AD 409 089

UNIVERSITY of PENNSYLVANIA
ELECTROMEDICAL LABORATORY
The Moore School of Electrical Engineering
PHILADELPHIA 4, PENNSYLVANIA

ONR

TECHNICAL REPORT NO. 37*

MECHANICAL EFFECTS OF AC FIELDS ON PARTICLES DISPERSED IN A LIQUID; BIOLOGICAL IMPLICATIONS

Lawrence D. Sher

Principal Investigator: H. P. Schwan

Electromedical Division
The Moore School of Electrical Engineering
University of Pennsylvania
Philadelphia 4, Pennsylvania

* This report was submitted by L. D. Sher as a thesis in partial fulfillment of the requirements for a Ph. D.

ACKNOWLEDGEMENT

Initial support for this work was provided by the Air Force Contract AF 30(602).

Since 1961 this work has been solely supported by the Office of Naval Research, Contract Nonr 551 (05).

TABLE OF CONTENTS

LIST OF FIGURES

BIBLIOGRAPHY

Abraham, M. and Becker, R.: The Classical Theory of Electricity and Magnetism. 2nd ed., Hafner, New York, 1949.

Abramson, H.A.: Electrophoresis. The Academy, New York, 1939.

Abramson, H.A., Moyer, L.S., and Gorin, M.H.: The Electrophoresis of Proteins. Reinhold, 1942.

Anne, A., Saito, M., Salati, O.M., and Schwan, H.P.: Penetration and thermal dissipation of microwaves in tissues. Report No. 62-13, Dept. of Biomed. Electronic Eng., Univ. of Pa.

Bach, S. et al.: Effects of radio-frequency energy on human gamma globulin, in Vol. I of Biological Effects of Microwave Radiation. Plenum Press, New York, 1961.

Blüh, O.: Einige bei der Untersuchung von Kolloiden im Wechselfeld auftretende Erscheinungen. Kolloid Z., 37, 267, (1925).

Blüh, O.: Untersuchung von Kolloidpartikeln in Wechselfeldern verschiedener Frequenzen. Ann. Physik, 78, 177, (1925); ibid., 79, 143, (1926) (short additional note); ibid., 80, 181, (1926) (errata).

Brown, F.A. Jr.: Response to pervasive geophysical factors and the biological clock problem. Symposia Quant. Biol., 25, 57, (1960).

Brown, F.A. Jr.: Extrinsic rhythmicality; a reference frame for biological rhythms under so-called constant conditions. Ann. N.Y. Acad. Sci., 98, 775, (1962).

Colloid Science, Vol. 1. H. R. Kruyt, ed. Elsevier, New York, 1952.

Cotton, A. and Mouton, H.: Etude directe du transport dans le courant des particules ultramicroscopiques, Compt. Rend. Acad. Sci., 138, 1584 and 1692, (1904).

Debye, P. and Debye, P.P. Jr.: The Collected Papers of Peter J. W. Debye, p. 697. Interscience. New York, 1954.

Debye, P. et al.: Experiments on polymer solution in inhomogeneous electrical fields. J. Chem. Phys., 22, 152, (1954).

Eigen, M., and Schwarz, G.: Orientation field effect of polyelectrolytes in solution. J. Coll. Sci., 12, 181, (1957).

Frey, A.H.: Human auditory system response to modulated electromagnetic energy. J. Appl. Physiol., 17, 689, (1962).

Fricke, H., Schwan, H.P., Li. K., and Bryson, V.: A dielectric study of the low-conductance surface membrane in E. coli. Nature, 177, 134, (1956).

Furedi, A.A. and Valentive, R.C.: Factors involved in the orientation of microscopic particles in suspensions influenced by radio-frequency fields. Biochim. et Biophys. Acta, 56, 33, (Jan.) (1962).

Heller, J.H. and Teixeira-Pinto, A.A.: A new physical method for creating chromosomal aberration. Nature, 183, 905, (1959).

Herrick, J.F.: Pearl chain formation. Proceedings of the Second Tri-Service Conference on Biological Effects of Microwave Energy, 8-10 July 1958.

James, A.M.: The Electrochemistry of the Bacterial Surface, p. 98 in vol. 8 of Progress in Biophysics and Biophysical Chemistry. Pergamon, New York, 1957.

James, I.A.M., and Loveday, D.E.E.: Microelectrophoresis. Chemical Products, 21, 357, (1958) (part I); ibid., 21, 408, (1958) (part II).

Joos, G.: Theoretical Physics. 2nd ed., Hafner, New York, 1950.

Knoll, M. et al.: Reproduzierbarkeit von electrisch angeregten Lichterscheinungen (Phosphenen) bei zwei Versuchspersonen innerhalb von sechs Monaten. Elektromedizin, 7, No. 4, 235, (1962).

Krasny-Ergen, W.: Nicht-thermische Wirkingen elektrischer Schwingungen auf Kolloid. Hochfreq. u. Electroak., 48, 126, (1936).

Krasny-Ergen, W.: Zwei leitende isolierte Kugeln in homogenen elektrischen Feld. Ann. der Physik. Ser. 5, 27, 459, (1936).

Krasny-Ergen, W.: Der Feldverlauf im Bereich sehr kurzer Wellen; spontane Drehfelder. Hochfreq. u. Electroak., 49, 195, (1937).

Lamb, H.: Hydrodynamics. Article 357. 6th ed., Cambridge, 1932.

Liebesny, P.: Referate u. Mitteil. Internat. Kong. f. Kurzwellen. Vienna, 1937.

Liebesny, P.: Arch. Phys. Ther. 19, 736, (1939).

Lissman, H.W.: Electric location by fishes. Sci. Amer., 208, No. 3, 50, (1963).

Maxwell, J.C.: A Treatise on Electricity and Magnetism, I, fig. V, art. 143. Clarendon Press, Oxford, 1892.

Muth, E.: Uber die Erscheinung der Perlschnurkettenbildung von Emulsionspartikelchen unter Einwirkung eines Wechselfeldes. Kolloid Z., 41, 97, (1927).

Ogawa, T.: Measurement of the electrical conductivity and dielectric constant without contacting electrodes. J. Appl. Physics, 32, 583, (1961).

O'Konski, C.T. and Haltner, A.J.: Electric properties of macromolecules I. A study of electric polarization in polyelectrolyte solutions by means of electric birefringence. J. Am. Chem. Soc., 79, 5634, (1957).

Peterlin, A. and Ribaric, M.: Dynamical theory of electrosedimentation. J. Chem. Phys. 31, 759, (1959).

Prock, A. and McConkey, G.: Inhomogeneous field method for the study of large polarizable particles. J. Chem. Phys., 32, 224, (1960).

Rajewsky, B.: Ultrashortwaves in Biology and Medicine. Georg Thieme, Leipzig. 1938.

Saito, M.: A model for pearl-chain formation. Internal report of the Dept. of Biomedical Electronic Eng., U. of Pa. In preparation for publication.

Saito, M. and Schwan, H.P.: The time constants of pearl-chain formation, in Vol. 1 of Biological Effects of Microwave Radiation. Plenum, New York, 1961.

Saito, M. and Schwarz, G.: The threshold for the orientation of a particle. Internal report of the Dept. of Biomed. Electronic Eng., Univ. of Pa. In preparation for publication.

Schwan, H.P.: Biophysics of Diathermy, in Therapeutic Heat. Ed. by S. Licht. Licht, New Haven, Conn. 1958.

Schwan, H.P.: Determination of Biological Impedances, in Vol. 6 of Physical Techniques in Medicine and Biology. Academic Press, New York, 1963.

Schwan, H.P. and Li, K.: Hazards due to total body irradiation by radar. Proc. I.R.E., 44, 1572, (1956).

Schwan, H.P., Schwarz, G., Maczuk, J., and Pauly, H.: On the low-frequency dielectric dispersion of colloidal particles in electrolyte solution. J. Phys. Chem., 66, 2626, (1962).

Schwarz, G.: Zur Theorie der Leitfähigkeitsanisotropie von Polyelektrolyten in Lösung. Z. Physik, 145, 563, (1956).

Schwarz, G.: Uber die Dispersion des Orientierungsfeldeffektes von Polyelektrolyten in hochfrequenten elektrischen Feldern. Z. Physik. Chem. (Frankfurt) 19, 286, (1959).

Schwarz, G.: A general expression for the energy of a dielectric body in a quasi-electrostatic electric field. Internal report of Dept. of Biomedical Electronic Eng., U. of Pa. Submitted for publication.

Siglaff, C.L. and Mazur, J.: Electrophoretic mobility and electrochemistry of latex systems. J. Colloid Science, 15, 437, (1960).

Smoluchowski, M.: in Graetz Handbuch der Electrizität und des Magnetismus, Vol. 2, p. 366. Leipzig. Barth, 1921.

Stratton, J.A.: Electromagnetic Theory. p. 206. McGraw-Hill, New York. 1941.

Svedberg, T. and Andersson, H.: Zur Messmethodik der elektrischen Kataphorese. Kolloid Z., 24, 156, (1919).

Teixeira-Pinto, A.A., Nejelski, L.L. Jr., Cutler, J.L., and Heller, J.H.: The behaviour of unicellular organisms in an electromagnetic field. Exp. Cell Res., 20, 548, (1960).

Trank, J.W.: A statistical study of the effects of electric fields on the movements of mammalian sperm cells. Proceedings of the 11th Annual Conference on Electrical Techniques in Medicine and Biology, Minneapolis, Minn., Nov. 1958.

White, P.: The theory of electro-osmotic circulation in varying fields. Phil. Mag., 26, 49, (1938).

I. Introduction

This dissertation explores the possibility that electromagnetic radiation may interact with biological material without the production of a significant amount of heating. A simple physical system is used to show that various non-thermal interactions are possible. These interactions are studied to see whether, or under what conditions, they may occur in the case of irradiation of biological material.

Numerous claims exist in the literature for non-thermal interactions between electric and magnetic fields and biological organisms: Garlic root tips have exhibited mutations when grown in a high-frequency field[1]; micro-organisms have swum in preferred directions associated with the field direction[2]; snails and planaria have shown the ability to sense the presence and polarity of very weak electric and magnetic fields[3,4]; several people have heard sounds which correspond to the frequency of modulation of an incident

---

[1] Heller, J.H. and Teixeira-Pinto, A.A.: A new physical method for creating chromosomal aberration. Nature, 183, 905, (1959).

[2] Teixeira-Pinto, A.A., Nejelski, L.L.Jr., Cutler, J.L., and Heller, J.H.: The behaviour of unicellular organisms in an electromagnetic field. Exp. Cell Res., 20, 548, (1960).

[3] Brown, F.A.Jr.: Response to pervasive geophysical factors and the biological clock problem. Symposia Quant. Biol., 25, 57, (1960).

[4] Brown, F.A.Jr.: Extrinsic rhythmicality; a reference frame for biological rhythms under so-called constant conditions. Ann. N.Y. Acad. Sci., 98, 775, (1962).

microwave beam[5]; some fish are able to navigate by detecting distortions in their self-generated electric fields[6]; visual stimuli have resulted in humans from fields too weak to depolarize visual neurons in the usually understood way[7]; and changes have been reported in the paper electrophoretic pattern of human gamma globulin after isothermal irradiation by microwaves[8].

Although the quality of these reports is not uniformly good, there is no doubt that a biologically significant interaction with electromagnetic fields is possible for which tissue heating is not the cause. There is no presently understood physical basis that can explain these diverse non-thermal effects.

One class of possible non-thermal effects may be the result of mechanical forces on polarizable particles due to impressed AC fields. These forces have their origin in classical considerations of the energy in a field, but their consequences are often unexpected. To resolve the question of whether these field-induced mechanical forces have biological

---

[5]Frey, A.H.: Human auditory system response to modulated electromagnetic energy. J. Appl. Physiol., 17, 689, (1962).

[6]Lissman, H.W.: Electric location by fishes. Sci. Amer., 208, No. 3, 50, (1963).

[7]Knoll, M. et al.: Reproduzierbarkeit von electrisch angeregten Lichterscheinungen (Phosphenen) bei zwei Versuchspersonen innerhalb von sechs Monaten. Elektromedizin, 7, No. 4, 235, (1962).

[8]Bach, S. et al.: Effects of radio-frequency energy on human gamma globulin, in vol. I of Biological Effects of Microwave Radiation. Plenum Press, New York, 1961.

consequences, this dissertation qualitatively and quantitatively explores the varied effects of such forces. At least four distinct effects are shown to be possible, each of which is discussed in a separate section. Both experiment and theory are brought to the issue; their successful comparison is shown to extrapolate to the conclusion that, for impressed fields which do not unduly heat the tissue, these forces may have biological manifestations on the cellular scale but are ineffectual for sizes smaller than those microscopically visible.

II. Investigative Program

A study of the mechanical effects of AC fields is greatly simplified when these effects can be directly observed. Therefore the subject of the experimental effort was the simplest physical system which would conveniently exhibit the desired behaviour. Such a system is a suspension of micron-sized particles in a simple liquid. The premise for this method is that the passive physical behaviour of biological material in an AC field may be explained in terms of its measurable passive physical properties. Conversely, the behaviour of comparatively simple particles, such as polystyrene spheres could be used to study the interaction, with full confidence that the relations so found would have general validity.

Four distinct mechanical effects were observed: (1) Forces in inhomogeneous fields, (2) AC electrophoresis, (3) orientation of non-spherical particles, and (4) pearl-chain formation. The first three may be observed on single particles in the field, but the fourth is an interaction between two or more particles brought on by their combined exposure to the field. The various effects are independent of each other and may occur simultaneously. Each of them is investigated separately with both theory and experiment where possible. Experimental measurements of the threshold for their occurrence are compared with theoretical predictions for these threshold values. Agreement then allows extrapolation of the theory to smaller particles of biological interest.

The theory for these four effects was available in pieces, some exact, some approximate, and some requiring correction or extension. Where necessary and/or possible, the theory was corrected or amended in order to force a more valid or direct confrontation between experiment and theory. The theory for each effect will be discussed in the pertinent section.

III. EXPERIMENTAL METHODS

A. Choice and description of cell and cell holder

There were many constraints, often conflicting, on the choice of a cell to contain the particle suspension. But the consideration of paramount importance was good microscopic viewability. The cell thus had to be small enough to fit on the stage of the Leitz Dialux microscope; the thickness of the liquid layer had to be small enough so that particle concentration of a few percent would not interfere with the proper sub-stage illumination; the liquid could not have contact with free air or else evaporation and resultant thermal convection would disturb the microscopic scene; and the cell had to permit the use of the 90x objective lens which has an oil-immersion working distance of 0.12 mm.

An electric field had to be applied to the suspension, so-contained, and the metal body of the objective lens obviously had to be kept out of the field. A useful but not vital requirement was that the electric field should be homogeneous throughout the viewing area. However, the necessity of generating several hundred volts per centimeter from sub-audio to the hundreds of megacycles led to the hope that the electrodes could be as closely spaced as possible, a geometry not conducive to homogeneous fields.

Finally, with the knowledge that polystyrene spheres were in short supply, and that cleaning them and silicone emulsions from glassware often was difficult, it appeared desirable to use small sample volumes and to eliminate the

need for cleaning if possible.

These considerations eventually led to a successful design for an expendable cell which could easily be built from commercially available components. This design, shown in fig. 1 and 2, uses a proprietary product, Parafilm, in an essential way[9]. Parafilm is a wax-like substance which comes in large sheets, about 0.1mm thick. Commonly used to seal the tops of open glassware, it sticks to glass when moderate pressure is applied. It is easily cut into shapes, although fine shapes are difficult to handle because of its stickiness and tendency to stretch. It softens at temperatures between 40° and 55°C and begins to flow at about 55° to 60°C. When Parafilm melts on glass, it sticks with considerable tenacity. These properties are used to advantage in the present application.

This design was chosen after rejection of two designs described in the literature. One had the sample fluid partially exposed to the air and was awkward to use[10,11]; the other had poor optical conditions for high magnification and had the electrodes too widely spaced.[12]

---

[9]Parafilm is manufactured by Marathon, a division of the American Can Co., Menasha, Wisconsin.

[10]Blüh, O.: Einige bei der Untersuchung von Kolloiden im Wechselfeld auftretende Erscheinungen. Kolloid Z., 37, 267, (1925).

[11]Herrick, J.F.: Pearl chain formation. Proceedings of the Second Tri-Service Conference on Biological Effects of Microwave Energy, 8-10 July 1958.

[12]Trank, J.W.: A statistical study of the effects of electric fields on the movements of mammalian sperm cells. Proceedings of the 11th Annual Conference on Electrical Techniques in Medicine and Biology, Minneapolis, Minn., Nov. 1958.

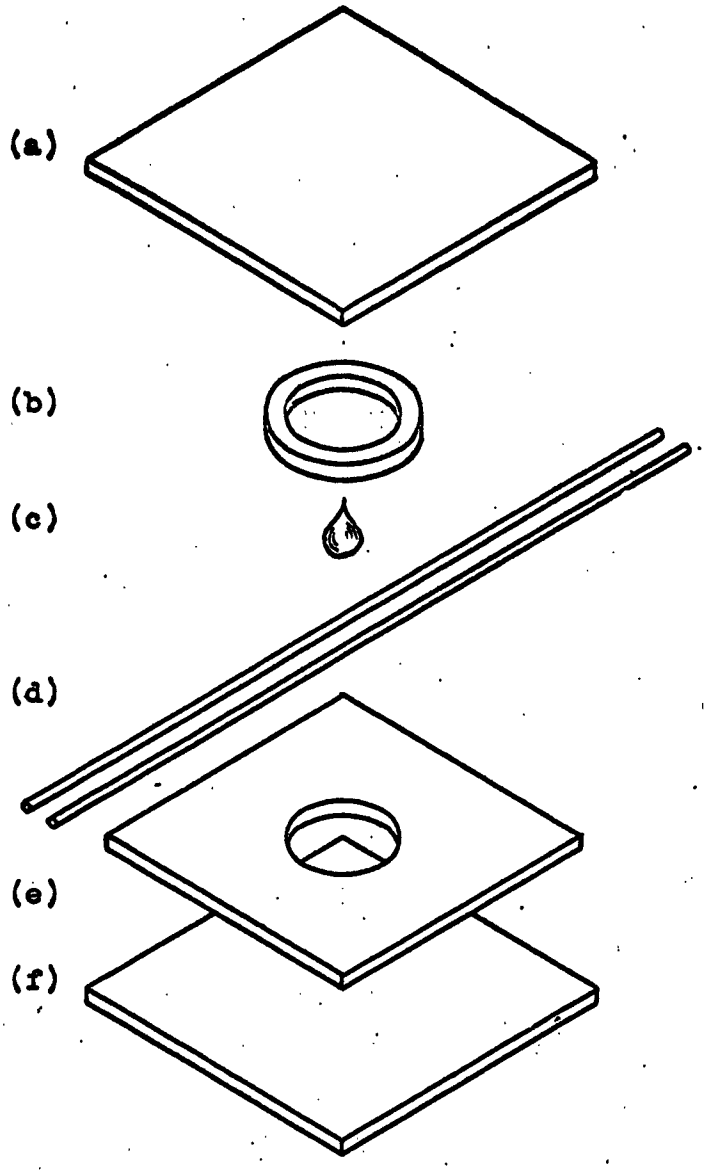

Figure 1. Exploded view of cell. Not to scale. (a) Top cover glass, No. 0, 100μ thick, 18mm square. (b) Annulus of Parafilm. (c) Sample fluid introduced with a dropping pipette, .4 mm^3 required. (d) Two parallel platinum wires, 65μ diam. reference grade Pt. (e) Sheet of Parafilm with a 7mm diam. hole for sample, 16mm square. (f) Bottom cover glass, No. 0, 100μ thick, 18mm square.

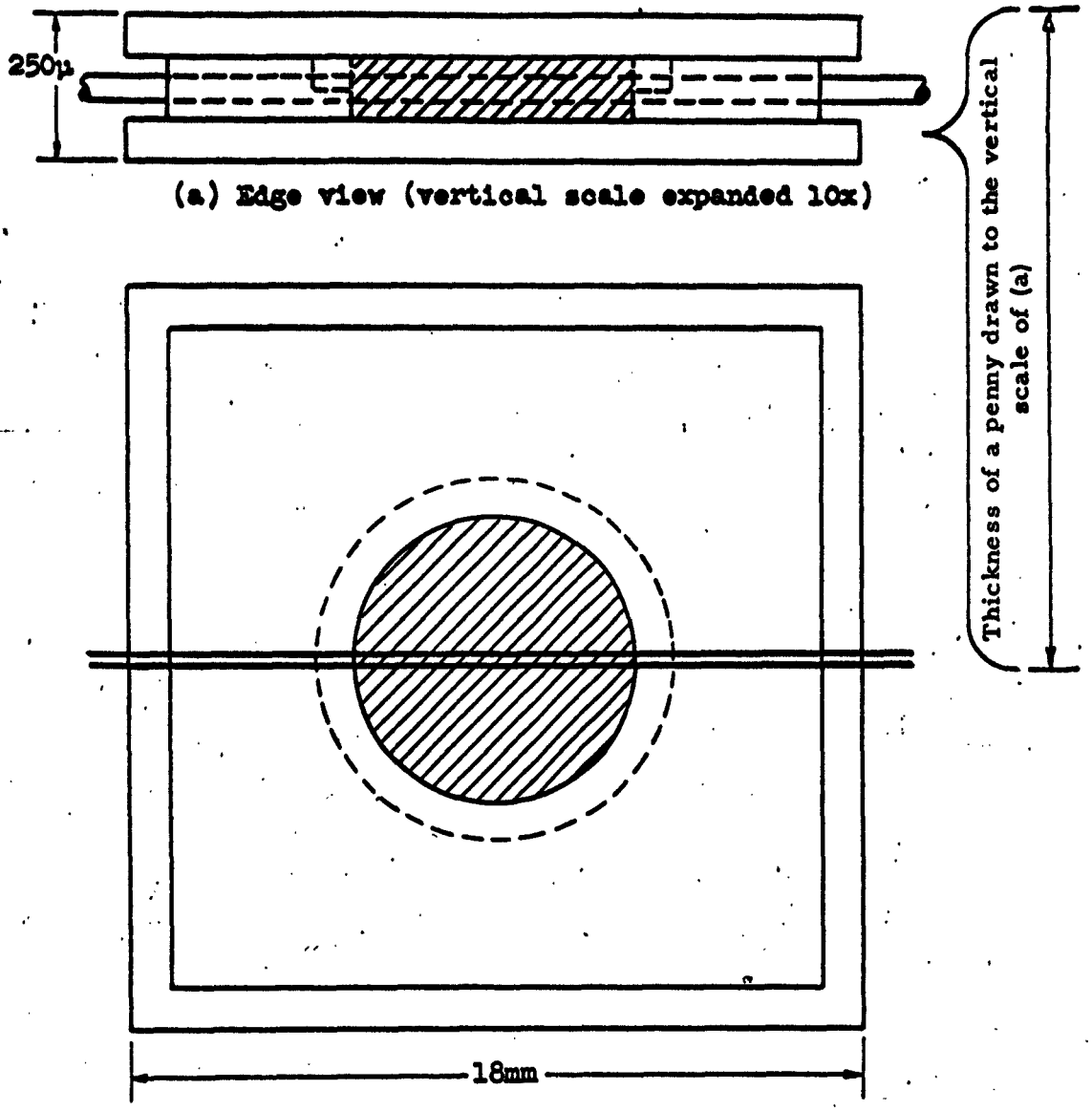

(a) Edge view (vertical scale expanded 10x)

(b) Top view

Figure 2. . Detailed views of assembled cell. Sample chamber is cross-hatched. Wires are shown undotted in (b) since thin film of Parafilm is almost transparent. Parafilm annulus (cf. fig. 1,b) is dotted, since it fuses into the larger sheet of Parafilm during the assembly process.

Assembly of the cell requires the use of a jig to hold the wires straight and accurately parallel, the cell being constructed around the wires while they are so held. The whole assembly process, which takes about 20 minutes, must be repeated using all new materials for each new sample. The method of assembly is now described in detail.

Approximately 22 cm. of wire is tied into a loop and is stretched as shown in fig. 3.

Figure 3. Schematic diagram of jig for assembling cells. Adjustable pegs hold wires parallel at a 250μ separation. Drawing to actual size. The dotted square shows where the cell is constructed.

The small closed circles are fixed pegs and the open circle is a freely movable peg which is drawn to the left by a spring. The spacing between the wires is adjustable by changing the positions of the fixed pegs. Typically, the clear space between the wires is 250μ = 4 wire diameters, and is uniform to within ± 4μ in the finished cell. Figure 4 shows the jig with a partially completed cell in place.

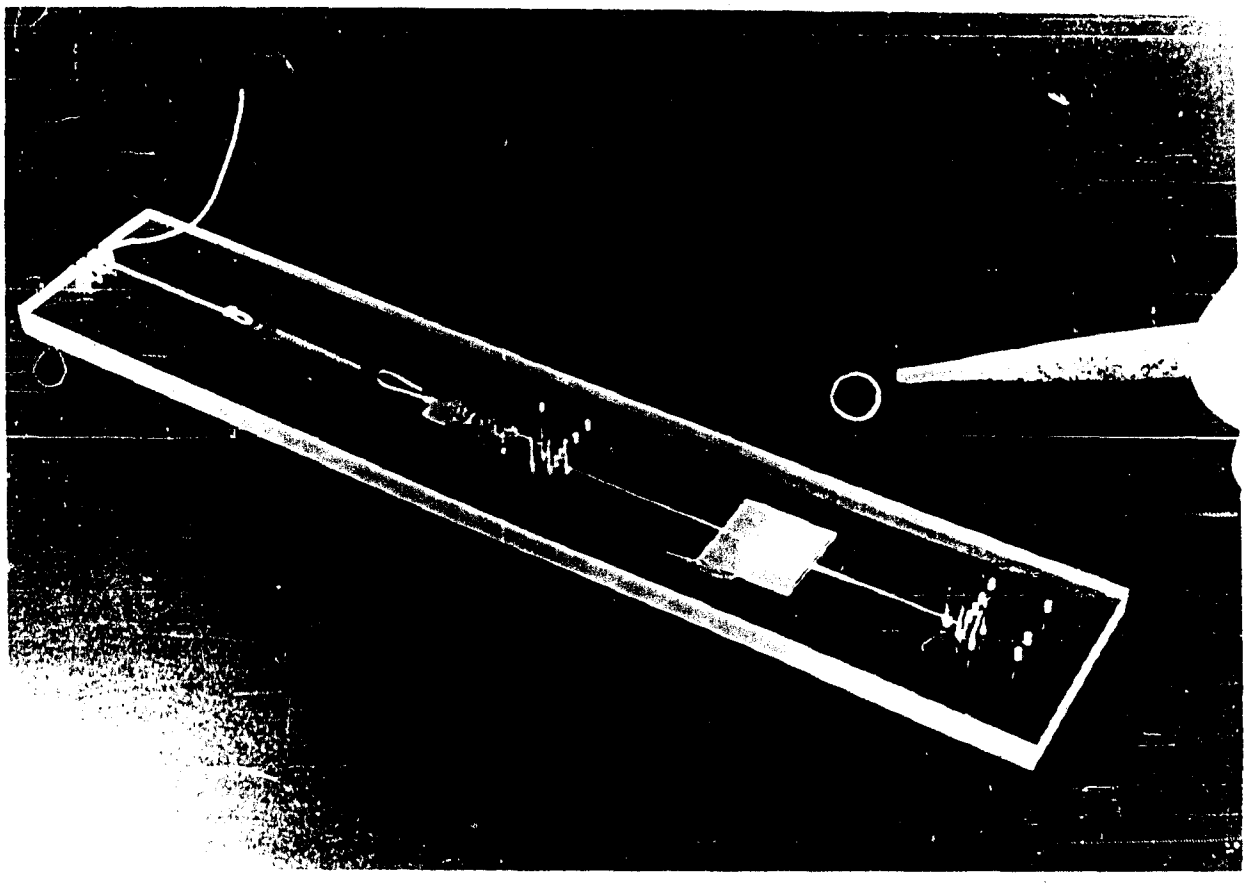

Figure 4. Jig with partially completed cell in place. The sample liquid is in its uncovered chamber and the cover together with the Parafilm annulus (cf. fig. 1 (a) and (b) is about to be placed on the assembly.

The cell-assembly procedure is as follows: A wire loop is put into the jig and stretched to a tension of about 75 grams (150 grams of spring tension). The wire loop is made coplanar by pushing it down the pegs until its full length lies on the plexiglass base plate, into which the pegs are fixed. Assembly of the lettered components (cf. fig. 1) begins by pressing the sheet of Parafilm (e) onto the bottom cover glass (f) with a small stainless steel spatula. This "lower" assembly is pushed under the wires to occupy the dotted square space in fig. 3. In this position the wires press lightly on the Parafilm, since the wires had to be raised to get the "lower" assembly into place. An "upper" assembly (a + b) is now made in exactly the same way and is stored temporarily. The sample liquid is introduced onto the lower assembly with a dropping pipette until there is a slight convexity of liquid in the sample chamber. The upper assembly is carefully lowered onto the lower, thus trapping the wires (this operation is pictured in fig. 4). The sandwich is now heated (method described below) until the Parafilm melts (about 55°C), which allows the two pieces of Parafilm to flow into each other and to adhere very tightly to the glasses. The result is a sealed unit capable of withstanding all normal handling.

A satisfactory method of heating was found with difficulty. Through a block of aluminum, about 4 x 3 x 2 cm, a 6 mm (diameter) hole was drilled through the center of the 4 x 3 faces. The block is heated to 100°C in boiling water,

is removed, and dried quickly with a paper towel. It is then carefully set on top of the complete cell assembly, the hole covering (not heating) the sample chamber. Slight additional pressure for a few seconds is sufficient to "grill the sandwich." The final thickness of the cell, or height of the sample chamber, is almost completely determined by the thickness of the Parafilm layer (e in fig. 1), since it softens but does not extrude. The annulus (b) does extrude slightly into the sample chamber because of the concentration of pressure at that point, resulting in a good seal where the wires enter and leave the liquid.

Final preparation for use requires only that the tension in the wire loop be released and the wires cut closely on one side and about 15 mm long on the other.

Figure 5. The finished cell ready for use. The penny is shown for a size comparison. The cell may be used with either side up.

Insertion of the cell into the cell holder completes the preparation for use. The cell holder has several functions: It allows the microscope stage manipulator to grip and move the cell as if it were a standard glass slide; it immobilizes the cell in a vertical sense so that oil immersion objectives can be used; and it allows electrical contact to be made with the platinum wires with no danger of pulling these wires. The photographs of the cell holder with and without the cell in place (fig. 6 and 7) are followed by a more detailed plan of its construction (fig. 8).

Figure 6. Cell holder without cell. Miniature alligator clips have been modified by filling in the jaws with solder and filing them flat so that they may grip fine wires with security but without damage.

Insertion of the cell into the cell holder completes the preparation for use. The cell holder has several functions: It allows the microscope stage manipulator to grip and move the cell as if it were a standard glass slide; it immobilizes the cell in a vertical sense so that oil immersion objectives can be used; and it allows electrical contact to be made with the platinum wires with no danger of pulling these wires. The photographs of the cell holder with and without the cell in place (fig. 6 and 7) are followed by a more detailed plan of its construction (fig. 8).

Figure 6. Cell holder without cell. Miniature alligator clips have been modified by filling in the jaws with solder and filing them flat so that they may grip fine wires with security but without damage.

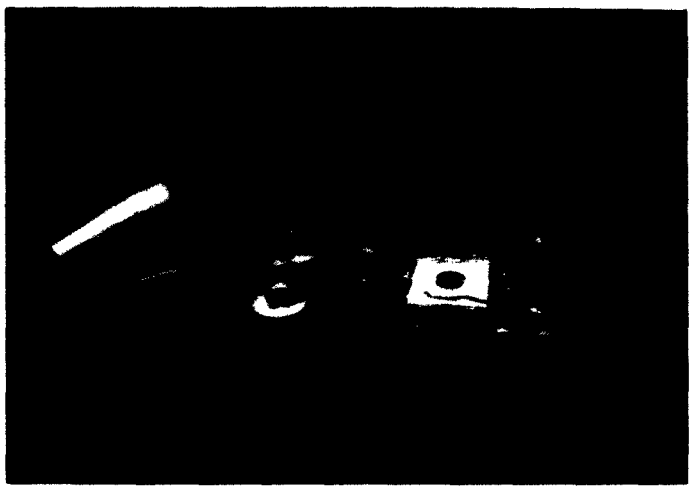

Figure 7. Cell holder with cell in place. Hold-down clips prevent the cell from sticking to the 90x oil-immersion objective lens as it is retracted. The geometry was chosen to optomize the microscopic view and to minimize lead length and inter-lead capacitance.

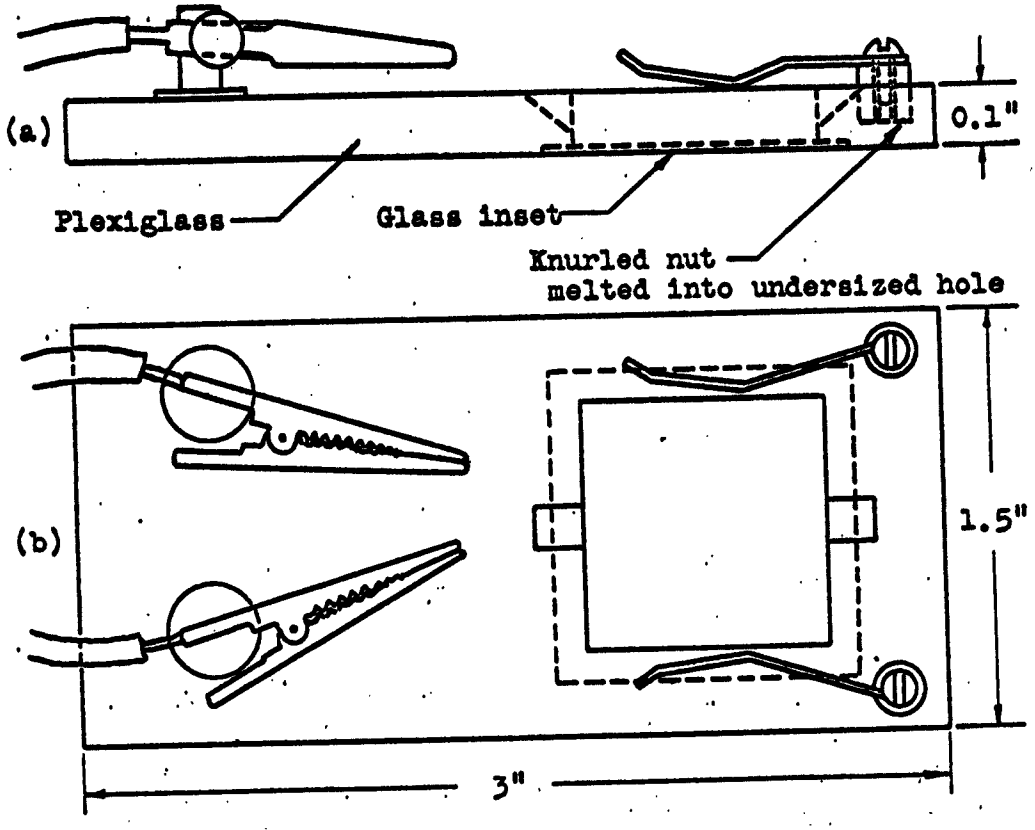

Figure 8. Construction details of cell holder. Spring clips used to hold the cell down are shown in their retracted position. Small alligator clips modified to grip fine wires are soldered to small pedestals which are glued to plexiglass. Drawing approximately to scale, except for vertical scale of (a) which is expanded for clarity.

The wires coming from the cell holder must be immobilized, since a pull on these wires would cause the cell holder to come out of the stage clamp. This immobilization has been combined with a cable junction point in the form of a bracket fixed to the microscope body, as shown in fig. 9.

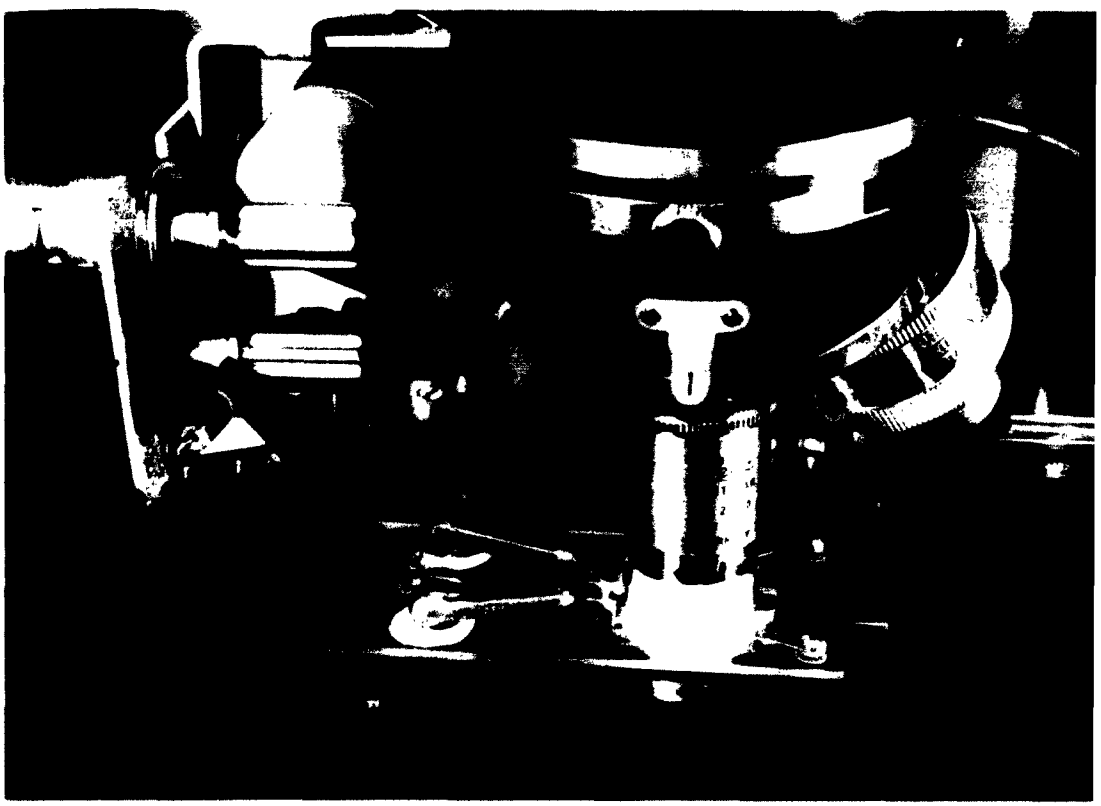

Figure 9. Stage of microscope with cell, cell holder, cable junction bracket, and VTVM probe in their working positions. Detail is lost in the cell's picture because of the bright sub-stage illumination. Resistor at left is normally not in the circuit, is used to measure the current through the cell.

A VTVM probe utilizes the same bracket for mechanical support and for electrical contact as shown. Thus voltage measurements are made about 8 cm. from the cell. The effect of the lead wires on potential measurement will be discussed in reference to fig. 15. A coaxial input cable may be attached to the coax-to-banana adaptor (General Radio type 874-Q2) which is a permanent (although removable) part of the bracket. A double wire input for low frequencies may be attached by using a banana plug in conjunction with a second coax-to-banana adaptor of the same type.

The finished cell has good viewability and photographic potential, good thermal dissapation, fairly homogeneous fields (see the next section for a discussion of homogeneity), is relatively simple to make, and may be discarded after use. If the contents of the cell undergoes any irreversible, detrimental change, however, it must be discarded and a new one built. Some difficulties of this type may be avoided by the proper corrective action; this topic is discussed in more detail in section VII.

In summary, a cell and cell holder have been designed for microscopic observation of the effects of alternating electrical fields on a suspension of micron-sized particles. The cell satisfies almost all of the many requirements placed upon it.

B. Homogeneity of field

Knowledge of the field configuration within the cell was necessary for two reasons: First, the actual value of the field strength could be determined by no other method; and second, non-thermal effects may result from inhomogeneities in the field (see section IV).

The measurement was based on the following analysis of the possible current paths between the electrodes:

Glass: $\kappa \sim 10^{-13}$ mho/cm ; $\epsilon \sim 5$

Water: $\kappa \sim 10^{-3}$ mho/cm ; $\epsilon \sim 80$

$$\frac{\text{Conductive current in aqueous medium}}{\text{Conductive current in glass}} \cong \frac{10^{-3}}{10^{-13}} \cong 10^{10}$$

$$\frac{\text{Susceptive current in aqueous medium}}{\text{Susceptive current in glass}} \cong \frac{80}{5} \cong 16$$

Thus both the conductive and the susceptive parts of the current are virtually completely confined to the aqueous medium. For this reason it is possible to plot the field lines with an analog which ignores the presence of the glass, i.e., which assumes that current density normal to the glass is zero everywhere. Of course the ratio of conductive to susceptive current in the aqueous medium changes with frequency, but the ratio is not of interest in this study of homogeneity.

The analog chosen was Teledeltos paper.[13] This paper has a thin uniform coating of a conductive material (containing carbon) with a surface resistivity of 4000 Ω/square. Potential in this thin sheet was used to represent the po-

---

[13] Made by Western Union Telegraph Co., 60 Hudson St., N.Y., N.Y.

tential in any section of the cell taken normally through the wires. The choice of a two dimensional analog was possible since any of the cell's parameters, including potential, is essentially constant in a direction parallel to the wires, the end effects being completely negligible.

The Teledeltos experiment is accomplished with the circuit shown in fig. 10.

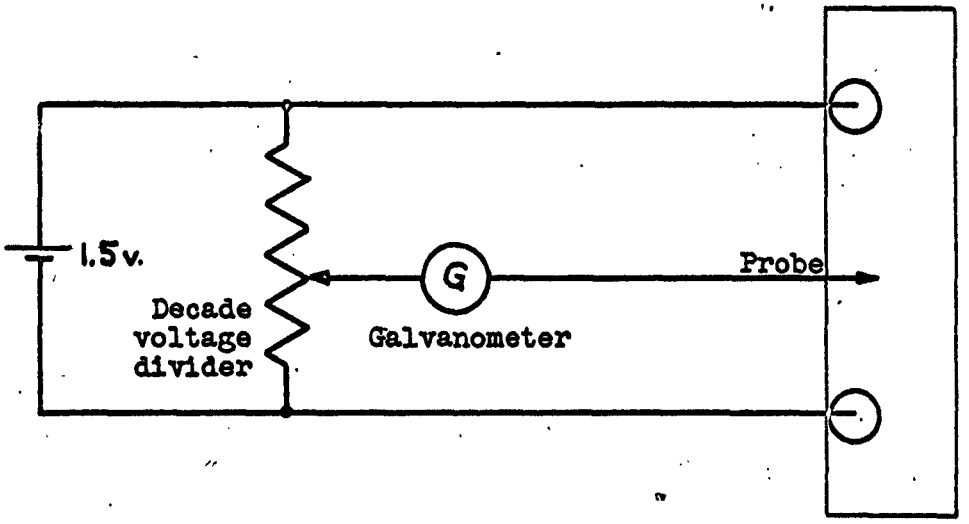

Figure 10. Field plotting with Teledeltos paper. This conductive paper, shown on the right, has two round electrodes which represent cross-sections of the wire electrodes.

Normally, areas of constant potential, such as cross-sections of solid conductors, are represented on the paper as appropriately shaped areas of silver paint. To minimize possible losses in the silver paint, however, the round electrodes used here were copper disks of the proper size fastened to

the paper with the silver paint as glue. Also it was relatively simple to attach wires to the copper. Under the Teledeltos paper was placed (in descending order) a sheet of carbon paper face down, a sheet of plain white paper, and glass. The end of the probe was polished to a smooth but fine point. When, by lightly moving the probe tip across the Teledeltos paper, a null was found on the galvanometer, a mark was registered on the white paper by pressing slightly with the probe tip. This procedure was repeated several times for each of nine equi-spaced settings on the decade voltage divider. Finally, the circular electrode outlines and the straight paper borders were traced onto the white paper, using the disconnected probe tip pressing through the carbon paper. In this manner a complete pictorial record of the potential distribution was obtained. Each record shows the equipotentials in intervals of 0.1 V, where V is the voltage applied between the electrodes. In all cases, the electrodes were placed far enough from the ends of the paper to minimize end effects. These long ends are not shown on the records in fig. 12. The procedure was repeated for several different electrode spacings and cell thicknesses, since these quantities may vary somewhat in practice. Figure 11 illustrates the cases treated and fig. 12 shows the actual field plots for these cases.

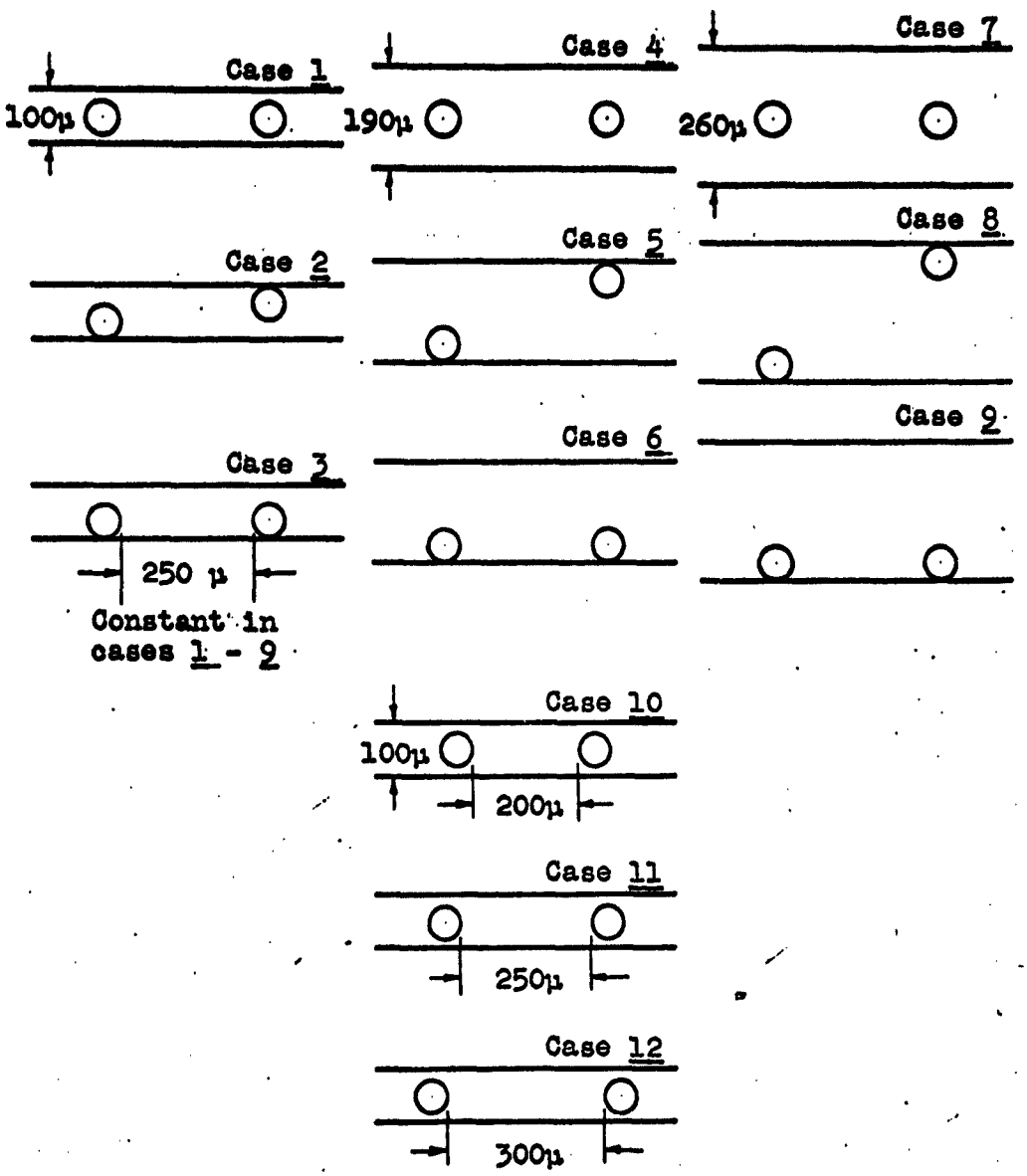

Figure 11. Variations of electrode spacings and cell thicknesses which encompass the ranges of variability encountered in practice. The field configuration was measured for each of these cases (see fig. 12). The cell thickness is constant for each vertical group of three cases. Note that cases 1 and 11 are identical.

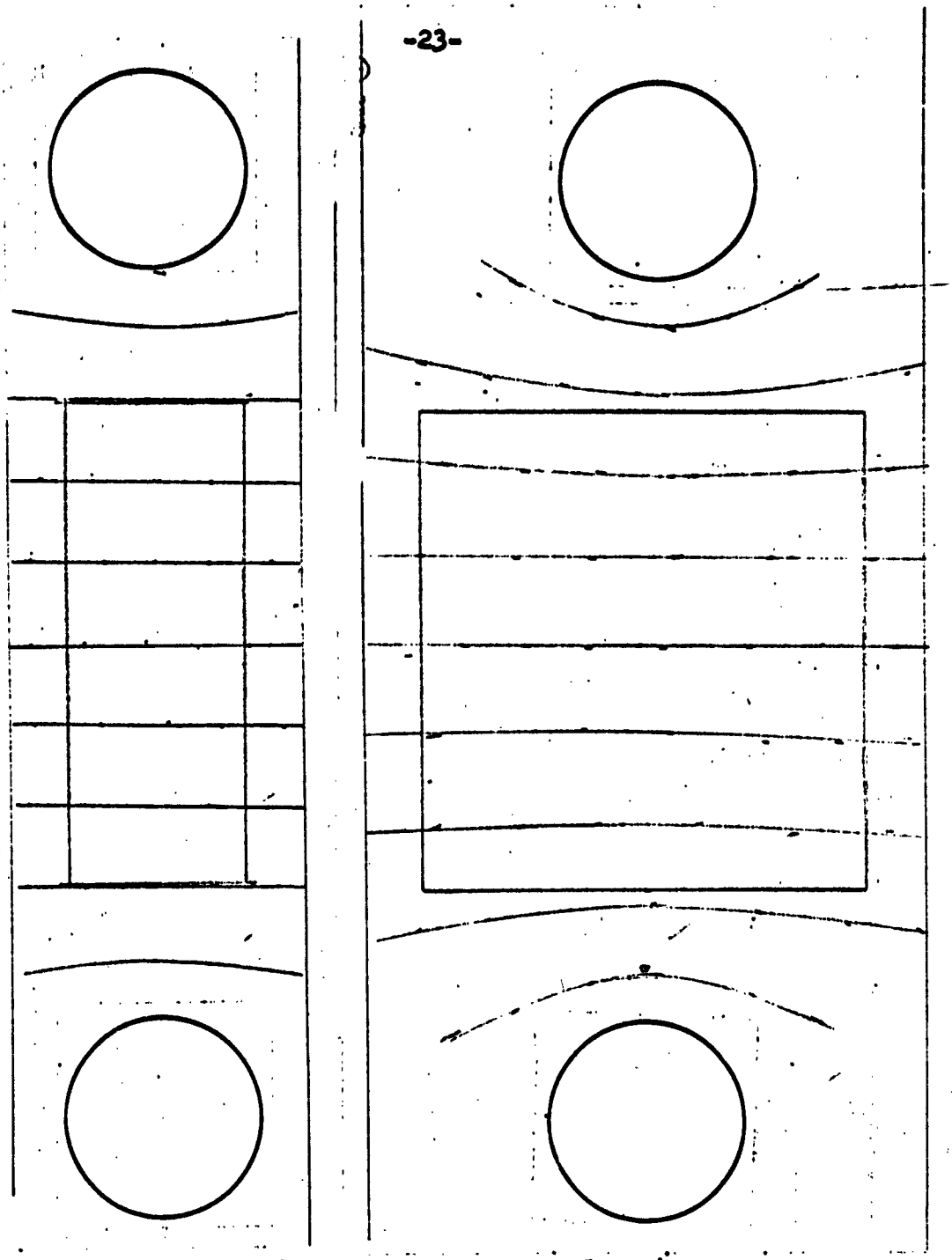

Cases 1 and 11 Case 4

Figure 12a. Field plots of the cell with varied electrode spacings and cell thicknesses (see fig. 11). Rectangle defines area viewed when taking measurements. Scale: 1mm = 2μ

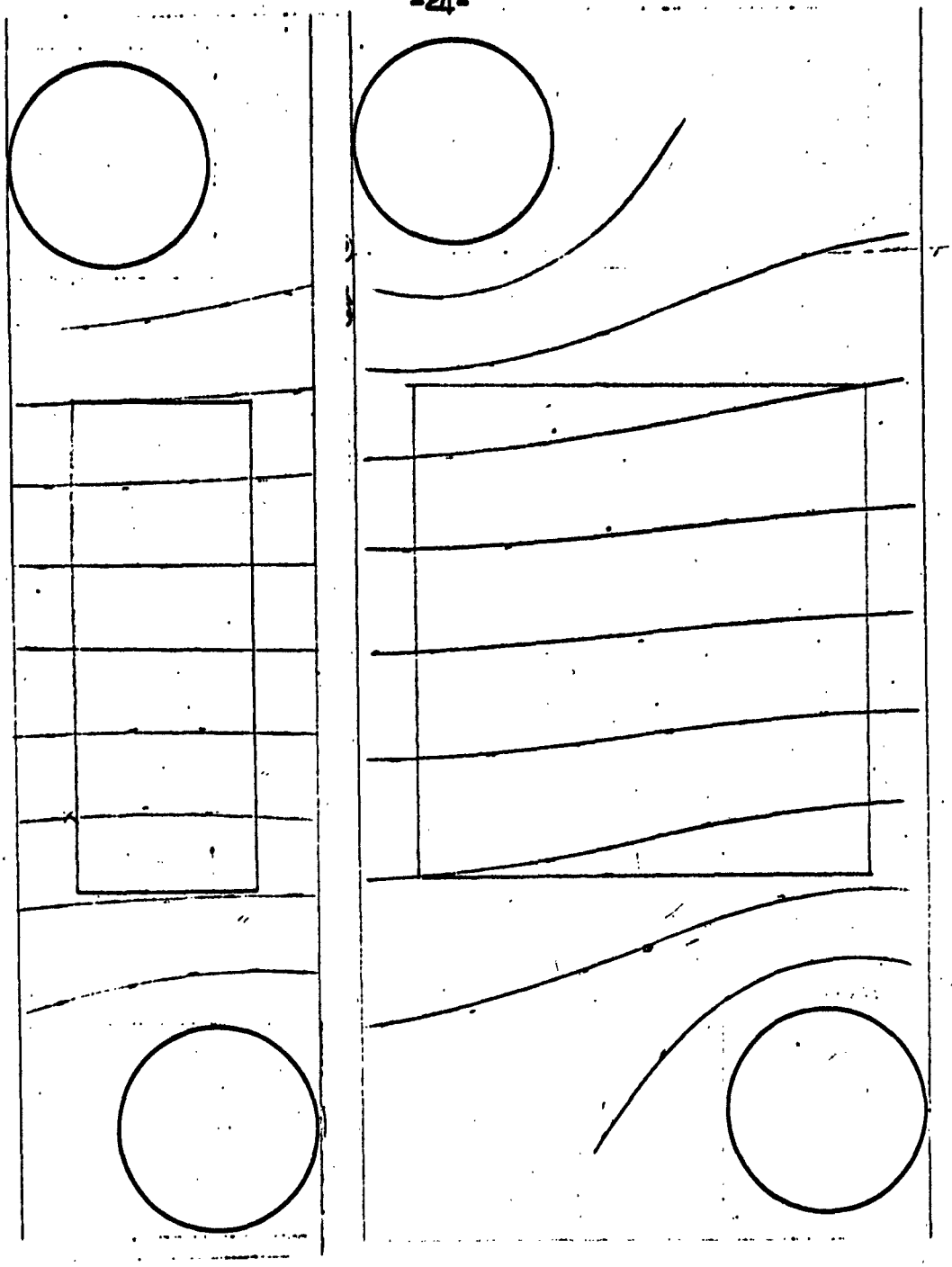

Case 2 Case 5

Figure 12b. Field plots of the cell with varied electrode spacings and cell thicknesses (see fig. 11). Rectangle defines area viewed when taking measurements. Scale: 1mm = 2μ

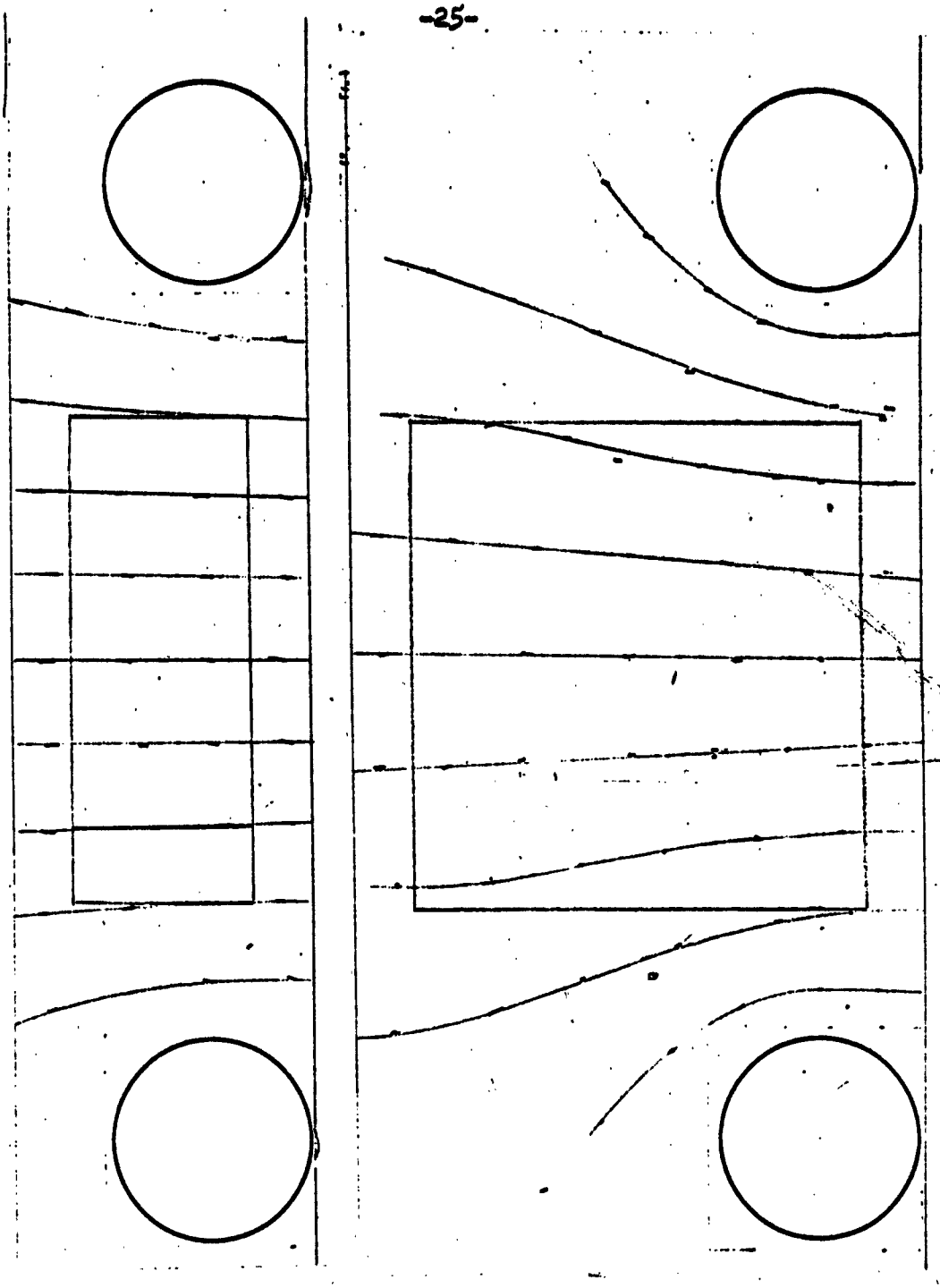

Case 3 Case 6

Figure 12c. Field plots of the cell with varied electrode spacings and cell thicknesses (see fig.11). Rectangle defines area viewed when taking measurements. Scale: 1mm = 2μ

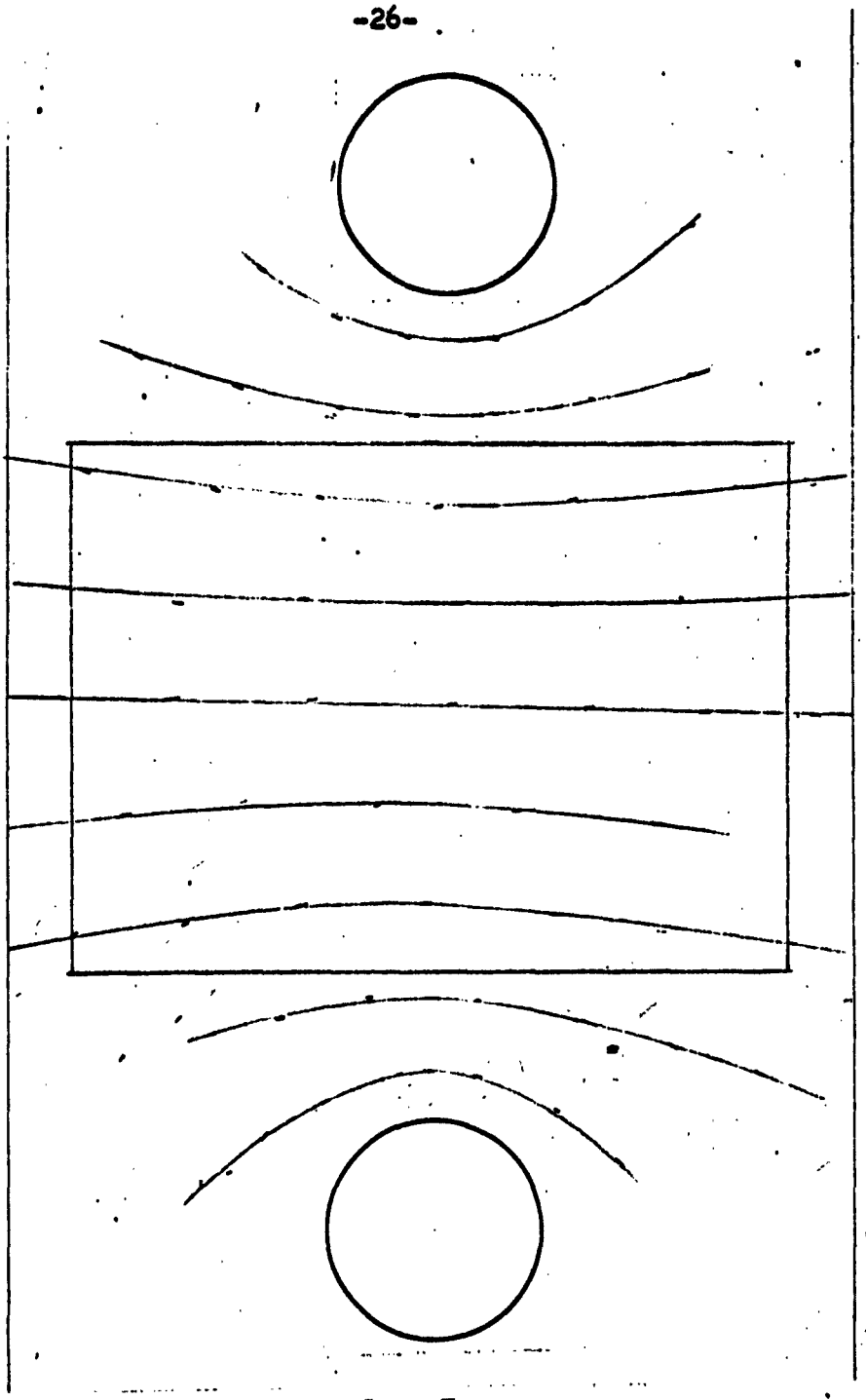

Case I

Figure 12d. Field plots of the cell with varied electrode spacings and cell thicknesses (see fig.11). Rectangle defines area viewed when taking measurements. Scale: 1mm = 2μ

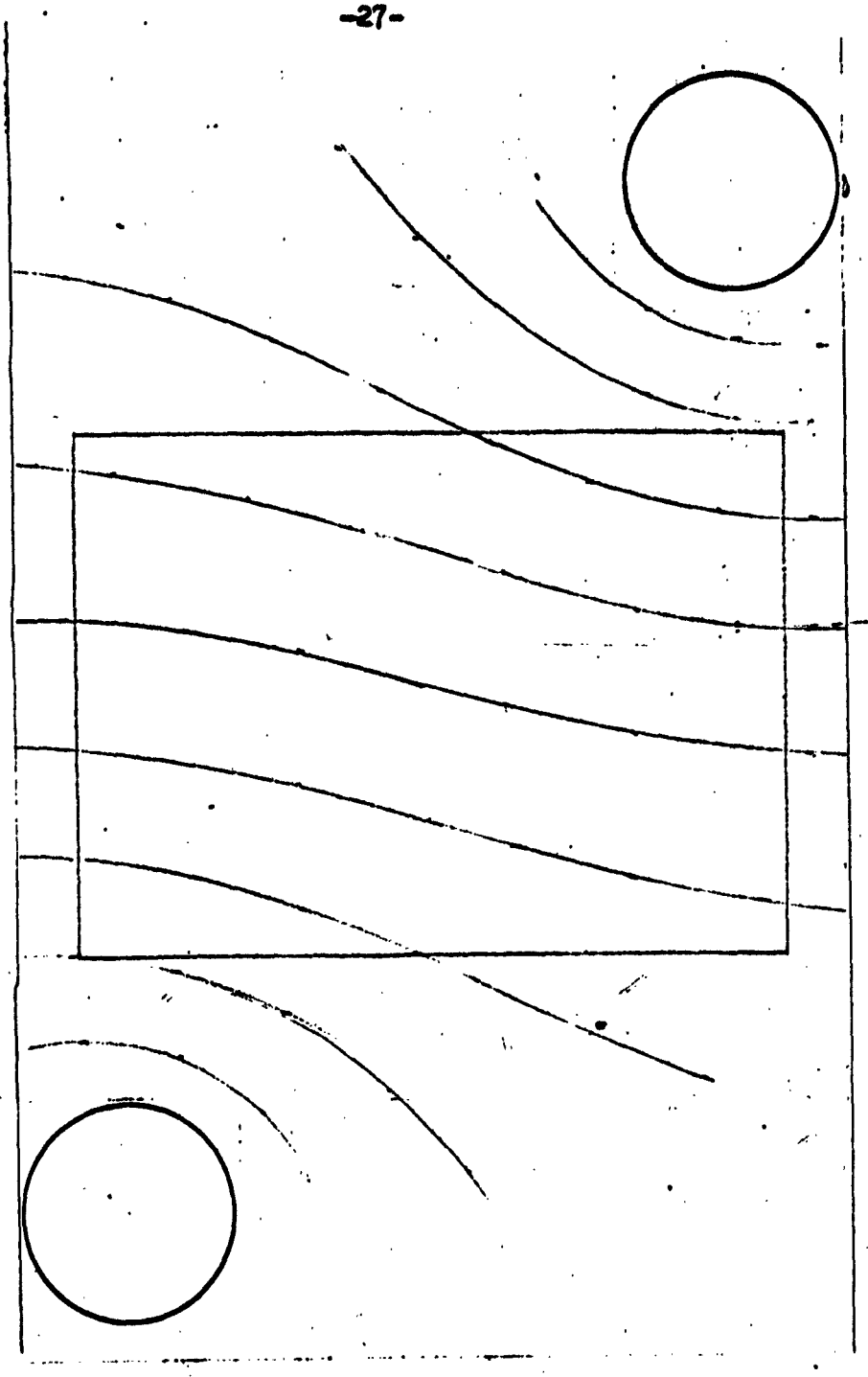

Case 8

Figure 12e. Field plots of the cell with varied electrode spacings and cell thicknesses (see fig.11). Rectangle defines area viewed when taking measurements. Scale: 1mm = 2μ

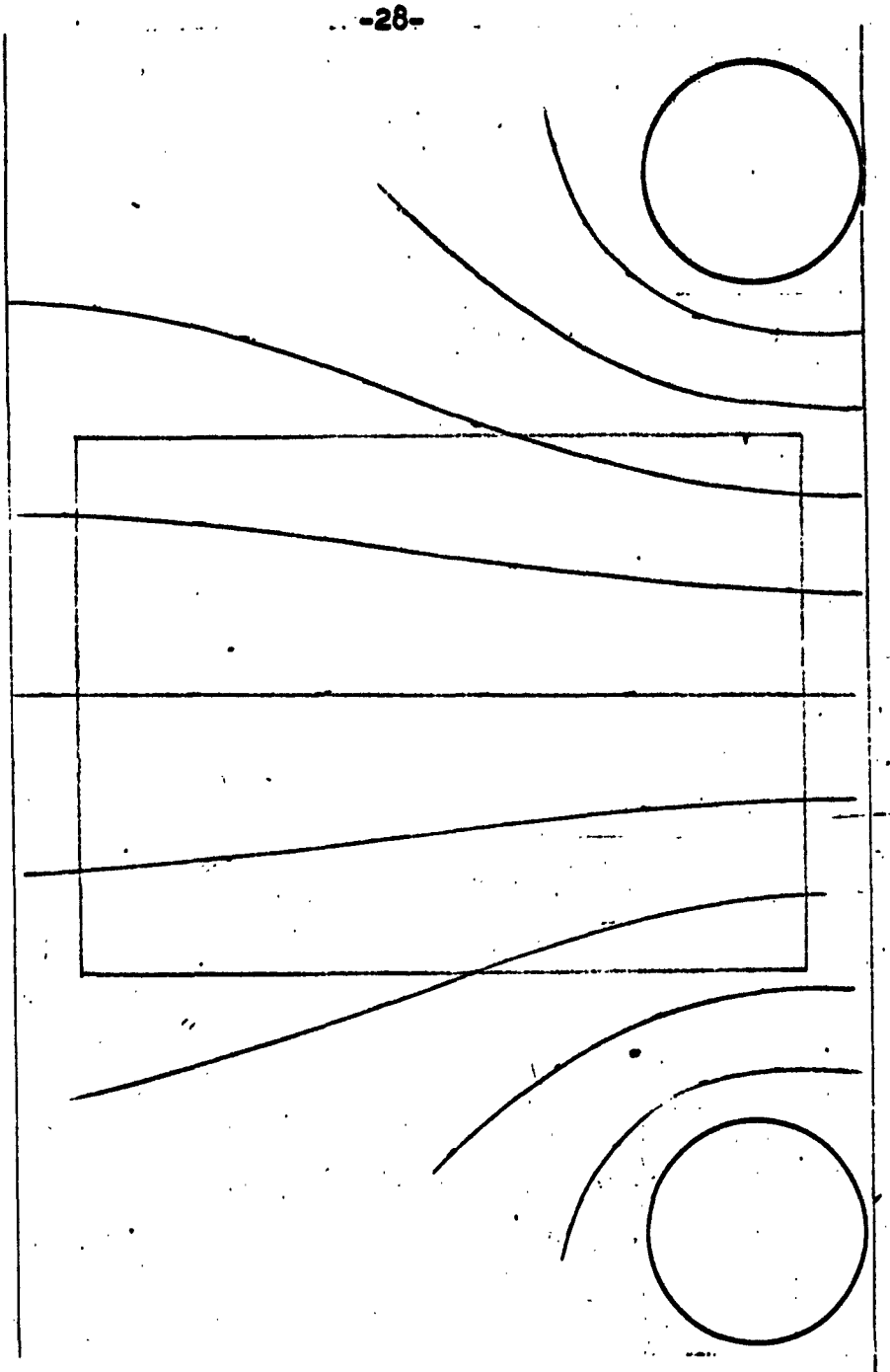

Case 9

Figure 12f. Field plots of the cell with varied electrode spacings and cell thicknesses (see fig.11). Rectangle defines area viewed when taking measurements. Scale: 1mm = 2μ

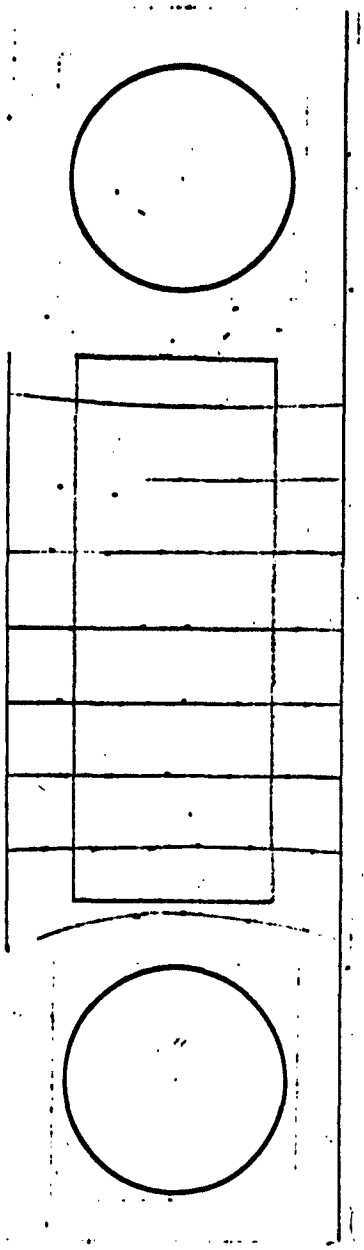

Case 10

Case 11 = Case 1, q.v.

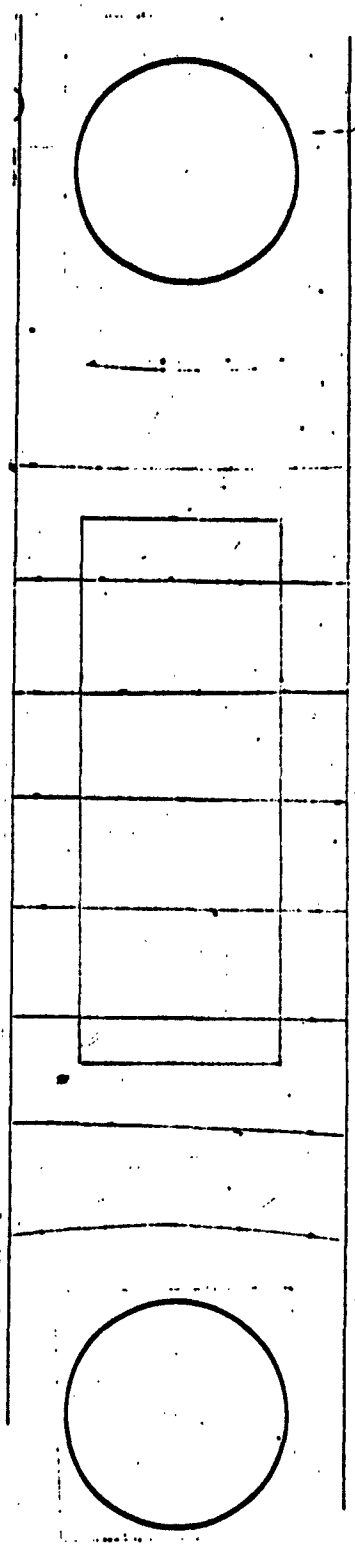

Case 12

Figure 12g. Field plots of the cell with varied electrode spacings and cell thicknesses (see fig.11). Rectangle defines area viewed when taking measurements. Scale: 1mm = 2μ

To relate these studies of homogeneity to the measurements taken in this cell, it was convenient to define a "field parameter" F which would relate the magnitude of the actual field strength in the area of observation to the magnitude of the "apparent" field strength. By "apparent" field strength is meant the (r.m.s.) voltage, V, between the electrodes divided by the distance, d, between their inner borders, the distance being measured in a direction parallel to the glass. The field parameter was defined so that

$$E_{actual} = F\, E_{apparent}$$
$$= F\, \frac{V}{d} \qquad (1)$$

Of course F is a function of position in any specific cell. However, since it would have been too difficult to record the position of each observation, the alternative of measuring F_{max}, $F_{center\ of\ cell}$, and F_{min} for each case was chosen. The proper graphical presentation of these F-values would, it was felt, provide sufficient means for achieving an experimental accuracy commensurate with the other accuracies (or inaccuracies) in this work.

Calculation of F from these field patterns is straightforward. Since $F = E_{actual}/E_{apparent}$, it is necessary only to measure these quantities from the record. E_{actual} is given by the potential difference (0.1 V) between two adjacent equipotentials divided by their orthogonal separation (in mm), i.e. a quantity whose units are V/mm, where V is unspecified. $E_{apparent}$ is given by V/d, as mentioned above, and so has the same units. Thus F is a pure number, free of V. The positions

of F_{max} and F_{min} for each case are found by observation but do not always occur at corresponding places in the different cases. All measurements of F refer to the field within the areas of observation, i.e., the rectangles in fig. 12. An effort was made to determine F as accurately as interpolation of these curves would permit. F is presented in fig. 13.

The "F correction" was applied to all measurements taken in the cell. In several cases, no record of the detailed geometry of the cell was made, except, of course, for the wire spacing, d, which was always recorded (see section IIID for a discussion of microscopic methods of measuring cell geometry). All of these data-deficient cases occur for early cells which used no Parafilm annulus in their construction; therefore their thickness is fairly uniform at about 100μ. For these cases, F = 0.90 was used.

It must be stressed that the cases were chosen to encompass the cell geometries found in practice. Thus cases 8 and 9 were never observed in actual cells. Also the values of F_{max} and F_{min} are not necessarily representative of more than a very small portion of the viewing area; they are included to help the experimenter with the interpretation of the data.

In a few cases, observations were not made in the defined viewing area, but rather near the bottom of the cell. Special measurements of $F_{bottom\ of\ cell}$ were made from fig. 12 for these cases. Fig. 13 does not show these values.

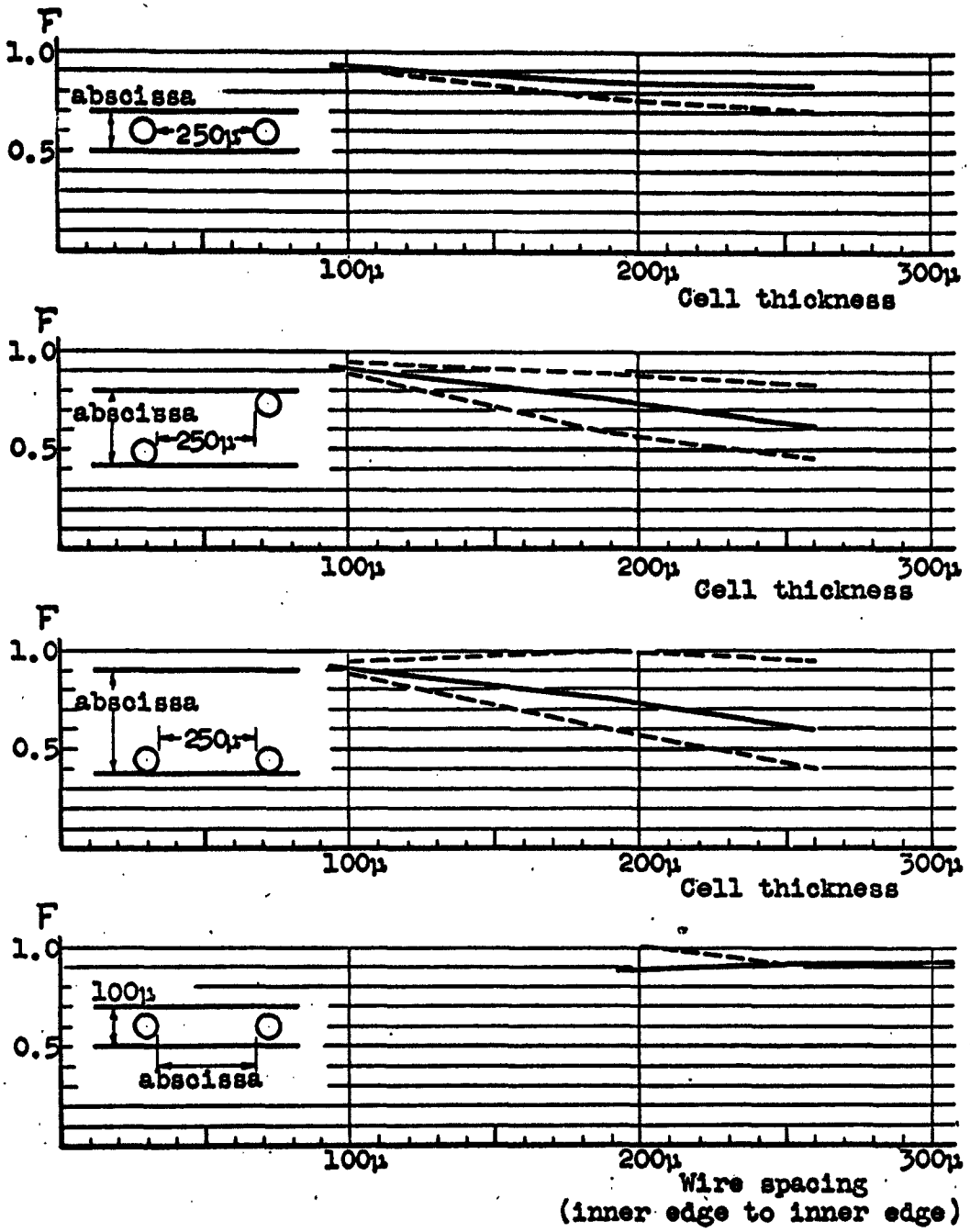

Figure 13. Field parameter F as a function of cell thickness and electrode configuration. The solid line in each graph represents F as measured in the center of the cell. The dotted lines above and/or below represent the values of F_{max} and/or F_{min} (see text).

C. Electrode polarization

The total impedance of the cell is composed of two series impedances: the fluid impedance and the boundary or surface impedance existing at the Pt-liquid interface. A portion of the applied voltage therefore is lost at these interfaces, the phenomenon being called electrode polarization. Accurate knowledge of the magnitude of electrode polarization was a prerequisite for these quantitative studies.

In general, the observed total resistance, R_T, is given by the approximate relation[14]

$$R_T = R_S + \Delta R \qquad (2)$$

where R_S = true, frequency-independent, sample resistance

ΔR = resistance contribution of electrode polarization, a power function of frequency

Since ΔR would be expected to be largest, and most troublesome, with high conductivity media, such as physiological saline ($K \sim 10^{-2}$ mho/cm), the first measurements were on that substance[15]. Fig. 14 shows the results of this measurement.

---

[14] Schwan, H. P.: Determination of Biological Impedances, in Vol. 6 of Physical Techniques in Medicine and Biology. Academic Press, New York, 1963.

[15] Measurements were made with a Hewlett-Packard Impedance Bridge, type 650-A.

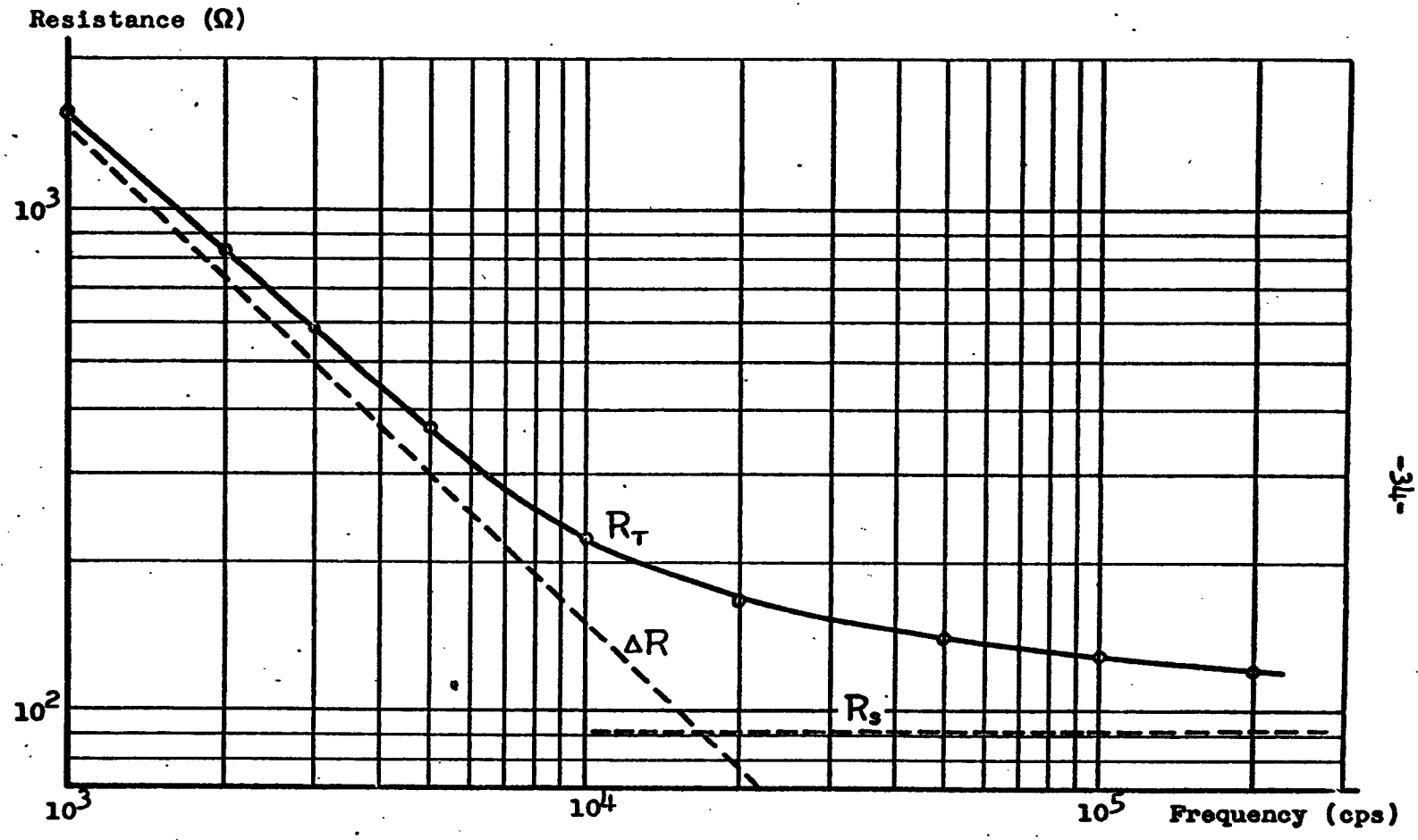

Figure 14. Total cell resistance as a function of sample and polarization resistances. Cell is filled with physiological saline. Dotted curves are chosen so that their sum will equal the solid curve, according to eq. (2).

From these measurements it can be concluded (1) that platinum electrodes must be retained, since some electrode polarization occurs even with them--copper electrodes would approximately double the polarization; and (2) that for frequencies much greater than 10 kc, polarization effects are tolerably small, but for f = 10 kc, electrode polarization absorbs about half of the applied potential. The few quantitative data which were taken in physiological saline, therefore, used frequencies well above 10 kc.

A similar measurement was made of the cell when filled with the low-conductivity polystyrene suspensions. The results of the measurements are shown in fig. 15a. From the frequency-independence of the low frequency part of the curve, it is clear that electrode polarization may be neglected. The drop-off above 1 Mc is due to the shunt capacitance of the leads and of the cell itself. This capacitance was measured independently and found to be of the order of 10μμf. At 1 Mc, therefore, the reactance and resistance of the cell are both about 10^4 ohm. Above 1 Mc, the cell will appear to be a pure capacitance. The approximately linear drop-off is the result of the relation

$$|Z_{cell}| \approx \frac{1}{\omega C} \quad , \qquad \text{for } f > 1 \text{ Mc}$$

$$\approx \frac{1}{2\pi C} f^{-1}$$

$$\ln|Z_{cell}| \approx \ln \frac{1}{2\pi C} - \ln f \qquad (3)$$

The curve should, and does, have a constant negative slope above 1 Mc. At about 100 Mc, the effect of lead inductance.

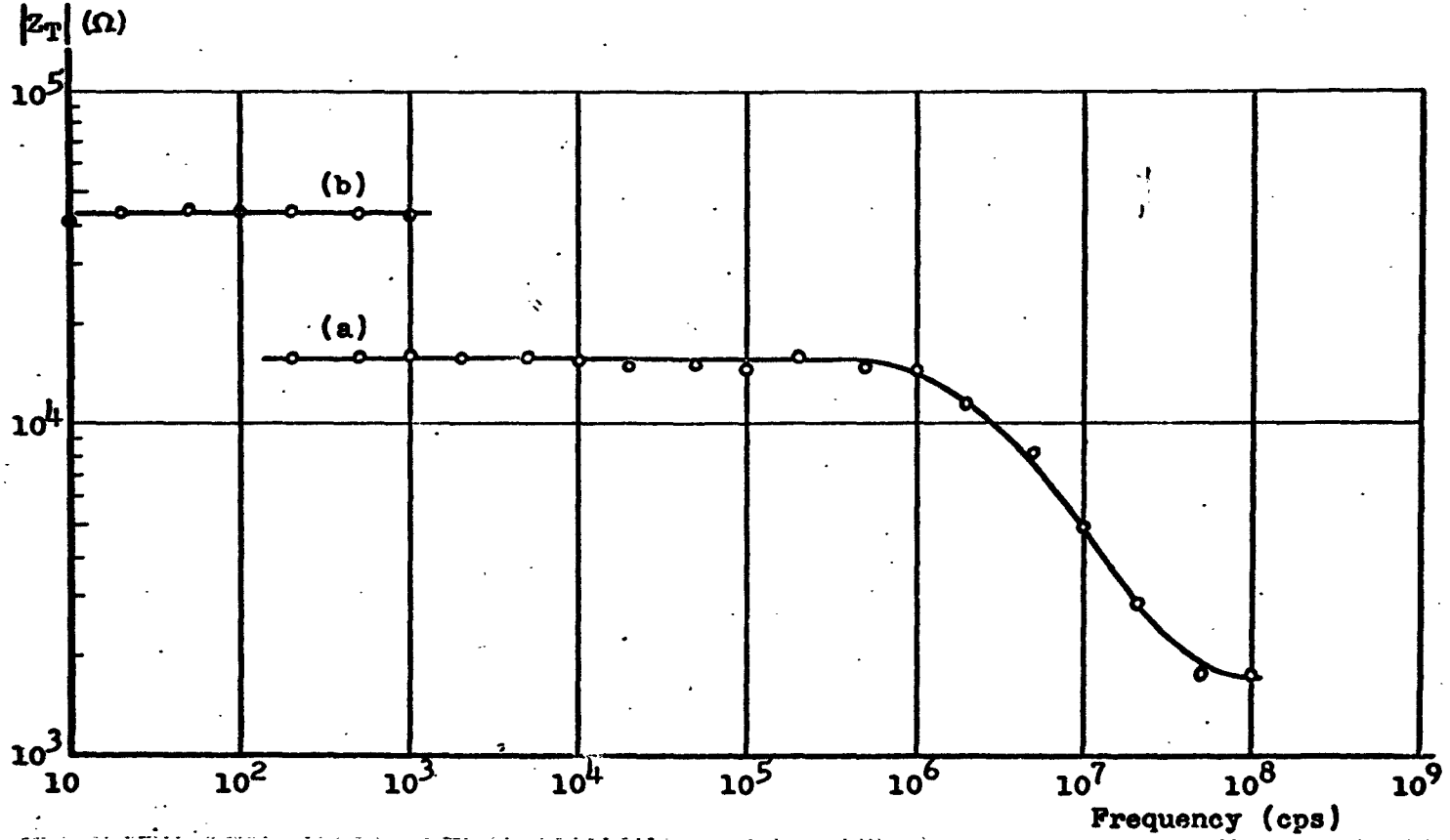

Figure 15. Impedance of the cell (a) when filled with a 1.17μ polystyrene sphere suspension, electrode spacing ≈ 0.3mm; (b) when similarly filled, electrode spacing ≈ 0.8mm for AC electrophoresis studies at very low frequencies. Flatness of curves at low frequencies shows that electrode polarization is not contributing significantly to Z_T. Impedance values measured with a Hewlett-Packard VTVM, model 410A, by using a series resistor for current determination.

begins to appear. Very few quantitative data for non-thermal effects were taken at 100 Mc and none were taken above it.

In conclusion, the amount of electrode polarization was found to be negligible for all frequencies of interest when low conductivity material is used. When high conductivity material is used, measurements must be limited to frequencies well above 10 kc if electrode polarization is not to be taken into account.

D. Microscopic methods

A Leitz Dialux microscope was used throughout this study. Illumination was incandescent and, with the exception mentioned in reference to fig. 23, was self-contained. A Heine condensor provided bright field, phase contrast, and dark field illumination in a continuum of available settings, which were used as required. Three objective lenses, 10x, 40x, and 90x (oil immersion), turret mounted, were used in conjunction with a 25x periplanatic eyepiece for viewing and a 10x Huygens eyepiece for photography.

Photographic facilities consisted of a Polaroid-Land camera attached to the lens body of the microscope by means of the Leitz Aristophot stand and suitable bellows and reflex viewer. Type 47 (ASA 3000) film was normally used to minimize the required exposure time.

Measurements of microscopic distances can be made in three dimensions. Length and width are measured with an eyepiece reticle calibrated, for each objective lens, against a calibrated slide (2mm divided into 200 parts). For example, this reticle was used to measure the diameter of spherical particles by measuring the length of a straight chain of such particles. The technique is described in more detail in reference to fig. 36. General measurement of fixed lengths over 10μ are probably accurate to within 1%. Measurements of depth are conveniently made using the calibrated stage elevator control. The apparent depth from one plane of focus to another is given on the "fine" elevator knob directly in

microns. The true depth may then be found be multiplying the apparent depth by the index of refraction of the medium in which the plane of focus was raised or lowered. Depth measurement by this method may have an error of ±5μ or ±5% (whichever is greater), but it is sufficiently accurate for all purposes of this study.

IV. FORCES IN INHOMOGENEOUS FIELDS[16]

A. Introduction and theory

A small particle of complex dielectric constant ϵ_1^* is suspended in a medium ϵ_2^* and is exposed to an alternating electric field whose effective (r.m.s.) value at the site of the particle, prior to its insertion, is E_o. The potential energy, ΔU, associated with the presence of the particle in the field is given by[17,18]

$$\Delta U = \frac{1}{2} \mathrm{Re} \int_{V_1} \tilde{\epsilon}_2^* \left(1 - \frac{\epsilon_1^*}{\epsilon_2^*}\right) E_1 \cdot \tilde{E}_o \, dV \qquad (1)$$

where E_1 = the effective field inside the particle

V_1 = the volume of the particle

$\sim$ = the complex conjugate

Assuming that (a) the media are homogeneous and isotropic and (b) the particle is a sphere whose size is sufficiently small so that over its extent the impressed field is homogeneous to a first approximation, then the internal field is also homogeneous to a first approximation. Its value is

$$E_1 = \frac{3\epsilon_2^*}{\epsilon_1^* + 2\epsilon_2^*} E_o \qquad (2)$$

Then

$$\Delta U = -\frac{3}{2} \mathrm{Re} \int_{V_1} \epsilon_2^* \frac{\epsilon_1^* - \epsilon_2^*}{\epsilon_1^* + 2\epsilon_2^*} E_o^2 \, dV \qquad (3)$$

---

[16] Called "ponderomotive forces" in Joos, G.: Theoretical Physics. 2nd ed., Hafner, N.Y., 1950; and in Abraham, M. and Becker, R.: The Classical Theory of Electricity and Magnetism. 2nd ed., Hafner, N.Y., 1949.

[17] Schwarz, G.: A general expression for the energy of a dielectric body in a quasi-electrostatic electric field. Internal report of Dept. of Biomedical Electronic Eng., Univ. of Pa. Submitted for publication.

[18] The MKS system of units is used.

The particle will experience a force F in this field where

$$F = -\nabla(\Delta U) \tag{4}$$

$$= \frac{3}{2} V_1 \, \mathrm{Re}\left(\epsilon_2^* \frac{\epsilon_1^* - \epsilon_2^*}{\epsilon_1^* + 2\epsilon_2^*}\right) \nabla E_0^2 \tag{5}$$

In the case of loss-free dielectric materials, eq. (4) reduces to a well-known relation[19]

$$F = \frac{3}{2} V_1 \, \epsilon_2 \frac{\epsilon_1 - \epsilon_2}{\epsilon_1 + 2\epsilon_2} \nabla E_0^2 \tag{6}$$

In view of these results, it is seen that a particle experiences a force whose magnitude increases with (a) the amount of the inhomogeneity, (b) a function describing the difference in electrical properties of the two media, and (c) the volume of the particle. Equation (5) will provide an explanation for several effects observed in the cell and will provide a quantitative basis for discussions of biological effects.

The creation of concentration gradients by the action of purposely-applied inhomogeneous fields on suspensions of polarizable ($\epsilon_1^* - \epsilon_2^* \neq 0$) particles has been given the name of electrosedimentation[20,21]. The method has been proposed for

---

[19] Abraham, M. and Becker, R.: Ref. cit., p. 91.

[20] Debye, P. et al.: Experiments on polymer solution in inhomogeneous electrical fields. J. Chem. Phys., 22, 152, (1954).

[21] Debye, P. and Debye, P.P. Jr.: The Collected Papers of Peter J. W. Debye, p. 697. Interscience, New York, 1954.

the study of the physical properties of large (>100Å), compact (dense) macromolecules, for which the effect of electrosedimentation is most pronounced[22,23].

---

[22]Peterlin, A. and Ribaric, M.: Dynamical theory of electrosedimentation. J. Chem. Phys. 31, 759, (1959).

[23]Prock, A. and McConkey, G.: Inhomogeneous field method for the study of large polarizable particles. J. Chem. Phys., 32, 224, (1960).

B. Examples of forces due to inhomogeneous fields

The polystyrene and silicone particles primarily used in these studies had dielectric constants and conductivities which were considerably lower than those of their aqueous suspending media. So referring to eq. (4), it may be seen that the direction of the force would always be toward areas of weaker field strength.

Figure 16 shows an interesting (composite) photograph of a small portion of a cell in which pearl chains have formed between the wire electrodes. The pertinent observation in this photograph is that there are two parallel areas adjacent to and between the wires in which there are virtually no particles or chains. Referring to fig. 12, it may be seen that these areas are those in which the inhomogeneity is a maximum. Over the period of three hours during which the field was applied, the chains that formed in those areas near the wires responded to the inhomogeneity by leaving the area. Once outside the wires, the chains broke up due to a lack of sufficient field strength and the individual globules remained outside in a random distribution. The chains which formed in the mid-area between the wires remained. As they slowly drifted to and fro, they stuck to each other, side to side, whenever they randomly made contact. Of course, neither the pearl chains nor the effects of field inhomogeneity required three hours to appear. The extra time was provided for the very slow drifting of completed chains to become resolved into a final pattern. The

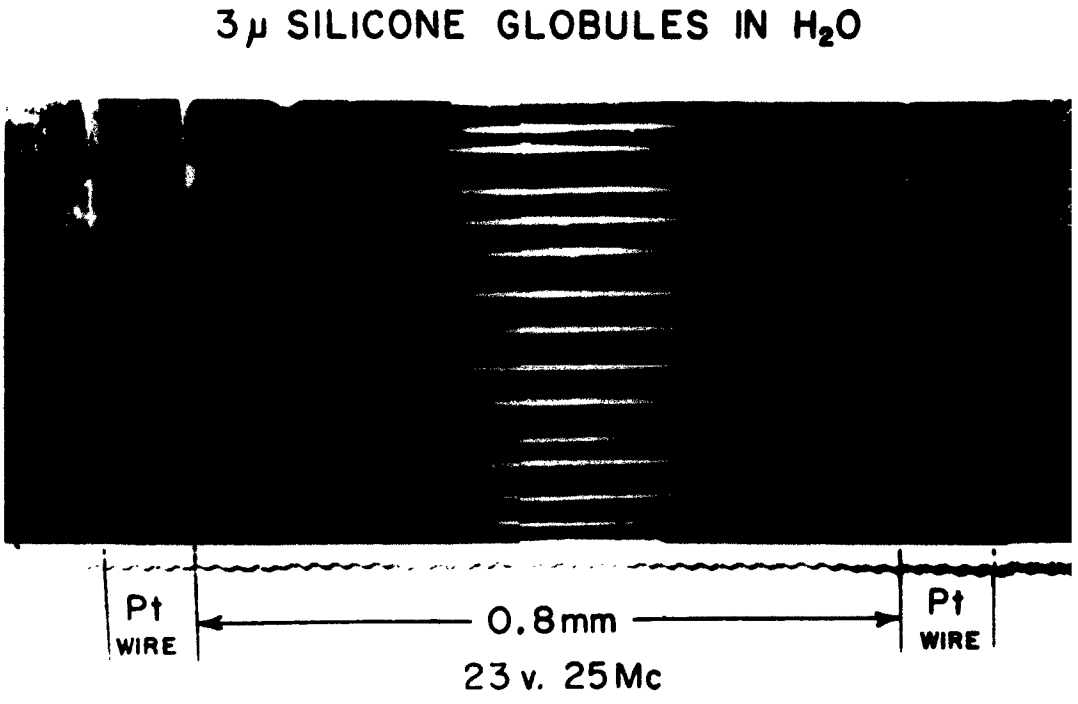

Figure 16. Composite photograph of pearl-chain formation in a silicone emulsion. The stated particle size of 3μ is very rough (see fig. 17). Picture shows areas near the wires which have been cleared of particles by the force due to the field inhomogeneity there. Note that particles outside the field are randomly distributed.

surprising regularity of the spacing between chains is probably just a consequence of a slow statistical process which was given enough time for virtual completion.

A close-up photograph of the ends of some of these very well-developed chains appears as fig. 17. It is surely the paucity of available particles that makes these ends taper down to a single strand. And the paucity was caused by the inhomogeneity of the field.

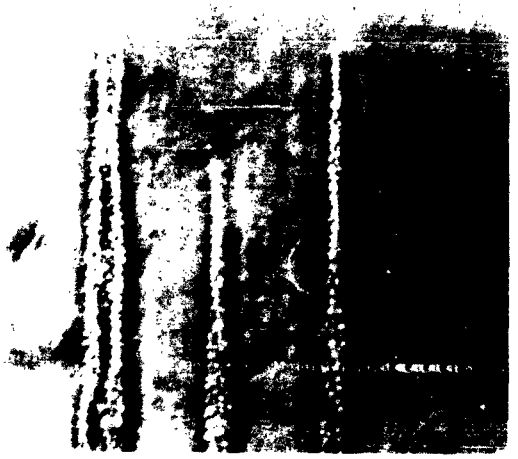

Figure 17. Detailed view of the ends of the pearl chains appearing in fig. 16.

Almost every time the effects of inhomogeneous-field forces appeared, they were unexpected. But never was the effect more surprising or dramatic than in the cell with tapered wire spacing. The idea was to have a single applied voltage result in a field strength which would vary with

distance along the wires. Although an evident grad E existed in a direction parallel to the wires, the particles did not visibly react to that comparatively weak force. Figure 18 illustrates the effect which occurred. The space between the wires at the left was necessarily very small, about 60μ or one wire diameter, so that the field was highly inhomogeneous there. Upon application of the field, all of the

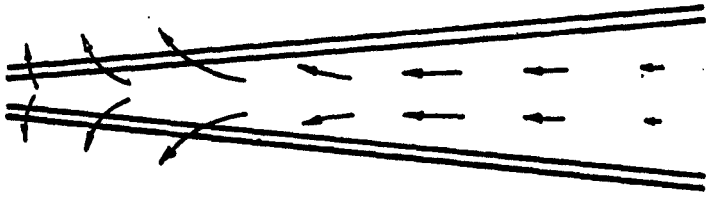

Figure 18. Particles leaving the space between tapered electrodes. Exodus at the left is due to the field inhomogeneity. Particles at right diffuse toward newly cleared area at left, then are forced out also.

particles in the narrow area left immediately (in about one second) in response to the force. The remaining particles then diffused into the evacuated area in a vain attempt to restore the concentration. The overall result was that the entire area between the wires was essentially clear within thirty seconds. The action clearly resembled that of a pump and , in fact, has been used for that purpose.

Another illustration of an unexpected effect was the concentration gradient found in the vicinity of air bubbles. Fig. 19 shows several air bubbles between the wires of a cell filled with a silicone emulsion. It can be seen that there are flare-like areas near the bubbles which have an augmented

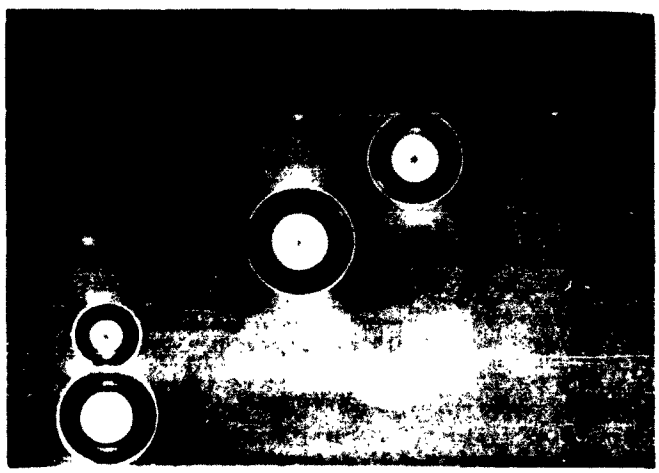

Figure 19. Air bubbles in a cell filled with a silicone emulsion. Lower wire is just visible. Note the concentration gradients around the bubbles. Also note the pearl-chain-like disposition of two of the bubbles. Bubbles do form chains.

concentration of particles (individual particles are too small to be seen in this photograph) and other diffuse areas with a deficiency of particles, as compared to the concentration of particles in the bulk. It is believed that this phenomenon is another manifestation of the forces in inhomogeneous fields and that the explanation is that given in fig. 20.

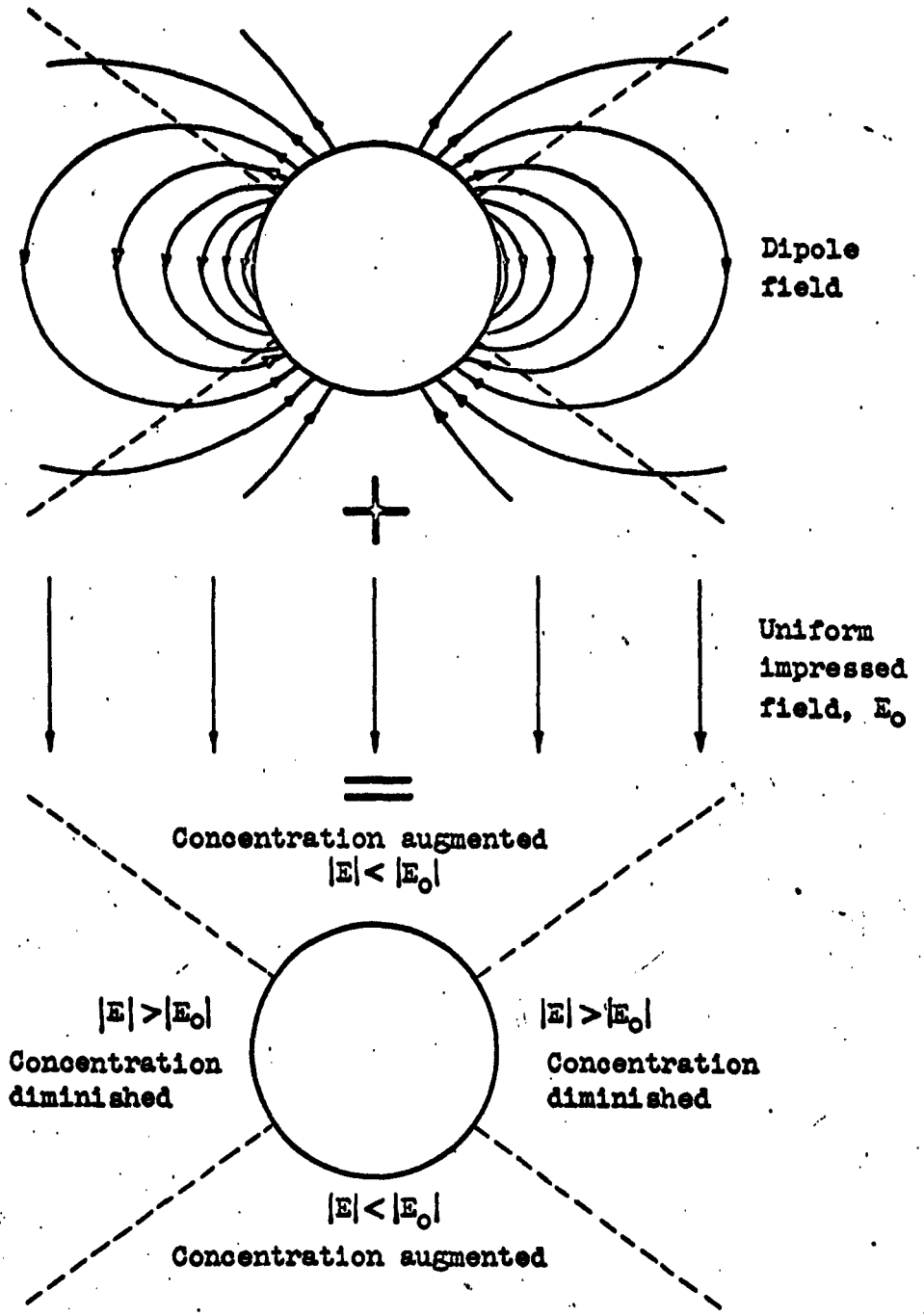

Figure 20. A study of the magnitude of the electric field in the vicinity of a dielectric sphere subjected to a uniform impressed field. The concentration of small particles in the medium surrounding the sphere is modified by changes in E.

Fig. 20 graphically shows that the perturbation of the field by an air bubble may be idealized as the field of a dipole[24,25]. This dipole field, when added to the pre-existing field, E_o, gives a resultant field, E, whose magnitude changes from values greater than E_o to values less than E_o at the dotted lines indicated. The particles in areas of augmented field strength tend to leave, and those in areas of diminished strength have unexpected company. The angles visible in the photograph do not exactly correspond to those in the drawing because of the tightly confined geometry of the large bubble.

C. Conclusion

Several examples of the effects of forces in inhomogeneous fields have been described. Each has been the consequence of a fairly high gradient. Since the field strengths have been of the order of 100v/cm, and distances over which a sharp drop in this value would provoke an effect have been of the order of 100μ, the order of magnitude of the gradients has been about 10^4v/cm/cm. Biological implications of these forces will be discussed in more detail in section VIII.

---

[24] Stratton, J.A.: Electromagnetic Theory. p. 206. McGraw-Hill, New York. 1941.

[25] The configuration of the dipole field around a sphere was taken from Maxwell, J.C.: A Treatise on Electricity and Magnetism, I, fig. V, art. 143. Clarendon Press, Oxford, 1892.

V. A.C. Microelectrophoresis

A. Introduction

Electrophoresis is the movement of colloidal particles through a fluid under the action of an applied electric field. Commonly performed as a statistical study of the mobility of large numbers of macromolecules, it may also be done on a single suspended particle if the motion can be observed microscopically. The latter technique, known as microelectrophoresis, uses an applied D.C. electric field to cause the observed particle to move a fixed distance in a measured time interval. The calculated velocity per unit field strength is called the mobility of that particle when so suspended[26]. D.C. microelectrophoresis has met with varying degrees of success, depending on the apparatus and on the operator. It is primarily used for studying the surface properties of particles in the micron range of sizes[27].

A knowledge of the technique of D.C. microelectrophoresis should have been sufficient to predict the occurrence of the phenomenon at sufficiently low frequencies, especially with the highly mobile 1.17μ polystyrene spheres. But the

---

[26] One of the first observations of D.C. microelectrophoresis was that by Cotton, A. and Mouton, H.: Étude directe du transport dans le courant des particules ultramicroscopiques. Compt. Rend. Acad. Sci., 138, 1584 and 1692, (1904).

[27] For a clear and instructive review of all facets of D.C. microelectrophoresis see James, A. M.: The Electrochemistry of the Bacterial Surface, p. 98 in vol. 8 of Progress in Biophysics and Biophysical Chemistry. Pergamon, N.Y., 1957.

prediction came after the fact. While studying the low-frequency behaviour of pearl-chain formation with polystyrene spheres, it was observed, at about 20 cps, that each particle appeared as a line segment whose length varied with the magnitude of the field strength and with the reciprocal of frequency. Once observed, the phenomenon was realized to be another non-thermal effect of alternating electric fields--hence its inclusion here.[28]

A.C. microelectrophoresis is not new[29]. But it has not become a useful research tool, because of two inherent difficulties: the lack of a suitable method for measuring the amplitude of the alternating motion and the difficulty in correcting for the complicated alternating electro-osmotic effects. The latter problem will be discussed in more detail in section D-2. The obvious "solution" to the former problem is a visual measurement of the apparent motion with an eyepiece reticle. But this measurement is difficult to the point of impossibility. It must be done at sufficiently high magnification (~100x) so that the possibility of aligning the particle's track with the fixed reticle is obviated by random or convective drifting of the particle's "rest" position. In other words, the apparent line of motion of the particle does not stand still. The present study started with an attempt to eliminate the problem of drifting.

---

[28] The phenomenon could be called A.C. electrophoresis, since the use of a microscope is mandatory in the A.C. case.

[29] Svedberg, T. and Andersson, H.: Zur Messmethodik der elektrischen Kataphorese. Kolloid Z., 24, 156, (1919).

B. Experimental methods

1. Separation of drift from mobility

Although a single particle in dark field illumination could be microscopically observed to oscillate and had the visual appearance of a line segment for frequencies over 5 cps, the length of the track could not easily be measured due to drifting. Clearly a photographic record would not only render the drifting less cumbersome but it would allow one to find the average of simultaneous measurements on many separate particles. Drifting, however, was not entirely overcome by photography, because it could not be guaranteed that the line segment on the photographic record was the exact superposition of several oscillations[30]. Each successive oscillation could add to the apparent length of the track if the drifting were in that direction. And in fact this situation subsequently was found to be the case.

The problem was overcome, following a suggestion of H. P. Schwan, by moving the stage of the microscope in a direction perpendicular to the oscillation while the picture was being taken. Figure 21 illustrates the problem and its solution. It can clearly be seen in (c) that the amplitude

---

[30] The following excerpt is translated from Svedberg, T. and Andersson, H.: Zur Messmethodik der elektrischen Kataphorese. Kolloid Z., 24, 156, (1919). "It was found impossible to use photographic registration of the motion since succeeding swings did not superimpose. Visual measurements were made using an eyepiece reticule."

of the oscillation and the drifting of the origin are clearly separated. Furthermore, it is apparent that two cycles of the applied field is sufficient to achieve this separation. Therefore, since the heat development in the liquid due to the applied field is not negligible, it will be helpful to limit application of the field to two cycles. How this is done follows the related discussion of the problem of providing proper illumination to the cell.

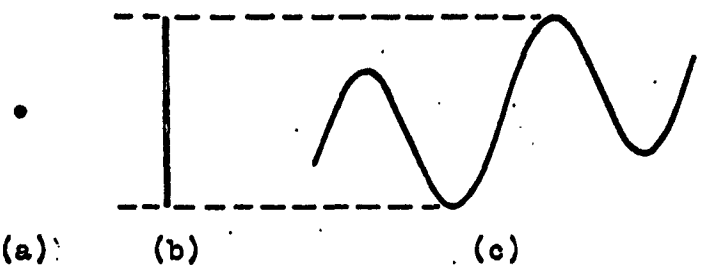

Figure 21. Diagram of the photographic record of a suspended charged particle. (a) No electric field is applied. The particle is stationary. (b) A sinusoidal field is applied. The vertical segment is the superposition of several "swings." (c) Same as (b) except that microscope stage is moved during the exposure.

2. Special illumination

Naturally, dark field illumination was a necessity, since only in that way would the track of the particle register on the film. In fact, normal dark field illumination as provided by the Heine condensor was not always sufficiently bright; the particle's image moved across the emulsion at

considerable speed leaving little exposure in its wake. An aggravating factor was the normally dull and thick track left by a particle larger than a 1.2μ polystyrene sphere, such as an erythrocyte or an erythrocyte ghost. The solution to both problems, i.e., faintness of the track and thickness which makes amplitude measurement difficult, was to design a different kind of dark field illumination.

The principle of dark field illumination is that an object should be seen only by the light which it scatters.

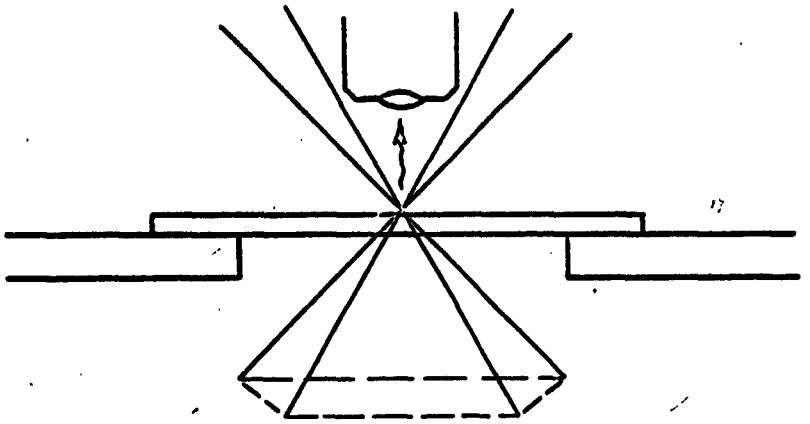

Figure 22. Normal dark-field illumination. Hollow cone of light converges on sample, then diverges to miss objective lens. Only light scattered by the sample enters objective.

Where there are no particles, there is no scattering, and hence nothing is seen. In other words, there is a dark field. The principle is illustrated in fig. 22. Illumination from beneath the stage is in the form of a circularly symmetric hollow cone, so that none of the rays directly enters the objective lens. An object caught in this crossfire scatters

some of the light and some of these scattered rays enter the objective lens betraying the presence of the scatterer. A large object generally appears duller than a small one, since light is scattered most efficiently by the borders. And as the image of these bright borders moves on the film, the track is wide and dull. What was needed was a way of illuminating a large particle so that it would appear to be small, that is, so that it would appear to be a bright point of light. Such a scheme was devised.

The normal Heine condensor was removed from its mount and a series of mirrors was put in its place, the first being plane and the second concave (converging). The self-contained lamp in the base of the microscope could still be used, and, in fact, its light output could be utilized more efficiently than in the standard scheme. Instead of circularly-symmetric, dark field illumination, the new system gave a very intense, unsymmetrical beam which converged to a maximum intensity near the stage surface. Figure 23 illustrates the light path.

The effect of this highly unsymmetrical illumination was to change the normal "bright" outline of an erythrocyte ghost, for example, to a pair of bright points, corresponding to the sides toward and away from the source. Because the stage movement during the exposure was perpendicular to the line connecting these two points of light, the track of each particle would change from a wide dull track to a pair of identical bright lines. Figures 24 and 25 show erythrocyte ghosts in normal and in modified dark field illumination.

Figure 23. Modified dark field illumination. The first mirror is plane, the second concave. A shutter riding in the condensor holder can interrupt the beam at its narrowest point.

Figure 24. Erythrocyte ghosts in normal dark field illumination as provided by the Heine condensor.

Figure 25. Erythrocyte ghosts in modified dark field illumination as provided by the arrangement shown in fig. 23. Each ghost appears as two (ghostly) points of light.

Since the intensity of this new dark field illumination was, and needed to be, so great, it was found expedient, in order to minimize heating of the illuminated object, to use a shutter in the beam whose open-time became the effective photographic exposure time. A picture was taken by opening the camera shutter on "time," removing the slide in front of the film and briefly opening the beam-interrupting shutter. Even though the film normally used in this work had an ASA 3000 exposure index (Polaroid Type 47), the effective f-aperture of the camera was so small that exposing the film to the unilluminated stage was permissable. The beam-interrupting shutter can be seen to be near the narrowest part of the beam in fig. 23.

3. Automatic sequencer

To move the stage during the exposure, to turn on a 10 cps field for two cycles, and to light the stage for about the same period required too much manual dexterity for the production of consistent results. These operations clearly demanded automation. But in this sequence of operations, the time intervals were long compared to those common in electronic devices and short compared to those common in mechanical devices. Nevertheless, a simple method, using relays, was devised which not only accomplished these goals satisfactorily but which had the bonus advantage of allowing an easier separation of superimposed, faint tracks on the film. The electromechanical device which was built to sequence the process is herein called the "sequencer."

Operation of the sequencer with a single "start" button performs several tasks as a function of time, as illustrated in figure 26.

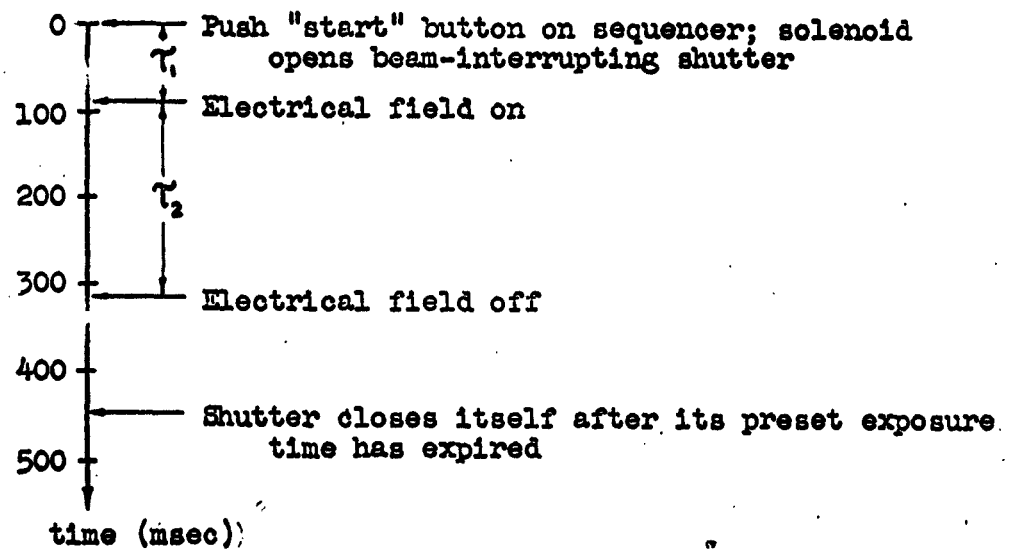

Figure 26. Time sequence of operations performed by the sequencer. τ_1 and τ_2 are the two time delays generated.

The operator must move the stage manually, and while so doing, a push on the sequencer's button completes the operation. Automatic movement of the stage could have been provided but was not seen to add any virtue except glamour to the method. It was found that 2 mm/sec of stage speed

was sufficient and that this speed corresponded to 40°/sec of angular movement of the appropriate stage control knob. By adding a 36 cm extension lever onto this knob, the motion was imparted manually with sufficient accuracy and smoothness and with little difficulty. It should be noted that exact control of stage speed adds no additional accuracy to the method.

The sequencer is described in detail in fig. 27 . The component values are those which give the delays τ_1 and τ_2 in fig. 26 .

Referring to fig. 26, it is seen that the field is on for only about half the time required for the complete picture. Both before the field goes on and after it goes off, the particle's image is moving but is not oscillating. Thus the sinusoidal track has a straight line as its start and one as its end. A typical result appears in fig. 28 . Note that the straight "tails" on the sinusoids allow one more easily to separate the tracks left by the individual particles.

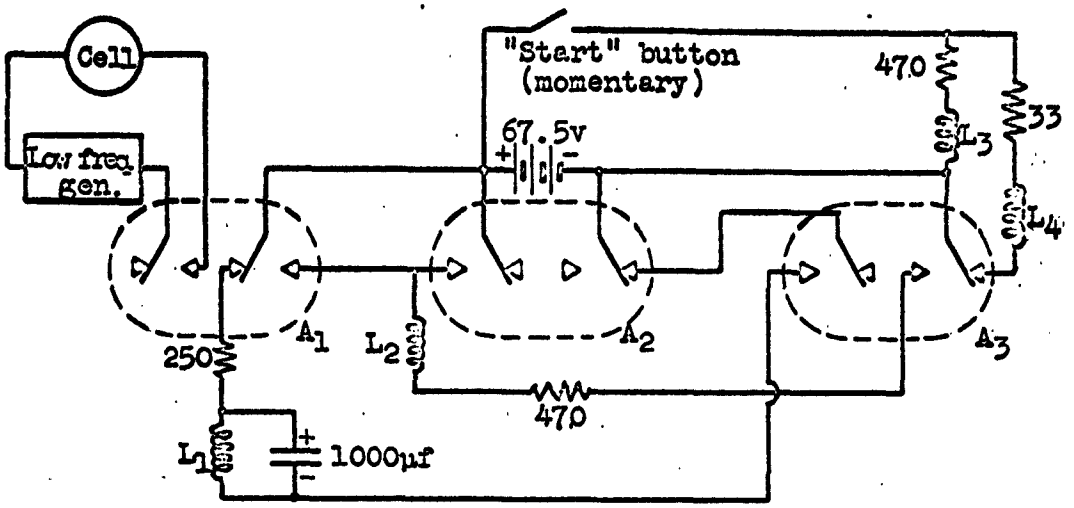

Figure 27 . Schematic of Sequencer (double time-delay generator) The 300Ω solenoids L_1, L_2, and L_3 operate the relays A_1, A_2, and A_3 with about 12v applied. L_4 is a shutter-operating solenoid. Operation of the circuit (refer to fig. 26): Each relay will be spoken of as being "off" if the contacts are made as illustrated and "on" otherwise. Closure of the "start" button allows relay A_3 to go on, but not before the shutter solenoid L_4 has been energized ($t \cong 0$). With A_3 on, the capacitor begins to charge up, finally allowing A_1 to go on ($t = \tau_1$). A_2 then goes on ($t \cong \tau_1$) and the capacitor begins to discharge through L_1. After $t = \tau_1 + \tau_2$, the capacitor has lost enough of its charge to allow A_1 to go off. However it does not charge up a second time because A_2 is on. The cycle is complete, repeating only if the button is released (A_2 and A_3 go off) and re-pushed.

C. Results

The photographs showed that the shiny wire electrodes were reflecting the light in such a manner that the dark field was changed to a gray field. So to improve the contrast, it was found necessary to use more widely spaced electrodes than for other kinds of observations. With this last modification, which also improved the homogeneity of the field, the photographs had the appearance shown in fig. 28 and 29.

Figure 28. Alternating electrophoresis patterns of 1.17μ polystyrene spheres. 10 cps sine wave applied.

Figure 29. Alternating electrophoresis patterns of 1.17μ polystyrene spheres. 10 cps square wave applied. Particles appear to reverse their course instantaneously, showing that inertial effects are not observable.

Comparison of these photographs with others taken of a calibrated slide is sufficient to establish a very accurate scale of size. However, the determination of mobility for these particles (particle velocity/field strength) requires the results of the following analysis of alternating electrophoresis.

D. Analysis of alternating electrophoresis

1. Electrical vs. inertial forces

A suspended particle with an effective net charge q in a DC electric field of strength E experiences a force qE. The particle's velocity increases until the viscous drag equals the electrical force. The terminal velocity $\dot{x}$ is given by

$$k\dot{x} = qE \tag{1}$$

where k is the coefficient of viscous drag. If the particle is spherical, $\dot{x}$ is sufficiently low, and there are no boundary effects, then Stokes law may be applied to give

$$k = 6\pi\eta a \tag{2}$$

where η = coefficient of viscosity and "a" = radius of sphere. It is now useful to define a parameter μ as mobility, with the units of particle velocity/field strength. (Particle velocity is used to emphasize that μ is defined for a particular particle.) Then

$$\dot{x} = \mu E \tag{3}$$

and

$$\mu = \frac{q}{k} \tag{4}$$

In an alternating electric field, a suspended, charged particle is subject to an alternating force. Motion is now resisted by viscous effects in the suspending medium and by inertia of the particle itself[31]. So, for a sinusoidal field,

---

[31] There is an inertial reaction from the liquid also. However it is of the same order of magnitude as the inertial reaction of the particle, which itself will be shown to be negligible.

the actual displacement, x, of the particle is given by the differential equation[32,33]

$$m\ddot{x} + k\dot{x} = qE \sin \omega t \tag{5}$$

where m = mass of the particle, k = coefficient of viscous drag, q = effective net charge on the particle, and E = amplitude of the applied electric field. Then

$$x = -\frac{qE}{\omega m\sqrt{\omega^2 + (k/m)^2}} \sin(\omega t + \theta) \tag{6}$$

where $\tan \theta = \frac{k/m}{\omega}$ (7)

Assuming a 1.17μ diameter polystyrene sphere[34] suspended in water, it is easily computed that

$$\tan \theta = \frac{3 \cdot 10^6}{f} \tag{8}$$

Thus the phase angle is essentially 90° for frequencies below 300 kc. Furthermore, at the low frequencies of interest, $\omega^2 \ll (k/m)^2$, so that eq. (6) reduces to

$$x = -\frac{qE}{\omega k} \cos \omega t \tag{9}$$

$$= -\frac{\mu E}{\omega} \cos \omega t \tag{10}$$

$$= -A \cos \omega t \quad , \quad \text{where } A = \frac{\mu E}{\omega} \tag{11}$$

Then $\mu = \frac{\omega A}{E}$ (12)

---

[32]Bluh, O.: Untersuchung von Kolloidpartikeln in Wechselfeldern verschiedener Frequenzen. Ann. Physik, 78, 177, (1925); ibid., 79, 143, (1926) (short additional note); ibid., 80, 181, (1926) (errata).

[33]Lamb, H.: Hydrodynamics. Article 357. 6th ed., Cambridge, 1932.

[34]It is unfortunate that mobility and micron are both designated by the symbol μ, but this is the custom. The context should obviate the ambiguity.

The amplitude A is measured from the photographic record, as illustrated in fig. 30 . Since ω and E are known, the use of eq. (12) gives a value for mobility in a fairly direct fashion.

In effect, the preceding development shows that, for all frequencies of practical interest, the terminal velocity of the particle is reached in a negligibly small time. Thus it is possible to say that

$$\dot{x} = \mu E(t) \qquad (13)$$

Therefore

$$x = \mu \int E(t)\, dt \quad , \qquad (14)$$

and if $E(t) = E \sin \omega t$, we have directly that

$$x = -\frac{\mu E}{\omega} \cos \omega t \qquad (15)$$

which is the same as eq. (10).

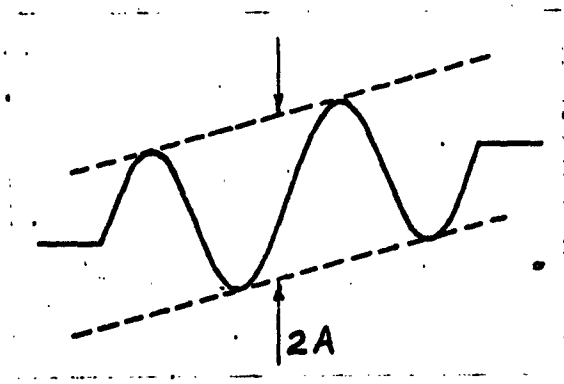

Figure 30. Measurement of amplitude from photographic record

From eq. (14) it can be seen that if E(t) is a square wave, then x(t) will be a triangular wave. The conversion of the amplitude of the triangular wave to a value of mobility proceeds in the same manner as the sine wave case, with the formula for μ being derived in the same simple manner.

2. Alternating electro-osmosis

Electro-osmosis, like electrophoresis, is one of a group of phenomena which have a common origin in the asymmetrical distribution of electric charges at an interface, "the electrical double layer." If an electrical field is applied to a system consisting of a solid and a liquid phase, there will be movement of one phase relative to the other. The velocity will depend upon the boundary potential across the plane of shear, the so-called zeta-potential.

The liquid environment of the particles has a certain zeta-potential with respect to the glass walls of the cell. This potential would be the same as that with respect to the particles only if the surface properties of the particles were identical to that of the glass. Therefore, an applied electric field will cause the liquid to move with respect to the glass walls (electro-osmosis) at a velocity which is different from the velocity of polystyrene particles with respect to the liquid (electrophoresis).

In a flat glass cell, a DC field will cause the two boundary layers of liquid to move in the same direction at the same velocity. The bulk of the liquid will eventually achieve the same uniform velocity due to its viscosity. However, if the cell is closed, the liquid cannot have a net flow across any cross-section of the cell. Therefore a flow profile develops whose integral is zero over every cross-section. Particles observed to migrate in the cell are actually achieving their terminal velocities, according to eq. (1), with respect to the liquid which is itself moving.

So the vector sum of particle and liquid velocities is the actual quantity measured. If the electro-osmotic flow profile is known, a suitable calculation isolates the electrophoretic component.

In a flat cell, DC electro-osmosis is relatively easy to analyze [35 - 38]. Pressure, built up at one end of the closed cell by the attraction of that electrode for the entire liquid, results in laminar flow in the reverse direction, with the usual parabolic velocity profile. Thus, the total flow profile of the liquid is the sum of a constant electro-osmotic flow in one direction and a parabolic flow in the opposite direction. The two flows combine to give a parabolic velocity profile, $v_w(x)$, for which

$$\int_0^X v_w(x)\, dx = 0 \qquad (16)$$

where $v_w(x)$ = velocity of liquid (water) at a depth x

and X = total depth of cell.

Knowing that $v_w(x)$ is parabolic, it is easily shown that

$$v_w(0.21\ X) = v_w(0.79\ X) = 0 \qquad (17)$$

which means that there are two planes within the cell where

---

[35] Smoluchowski, M.: in Graetz Handbuch der Electrizität und des Magnetismus, Vol. 2, p. 366. Leipzig, Barth, 1921.

[36] Abramson, H. A., Moyer, L. S., and Gorin, M.H.: The Electrophoresis of Proteins. Reinhold, 1942.

[37] Colloid Science, Vol, 1. H. R. Kruyt, ed. Elsevier, N.Y., 1952.

[38] James, I.A.M., and Loveday, D.E.E.: Microelectrophoresis. Chemical Products, 21, 357, (1958) (part I); ibid. 21, 408, (1958) (part II).

the liquid is stationary. Electrophoretic observations made in these planes require no electro-osmotic correction. However, the most accurate measurements involve measurements of apparent electrophoretic velocity

$$v_{apparent}(x) = v_{true}(constant) + v_w(x) \qquad (18)$$

as a function of depth, x. Subsequent use of eq. (16) gives an accurate graphical determination of v_{true}, which is the true, constant electrophoretic velocity.

These procedures were carried out recently for a detailed study of the DC electrophoretic mobility of 1.7μ polystyrene spheres[39]. These data are useful for comparison with those taken here for 1.17μ polystyrene spheres, since the mobility should be independent of size[40].

Analysis of alternating electro-osmosis is severely complicated by the inertia of the liquid. An analysis has been made[41], but since its discovery by this author was very recent, there has not been sufficient time to include it here.

Experimental measurements of the apparent (uncorrected) AC-electrophoretic mobility were made in the cell (previously described) as a function of depth. If the electro-osmotic correction were the same as in the DC case, the data should be parabolic, but fig. 31 shows that something more is involved.

---

[39] Siglaff, C.L. and Mazur, J.: Electrophoretic mobility and electrochemistry of latex systems. J. Colloid Science, 15, 437, (1960).

[40] Abramson, H.A.: Electrophoresis. The Academy, New York, 1939

[41] White, P.: The theory of electro-osmotic circulation in varying fields. Phil. Mag., 26, 49, (1938).

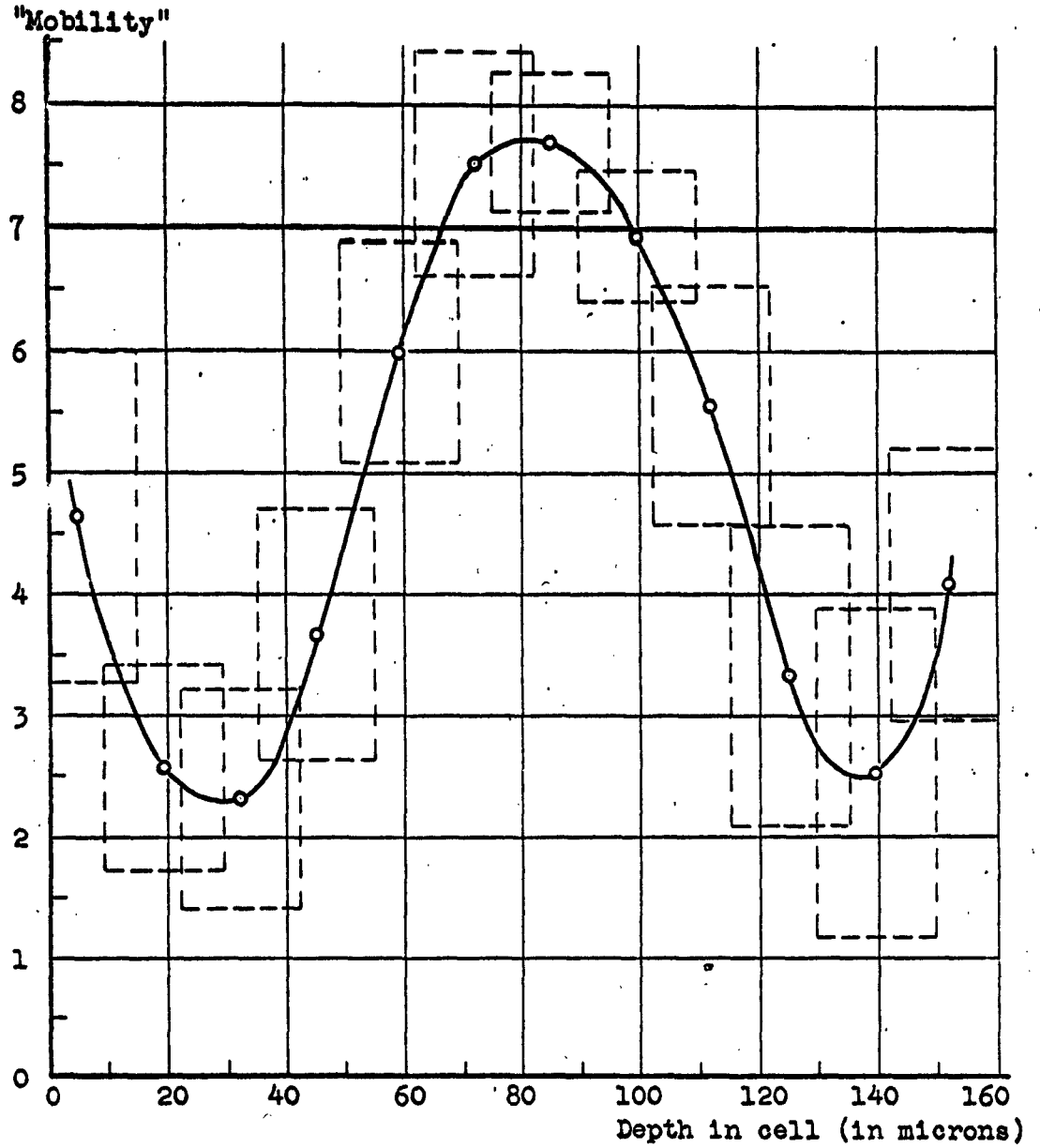

Figure 31. Electrophoretic behaviour of 1.17μ polystyrene spheres in water. Ordinate is amplitude of alternating migration (in mm) as measured from photographs (see fig. 30). Width of dotted rectangles is photomicrographic depth of field; height is one standard deviation above and below the mean A-value for each depth (see fig.32). Total curve is result of measurements on 262 particles. Applied field: 179v/cm, 10cps.

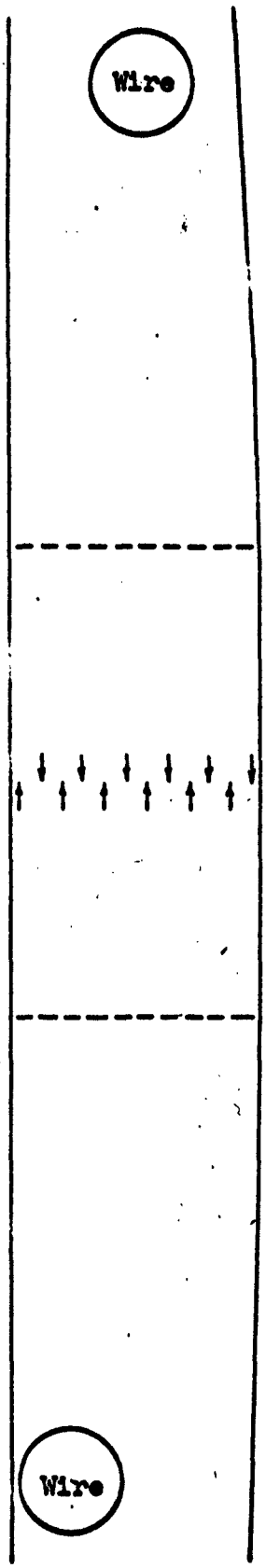

Figure 32. Cross-section of cell in which data for fig. 31 were taken. Arrows show depths at which photographs were taken, one at each depth. Dotted lines define area of cell seen on the photographs. Wire separation = 795μ.

Short of a complete theoretical analysis of electro-osmosis, several preliminary conclusions may be drawn from fig. 31:

(1) The most striking quality of the curve is its symmetry. In view of the fact that 1.17μ polystyrene spheres settle out at a rate which is not negligible as compared to the rate of taking the 12 pictures required, it is reasonable to blame part of the asymmetry on settling. The pictures were taken at increasing depths at approximately 30-second intervals.

(2) The maximum apparent mobility does occur at the exact center, just as in the DC case. Also, the general shape suggests a parabola with perturbations at the walls. Since a DC measurement would have given a parabola, and since the electro-osnotic effect has its origin at the walls, one is left with a feeling that the curve will succumb to a proper analysis.

(3) The average of the maximum and minimum values of mobility calculated from this curve is 2.46 $\frac{\mu/\text{sec}}{\text{v/cm}}$. This value is compared to published data in fig. 33, although the concentration of soap is not known in the present measurement[42]. However it is surely less that 10^{-3} mole/liter, since the polystyrene suspension is diluted by about 100x from its original prepared form before it is used.

---

[42] Siglaff, C.L. and Mazur, J.: Ref. cit.

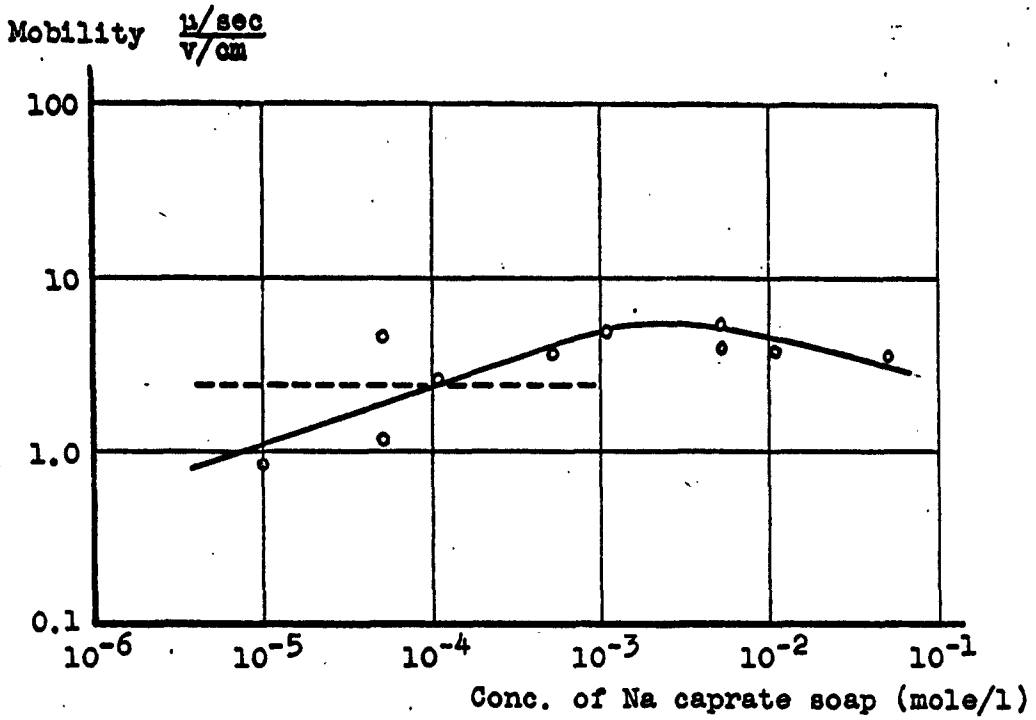

Figure 33. Comparison of published DC electrophoretic mobility with calculated approximate value of AC electroporetic mobility. Circles and fitted solid line are for the DC measurements on 1.7μ polystyrene spheres. Dotted line is the average value of AC electrophoretic mobility calculated from the data in fig. 31 for 1.17μ polystyrene spheres. The likely range of soap concentration in the AC case is indicated by the length of the dotted line. There should be no dependence of mobility on size per se.

E. Optomization of waveform, amplitude, and frequency

Considerable heat is developed in physiological saline or liquids of equivalent conductivity when the necessarily high electric field is applied. If the technique is to be useful for biological work, this heat must be minimized. The problem is complicated by the interaction of the parameters which determine the heat development: waveform, amplitude, and frequency. The present discussion attempts to elucidate these interactions and to specify the method of optomization.

It will be assumed that the applied field, E(t), satisfies the following mild conditions (where T is the fundamental period):

$$E(m\,\tfrac{T}{2}) = 0\,, \quad m = 0,\ 1,\ 2,\ \ldots$$
$$\neq 0\,, \quad \text{otherwise,} \tag{19}$$

and
$$\int_0^T E(t)\,dt = 0 \tag{20}$$

Then from eq. (14)

$$\text{Amplitude of particle's motion} \propto \int_0^{\frac{T}{2}} E(t)\,dt \tag{21}$$

$$\text{Heat developed per cycle} \propto \int_0^T E^2(t)\,dt \tag{22}$$

Because the field must be applied for only (about) two cycles and no heat can leave the fluid during that time, the total heat developed is the important quantity in determining the temperature rise of the sample. Thus it is necessary to maximize the ratio of amplitude of motion to heat developed per cycle. This quantity will be called A/H.

To maximize A/H as a function of waveform, several different waveforms are chosen which would be experimentally

convenient. In all cases, the amplitude of the field strength is held constant at unity.

Sine wave: $E(t) = \sin \omega t$

Then $A/H = \int_0^T \sin \omega t \, dt \Big/ \int_0^T \sin^2 \omega t \, dt = 0.64$.

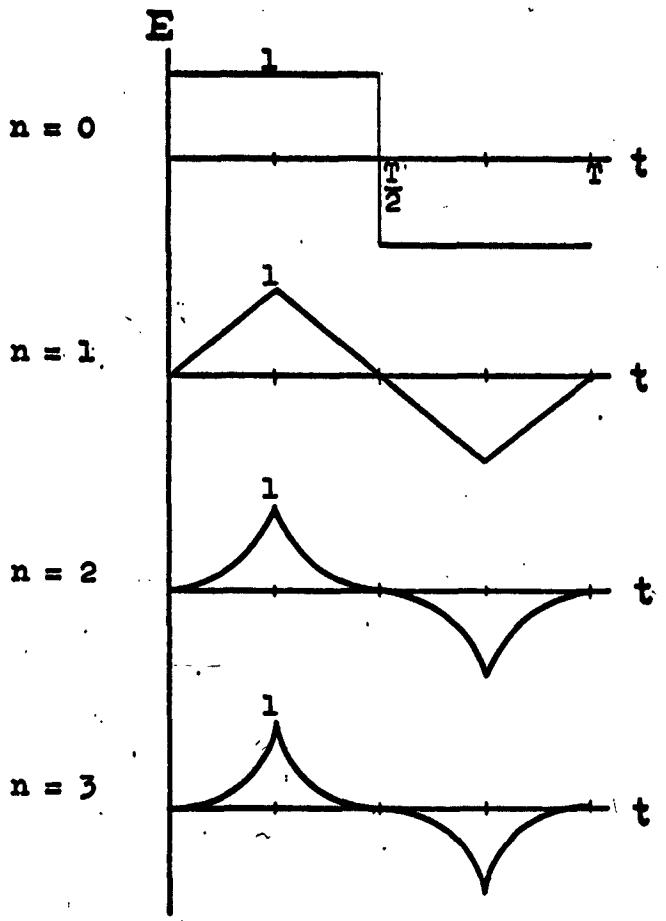

Figure 34. Waveforms investigated for their resultant ratio of amplitude to heat (see text).

Other waveforms: Consider waveforms of the form $E(t) = (\frac{4}{T})^n t^n$, $n = 0, 1, 2, \ldots, 0 \leq t \leq \frac{T}{4}$, where the waveform is extended as illustrated in fig. 34 .

For any waveform of this type, we have

$$A/H = 2\int_0^{\frac{T}{4}} \left(\frac{4}{T}\right)^n t^n \, dt \Big/ 4\int_0^{\frac{T}{4}} \left(\frac{4}{T}\right)^{2n} t^{2n} \, dt$$

$$= \frac{2n + 1}{2(n + 1)}$$

Note that $\lim_{n \to \infty} A/H = 1$. Figure 35 presents these results

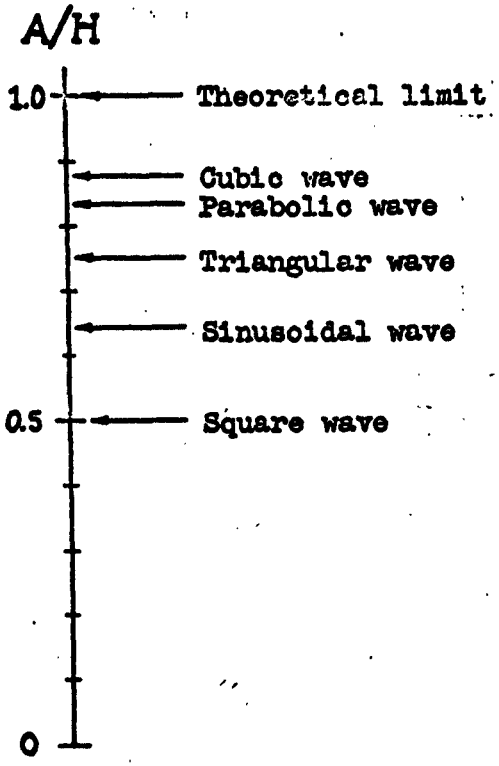

Figure 35. Ratio of amplitude of motion to heat developed in the suspending fluid per cycle, as a function of waveform.

in an instructive graphical form.

From a viewpoint of convenience, the triangular wave is probably the best. It must be recalled that the path of the particle will be "parabolic" in a "triangular" field, i.e., it will look like the n = 2 curve in fig. 34.

Referring to eq. (11), that $A = \mu E/\omega$, the following question may now be raised: If the amplitude of the motion needs to be doubled, should the frequency be halved or the amplitude of the electric field be doubled? It is easily seen from the relation for the heat developed per cycle, eq. (22), that halving the frequency doubles the heat, while doubling the amplitude gives four times the heat. Thus the frequency should be halved. But the same consideration may be applied repeatedly, resulting in the following set of optomization rules:

1. The frequency should be made as low as possible. The lower limit is determined by the requirement that the particle migrate "rapidly" about a "slowly" drifting origin.

2. The electric field should be raised to give the desired amplitude.

3. The waveform should be triangular or sinusoidal, with triangular giving 17% less heat per cycle than sinusoidal.

F. Conclusion

The phenomenon of AC electrophoresis, found by chance, has been pursued to the point where quantitative measurements of mobility are possible. Measurements agree moderately well with published data. To fully realize the potential accuracy of the AC electrophoretic measurement, compensation for AC electro-osmosis must be introduced. This refinement should be possible with available theory and is the next step in the development of this method into a useful quantitative technique.

Although somewhat premature, a tentative comparison of AC and DC microelectrophoretic techniques is now possible. It is true that the AC method is drift-free, but improvements in the DC method, such as an all-enclosing, temperature-regulated, water bath, have obviated drifting to a large extent. However, the AC method, as proposed here, does have two features of potential worth: First, measurements are made on many particles simultaneously, which is an unqualified virtue. Second, the higher particle velocities and accelerations in the AC technique may elucidate surface properties which cannot be resolved by the relatively slow drift in a DC field. For example, Blüh[43] suggests that the loosely bound surface layer of water on a particle may partially be ripped off by a rapid, alternating migration, leading to a change of mobility with frequency. So one properly may conclude that AC electrophoresis is fertile ground for more work.

---

[43] Blüh, O.: Ref. cit.

Although the amplitude of alternating migration falls off as f^{-1} (see eq. 11), its presence at high frequencies should be detectable, at least in principle, by dielectric measurements[44]. If the volume concentration of 1.17μ (diam.) particles is ~30%, a dielectric dispersion will occur whose characteristic frequency is ~3 Mc and whose magnitude is ~1 dielectric unit. This increase of ϵ with frequency may be called a "negative dispersion," since it is the only known case of ϵ increasing with frequency.

There is no reason to believe that AC electrophoresis at radio frequencies should have any biological significance.

---

[44]Schwan, H.P., Schwarz, G., Maczuk, J., and Pauly, H.: On the low-frequency dielectric dispersion of colloidal particles in electrolyte solution. J. Phys. Chem., 66, 2626, (1962).

VI. ORIENTATION

A. Introduction and theory

If a sufficiently strong AC field is impressed on a single, non-spherical, micron-sized particle polarizable in its suspending fluid, the particle may show a preferred orientation in the field. When the field is removed, the orientation will become random again. Thus the phenomenon of orientation may be described as a competition between electrical orienting forces and thermal randomizing forces.

If the frequency of the applied field is low (order of 1 kc), non-spherical, colloidal particles and poly-electrolytes may give evidence of orientation at relatively low field strengths. This phenomenon is the result of the movement of nearby counter ions in response to the individual alternations of the field polarity [45 - 48]. The counter ions are moved tangentially with the applied field, and a polarization of the ion atmosphere and an induced electric dipole moment of the particle result. Orientation of the particle occurs to a degree permitted by the frequency, since higher frequencies give less time for counter ion movement. In the Mc-range of fre-

---

[45] Schwarz, G.: Zur Theorie der Leitfähigkeitsanisotropie von Polyelektrolyten in Lösung. Z. Physik, 145, 563, (1956).

[46] Eigen, M., and Schwarz, G.: Orientation field effect of polyelectrolytes in solution. J. Coll. Sci., 12, 181, (1957).

[47] O'Konski, C.T. and Haltner, A.J.: Electric properties of macromolecules I. A study of electric polarization in polyelectrolyte solutions by means of electric birefringence. J. Am. Chem. Soc., 79, 5634, (1957).

[48] Schwarz, G.: Uber die Dispersion des Orientierungsfeldeffektes von Polyelektrolyten in hochfrequenten elektrischen Feldern. Z. Physik. Chem. (Frankfurt) 19, 286, (1959).

quencies of primary interest in the present study, this phenomenon can be neglected.

A striking demonstration of orientation at high frequencies was recently made by Teixeira-Pinto[49], who subjected the protozoa Euglena (a flagellate) to an AC field (~20 Mc). The Euglena, free to "swim," were observed to move either parallel or perpendicular to the electric field, depending on the frequency of the field. No theoretical explanation was given for the movement in preferred directions or for its frequency dependence. However, the effect can be ascribed entirely to an orientation phenomenon, as the Euglena, by waving their flagella, would move in the direction in which the field oriented them.

The present state of orientation theory is one of incompleteness. That a torque may exist on an ellipsoid in a field is well-known. Stratton[50], for example, treats the electrostatic case of perfect dielectric media and shows that an ellipsoid whose major axis is oriented along the applied field is in stable equilibrium, and that the equilibrium positions of the minor axes are unstable. However he does not include particles with significant Brownian motion. Another more general theory, treating lossy dielectric ellipsoids in an AC field has been reported by Ogawa[51]. This theory also

---

[49] Teixeira-Pinto, A.A., et. al.: Ref. cit.

[50] Stratton, J.A.: Ref. cit., p. 215.

[51] Ogawa, T.: Measurement of the electrical conductivity and dielectric constant without contacting electrodes. J. Appl. Phys., 32, 583, (1961).

treats large particles only, but it does show that orientations other than that parallel to the electric field may be stable. Saito and Schwarz[52] have made considerable progress in analyzing the most general case of the orientation of lossy, micron-sized particles. One tentative result, calculated in response to the experimental observation that orientation and pearl-chain formation seem to be related (fig. 36), agrees with these observations. The theory implies that the ratio of the threshold field strengths for these two effects should be primarily a function of the eccentricity of the particle. If this relation is true, then the much more complete analysis of the threshold for pearl-chain formation (section VII) may contribute to an analysis of the threshold for orientation.

At this time, there is no completely adequate theoretical treatment for orientation of general, thermally-active particles in an AC field. All that can be said is that alignment in a particular orientation with respect to the field direction will tend to occur if the electrical energy loss due to alignment, $-\Delta U$, is roughly comparable to the thermal energy, kT. The probability density, p, for that orientation corresponding to a change of energy ΔU, will be

$$p \sim \exp\left(-\frac{\Delta U}{kT}\right) \qquad (1)$$

Thus a suspension of many such particles will exhibit a Boltzmann distribution about some preferred orientation.

---

[52] Saito, M. and Schwarz, G.: The threshold for the orientation of a particle. Internal report of the Dept. of Biomed. Electronic Eng., Univ. of Pa. In preparation for publication.

B. Experimental results

Good quantitative data on non-spherical particles requires that the particles be as uniformly alike as possible. Inorganic particles fulfilling this requirement were never found, so that the bacterium Escherichia coli became the candidate of choice[53]. This bacterium is approximately a prolate spheroid, with major and minor axes of about 1.2μ and 0.6μ, respectively. It safely may be suspended in physiological saline or in distilled water, but in the latter, salt will leak out through the membrane and the rigid cell wall. The E. coli used for these measurements were in distilled water, whose final (after leakage) resistivities were measured[54] to be between 3×10^4 and 3×10^5 ohm-cm, depending on the number of resuspensions (washings) in distilled water. In view of the electrode polarization measurement in fig. 14, these "high" resistivities plus the use of a minimum frequency of 500 kc for quantitative measurements preclude any polarization difficulty.

At any given value of field strength, the orientation about the preferred direction is given by an exponential distribution function, as in eq. (1). Then, to say that at one field strength orientation is not evident and at a slightly higher field strength it is, requires a personal judgement. The difficulties inherent in such subjective measurements

---

[53] Kindly supplied by E.L. Carstensen, U.S. Army Biological Laboratories, Fort Detrick, Frederick, Md.

[54] Measurements were made on a General Radio Impedance Bridge, type 650-A.

are manifold. However, it is obvious that random orientation implies the ability to rotate and that firm orientation implies the converse. So one is able to equate the apparent onset of non-rotation with the threshold for orientation. The small size of E. coli is a further aid, since, as will be shown in section VII, these "particles" display an ability to rapidly (~1 sec) reach a new equilibrium after the field strength is changed. Therefore, there is relatively little difficulty to determine a consistent value for the threshold (± 5 to 10%).

1. Direction of orientation

E. coli would always align with their major axes parallel to the electric field. Frequencies were used between 1 kc and 100 Mc with no effect on this orientation. The threshold field strength was definitely a function of frequency, however.

2. Threshold field strength

Figure 36 shows the threshold field strength for the orientation and for the pearl-chain formation in E. coli. The constancy of the ordinate separating these curves is equivalent to the statement

$$\frac{E_{th}\ (\text{for p.c.f.})}{E_{th}\ (\text{for orientation})} = K_r \qquad (2)$$

where $K_r = 2.60 \pm 0.31$, or a variation of ±12%, well within the experimental error. That K_r is so stable, even with the pronounced frequency dependence shown in the thresholds, is strong evidence for a theoretical link between these two phenomena. An explanation for this frequency dependence

may be possible by combining the orientation theory of Saito and Schwarz with the available dielectric measurements of E. coli[55]. This analysis has not yet been carried out.

---

[55] Fricke, H., Schwan, H.P., Li, K., and Bryson, V.: A dielectric study of the low-conductance surface membrane in E. coli. Nature, 177, 134, (1956).

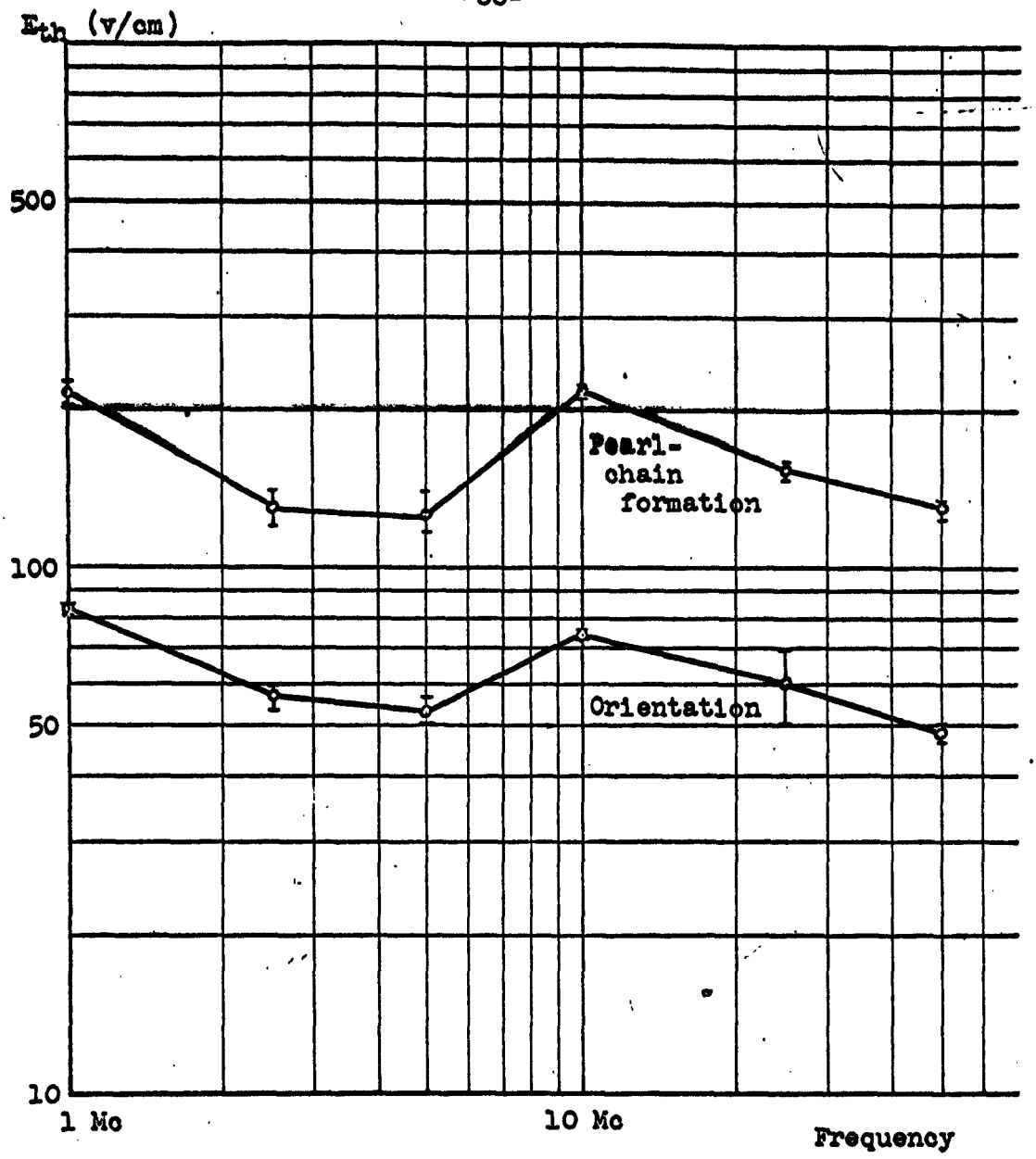

Figure 36. Comparison of threshold field strengths, E_{th}, for orientation and for pearl-chain formation of E. Coli in water. Similarity of curves shows close connection between underlying mechanisms. Each point is the average of three measurements whose spread is indicated.

C. Conclusion

Orientation of the major axis of E. coli has been obtained only in the direction parallel to the electric field. However, both the experiments of Teixeira-Pinto and the theory of Ogawa give reason to believe that other orientations are possible. The emerging theory of Saito and Schwarz may help to clarify the thresholds and directions for orientation and may be helpful in designing suitable experiments.

A close relationship has been demonstrated for the thresholds for orientation and for pearl-chain formation. In particular, orientation has been shown to occur for a field strength that is 2.6 times lower (or for an incident power density that is ~7 times lower) that that required for pearl-chain formation. For this reason alone orientation is of more biological interest than pearl-chain formation. But there is another reason: The histological prerequisites for orientation are much easier to satisfy than those for pearl-chain formation. It is much easier to imagine a single particle or even a part of a particle being oriented than it is to imagine a collection of freely moveable particles forming into chains. This idea will be expanded upon in section VIII, following the section on pearl-chain formation.

VII. PEARL-CHAIN FORMATION

A. Introduction

When a suspension of micron-sized particles is exposed to a sufficiently strong AC field, the particles arrange themselves into long chains, resembling strings of pearls. The chains break up when the field is removed, Brownian motion restoring the random distribution of particles. The phenomenon is known as pearl-chain formation and may be thought of as a competition between an "ordering force" of electrical origin and a "randomizing force" of thermal origin.

Pearl-chain formation was first reported by Muth in 1927[56]. Working with emulsions of fat particles, he observed the phenomenon in the presence of high-frequency fields. A theoretical analysis was undertaken in 1936 by Krasny-Ergen [57-59]. Although his treatment was limited to the case of perfectly conducting particles, it will be shown here that his methods had sufficient potency to be extendable to more complicated cases. Pearl-chain formation of red blood cells

---

[56] Muth, E.: Uber die Erscheinung der Perlschnurkettenbildung von Emulsionspartikelchen unter Einwirkung eines Wechselfeldes. Kolloid Z., 41, 97, (1927).

[57] Krasny-Ergen, W.: Nicht-thermische Wirkungen elektrischer Schwingungen auf Kolloid. Hochfreq. u. Electroak., 48, 126, (1936).

[58] Krasny-Ergen, W.: Zwei leitende isolierte Kugeln in homogenen elektrischen Feld. Ann. der Physik, Ser. 5, 27, 459, (1936).

[59] Krasny-Ergen, W.: Der Feldverlauf im Bereich sehr kurzer Wellen; spontane Drehfelder. Hochfreq. u. Electroak., 49, 195, (1937).

was reported in 1937 and 1939 by Liebesny[60,61]. Following a mention of the phenomenon by Rajewsky[62] in 1938, little was heard until 1958, when increasing use of microwave energy apparently stimulated a resurgence of interest. In that year, Herrick[63] made numerous qualitative observations; and Schwan[64], after reviewing Krasny-Ergen's progress in analyzing the effect, restated and extended the theoretical premise of a dipole-dipole interaction as being responsible for the attraction between particles. Furedi and Valentine made the next attempt at a theory after making numerous qualitative observations[65]. Their theory consists only of the derivation of an expression for the dipole-dipole force between lossy dielectric particles in an AC field. Unfortunately, it gives only the vaguest indications of chain formation. Their experimental cell is very primitive and it gives no more than a (meaningless) yes or no for pearl-chain formation.

Most recently, Saito, following the excellent lead of Krasny-Ergen, completed an exact analysis of pearl-chain for-

[60] Liebesny, P.: Referate u. Mitteil. Internat. Kong. f. Kurzwellen. Vienna. 1937.

[61] Liebesny, P.: Arch. Phys. Ther. 19, 736, (1939).

[62] Rajewsky, B.: Ultrashortwaves in Biology and Medicine. Georg Thieme, Leipzig. 1938.

[63] Herrick, J.F.: Pearl-chain formation. Proc. 2nd Ann. Tri-Service Conf. on Biol. Effects of Microwave Energy. July 8-10, 1958.

[64] Schwan, H.P.: Biophysics of Diathermy, in Therapeutic Heat. Ed. by S. Licht. Licht, New Haven, Conn. 1958.

[65] Furedi, A.A. and Valentine, R.C.: Factors involved in the orientation of microscopic particles in suspensions influenced by radio-frequency fields. Biochim. et Biophys. Acta, 56, 33, (Jan.), (1962).

mation for the case of perfectly conducting spheres in a pure dielectric medium (the case which Krasny-Ergen started to analyze), and for the pure dielectric case[66]. He also developed an approximate theory for this latter case which has the virtue of giving the threshold field strength in a simple, closed analytic expression (eq. 10). The error of the approximation is analyzed by a comparison with the exact theory and is found to be less than 20% (in terms of energy) unless the dielectric constant of the particle greatly exceeds that of the medium. An extension to this approximate theory, for the case of lossy dielectric media, has been made by this author, following some preliminary work in this direction by Saito. Approximate results for the transient behaviour of pearl-chain formation have also been derived by Saito[67].

In the following section of this dissertation, Saito's results are summarized, after being related to Krasny-Ergen's work. The extension to lossy dielectric media is then presented in detail. Measurements of the threshold for pearl-chain formation are summarized and are shown to validate the foregoing theory.

---

[66] Saito, M.: A model for pearl-chain formation. Internal report of the Dept. of Biomedical Electronic Eng., U. of Pa. In preparation for publication.

[67] Saito, M. and Schwan, H.P.: The time constants of pearl-chain formation, in Vol. 1 of Biological Effects of Microwave Radiation. Plenum, New York, 1961.

B. Summary of theory for pearl-chain formation

1. Perfectly conducting spheres in a dielectric medium--summary of theories of W. Krasny-Ergen[68] and M. Saito[69]

Although this case of pearl-chain formation has no biological significance, it is summarized here partly for historical perspective and partly as a relatively easy introduction to the theoretical treatment. The methods subsequently are applied to the more complicated case of perfect dielectric media.

The choice of the two-particle model, illustrated in fig. 37, was possibly the most important step toward an analytic treatment of pearl-chain formation. Application of an electric field[70] causes a separation of charges within the spheres in such a way that the perturbation of the impressed field, for each sphere acting alone, is the same as would be given by a concentric dipole. However, their proximity distorts the perfect dipole fields and, necessarily, the energy, U, associated with them. Since the spheres are highly mobile, they will tend to move toward a position which will minimize U.

It is convenient to speak of ΔU, the change in U when the particles approach (a negative quantity), rather than of U itself. Krasny-Ergen shows that this decrease of potential

---

[68] Krasny-Ergen, W.: Ref. cit.

[69] Saito, M.: Ref. cit.

[70] A quasi-static treatment suffices, even at microwave frequencies, because of the microscopic geometry.

energy due to the interaction of the fields surrounding the two perfectly conducting spheres is given by

$$\Delta U = KE_o^2 (f \cos^2\theta + g \sin^2\theta) \qquad (1)$$

where $K = 4\pi\epsilon a^3$ (in MKS units)

ϵ = dielectric constant of the medium

a, θ = as shown in fig. 1

E_o = strength of the impressed electric field

and f and g are given as complicated functions of r/a.

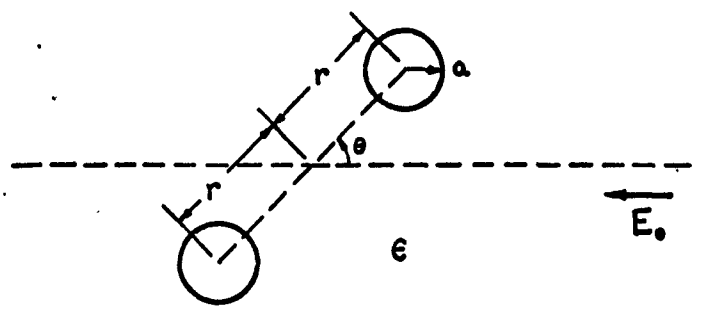

Figure 37. Two-particle model for pearl-chain formation, by Krasny-Ergen. Spheres are perfectly conducting, medium is perfect dielectric. Origin is fixed at midpoint of spheres.

The separation of the two spheres can now be seen to be governed by the Boltzmann Principle. This principle is a general law relating to the statistical energy distribution of large numbers of minute particles subject to thermal agitation and acted upon by a magnetic, an electric, or a gravitational field, or by inertia. In reference to fig. 36,

it says that the probability density, p, for finding a sphere at a distance r, when the system is in statistical equilibrium, is given by

$$p \sim \exp(-\Delta U/kT) \qquad (2)$$

Here $\Delta U = \Delta U(r)$ is the increment of potential energy suffered by the particle pair as their separation changes from "∞" to 2r. k is the Boltzmann constant and T is the absolute temperature. Although this principle was used by Krasny-Ergen for qualitative purposes (as far as eq. 2), he did not apply it quantitatively, and his contribution essentially stops at this point.

Saito now continues the development by calculating the mean value of the separation, i.e., the mean value of the separations of many sphere pairs, the general sphere pair being illustrated in fig.37. To calculate this value, it is necessary to use the distribution of separations (eq. 2). The mean separation is shown to be given by

$$\overline{r} = \frac{\iiint pr\ dv}{\iiint p\ dv} \qquad (3)$$

where the volume of integration is a sphere centered at the origin, with radius equal to R. The value of R is the average distance from the origin that the next sphere (other than the two in the model) will be found. It is related to the volume concentration of spheres by the approximate relation

$$\text{Concentration} = 74\% \left(\frac{a}{R}\right)^3 \qquad (4)$$

Thus the two-particle model has been related to an actual volume concentration of particles. Eq. (3) is evaluated numerically, with the results presented in fig.38.

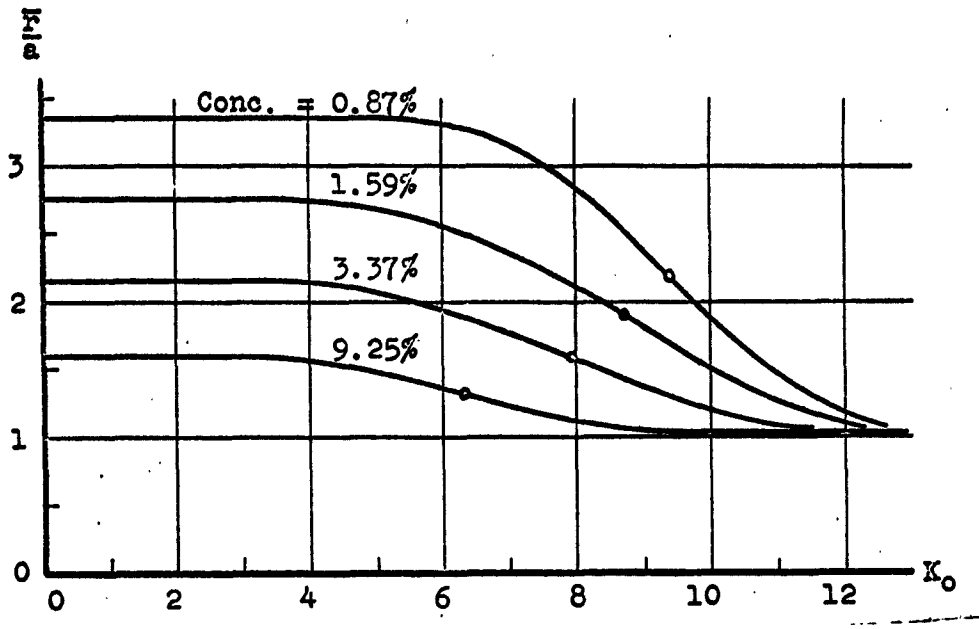

Figure 38. Normalized mean distance between perfectly conducting spheres, showing concentration effect. The abscissa is the energy change, measured in units of kT, which would occur if the two spheres came completely together in the direction parallel to the field. Thus $K_o = \frac{\Delta U}{kT}\Big]_{\theta=0°, r=a}$, where ΔU is calculated from eq. (1). The use of K_o is just a way of normalization and does not imply that the spheres are actually coming together or even moving. Note that $\bar{r}/a = 1$ is the condition of contact between the spheres. Dots on the curves indicate the threshold values (see following text).

Figure 38 shows that for a given volume concentration of particles, the mean separation of a particle pair decreases as the field strength increases ($E_o \sim K_o$). The theoretical definition for the threshold of pearl-chain formation is a logical consequence:

$$\left.\frac{\bar{r}}{a}\right|_{\text{threshold}} = \frac{1}{2}\left(\left.\frac{\bar{r}}{a}\right|_{\max} + \left.\frac{\bar{r}}{a}\right|_{\min}\right)$$

$$= \frac{1}{2}\left(\left.\frac{\bar{r}}{a}\right|_{\max} + 1\right) \qquad (5)$$

The threshold value of mean separation is indicated in fig. 38 for each of the four concentrations shown.

It can be concluded from these calculations, using the proposed definition for the threshold, that

(a) the onset of pearl-chain formation takes place when ΔU is about one order of magnitude greater than kT;

(b) higher particle volume concentrations do lower the threshold, but only by a small amount.

2. Perfect dielectric spheres in a perfect dielectric medium--summary of theory of M. Saito

The major new concern in this case is the need to calculate the decrease of potential energy associated with the electrical interaction of two dielectric spheres, a result analogous to eq. (1). The model is shown in fig. 39 .

It can be shown that the decrease of potential energy has the same form as eq. (1):

$$\Delta U = KE_0^2 (f \cos^2\theta + g \sin^2\theta) \qquad (6)$$

where K is a function of the dielectric constants ϵ_1 and ϵ_2 of the particle and medium respectively and f and g are functions of r/a, ϵ_1, and ϵ_2. The problem is thus to determine K, f, and g as functions of r/a, ϵ_1, and ϵ_2. The procedure is to solve the field distribution for the two separate cases $\theta = 0°$ and $\theta = 90°$, and to use the solutions to evaluate eq. (6) for each of those two cases. Since $Kf = \Delta U|_{\theta=0°}$ and

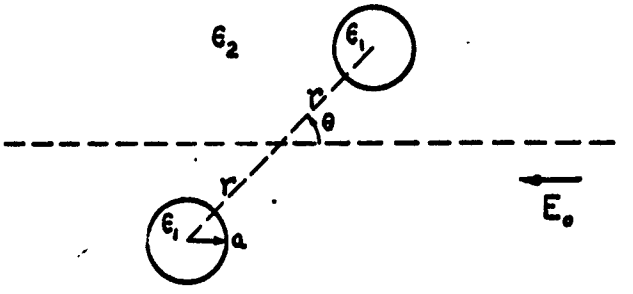

Figure 39. Two-particle model for pearl-chain formation with all dielectric media.

$Kg = \Delta U|_{\theta=90°}$, the result of this procedure is to have Kf and Kg, leaving k, f, and g undetermined to within a constant factor. The factor is found by treating the simplest case, that of $\epsilon_1 = \epsilon_2$, by a special method to be discussed in the next section, the dipole-approximation method.

The solution of the field distribution problem is based on an elementary principle that if all the induced charges at the surfaces of the spheres are regarded as the sources of the

field, then the field can be calculated in the same way as if these charges were located in a vacuum. So it is actually the induced surface charge density which is regarded as the unknown. The details of this lengthy solution are available from the original paper of Saito.

Analogous to the previous case, the results of the numerical integrations of eq. (3) may be presented in graphical form. Figure 40 shows the results only for one concentration, similar families of curves (available in the original paper) being necessary to describe the relationships for other concentrations.

The following conclusions may be drawn from the curves in fig. 40 :

(a) The onset of pearl-chain formation takes place when ΔU is about one order of magnitude greater than kT, unless $\epsilon_1 \gg \epsilon_2$.

(b) Higher particle volume concentrations lower the threshold, but only to a minor extent (this conclusion drawn from the curves for other concentrations which are not included here).

(c) Higher values of ϵ_1/ϵ_2 lower the threshold.

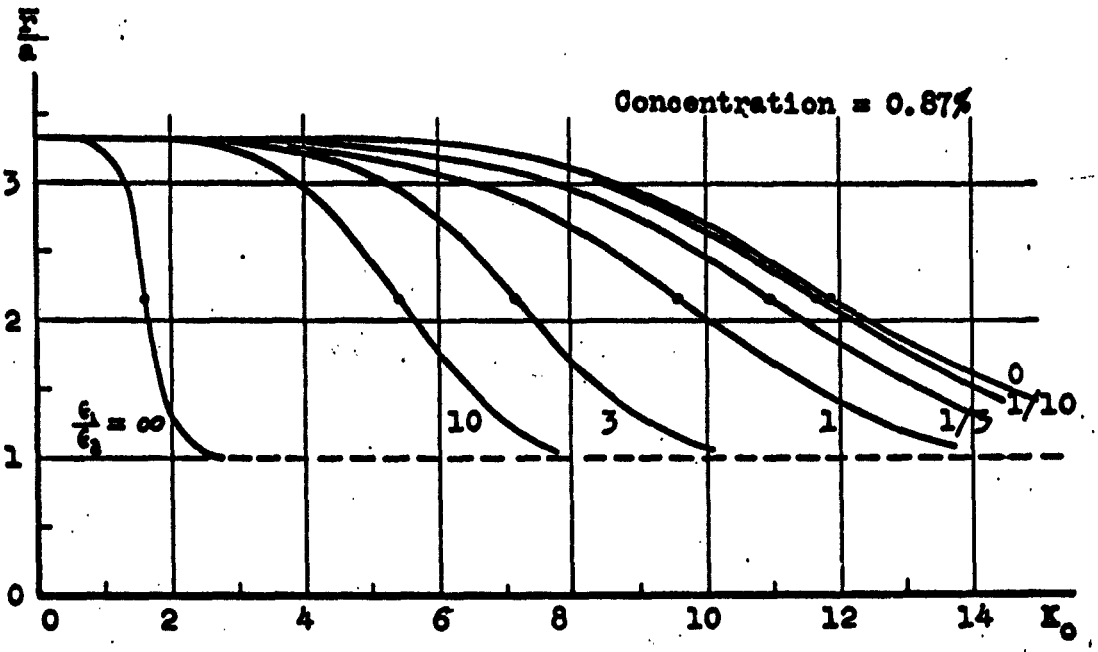

Figure 40. Normalized mean distance between the spheres, showing the effect of the ratio of dielectric constants, $\frac{\epsilon_1}{\epsilon_2}$. The abscissa $K_0 = \frac{\Delta U}{kT}\Big|_{\theta=0°, r=a}$, where ΔU is that expression found by neglecting the interaction between the spheres (see next section on "dipole approximation," eq. 7 and 8). The curve for $\epsilon_1/\epsilon_2 = 1$ was calculated from the "dipole approximation" theory (eq. 18), not from the exact theory (eq. 6). This curve represents the hypothetical case in which the spheres are indistinguishable from the medium and hence require an infinitely large applied field for pearl-chain formation (note in eq. 8 that finite K_0 corresponds to infinite E_0 if $\epsilon_1 = \epsilon_2$). And, by virtue of the assumptions in the dipole approximation, it also represents the case that the dipole fields of the spheres do not interact (cf. fig. 41).

3. Perfect dielectric spheres in a perfect dielectric medium: dipole approximation--summary of theory of M. Saito

The dipole approximation assumes that the dipole field surrounding each isolated sphere persists when the spheres are closely spaced. The model is the same as that in fig. 39. By neglecting the interaction between spheres, the theory not only is immensely simplified but it leads to a simple closed analytic expression for the threshold field strength. Therefore it is of interest to know by what amount the dipole approximation differs from the "exact" theory above. The dipole-approximation theory will be summarized briefly and the error of approximation discussed.

According to the assumption, the two spheres are producing dipole fields independently. Then ΔU may be equated to twice the potential energy of one dielectric sphere in the (induced) dipole field of the other. There results

$$\Delta U = K_0 kT \left(\frac{a}{r}\right)^3 P_2(\cos\theta) \qquad (7)$$

where

$$K_0 = \left.\frac{\Delta U}{kT}\right|_{\theta=0^\circ,\ r=a}$$

$$K_0 = \pi a^3 E_0^2 \left(\frac{\epsilon_1 - \epsilon_2}{\epsilon_1 + 2\epsilon_2}\right)^2 \frac{\epsilon_2}{kT} \qquad (8)$$

Substituting eq. (7) into eq. (3), the mean separation can be computed to be that shown in fig. 41.

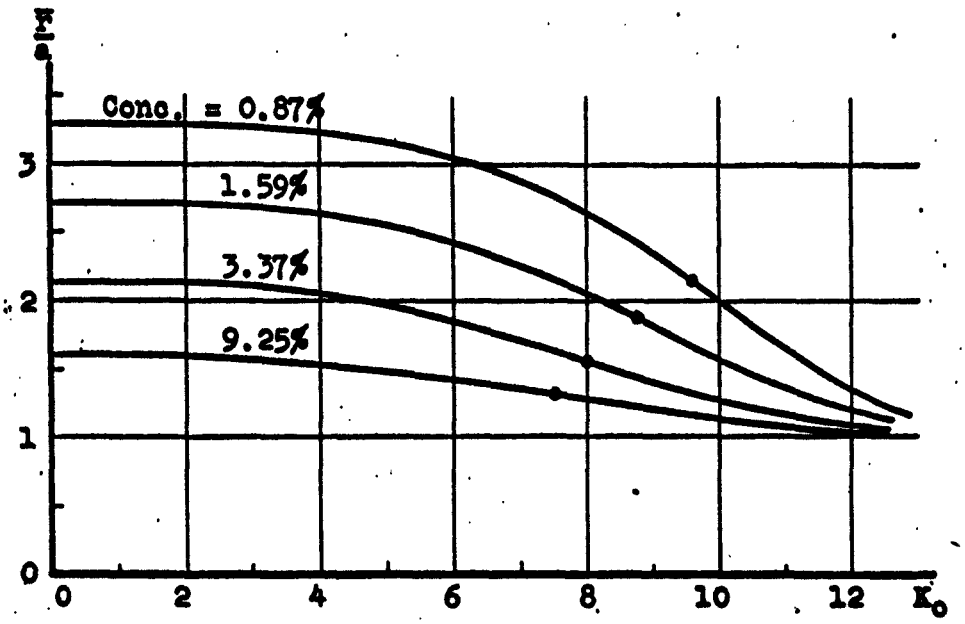

Figure 41. Normalized mean distance between the spheres, assuming no interaction. The abscissa, K_0, again is used as a way of normalization: From its explicit value in eq. (20) (with asterisks removed for this case), it can be seen that the value of the dielectric constant ratio, ϵ_1/ϵ_2, changes the relation between K_0 and E_0^2; but as a function of K_0, these curves are independent of ϵ_1/ϵ_2. Thus, as a result of the "dipole approximation," these curves, unlike those in fig. 40, are independent of the dielectric constant ratio.

It is suitable to point out here that pearl-chain formation is just another manifestation of the forces in inhomogeneous fields. In the present case, each particle reacts to being in the dipole (inhomogeneous) field of the other. The energy associated with this reaction, ΔU, is just the integral of the force with which they come together.

The validity of the dipole approximation is illustrated in fig. 42. The curves for other concentrations are very close to the curve shown, and therefore are omitted. It may be concluded that the dipole approximation is satisfactory except for the cases in which $\epsilon_1 >> \epsilon_2$.

A simple formula for the threshold field strength, E_{th}, follows directly from eq. (8):

$$E_{th} = \sqrt{\frac{K_{th}}{\pi}}\ a^{-\frac{3}{2}}\ \frac{\epsilon_1 + 2\epsilon_2}{|\epsilon_1 - \epsilon_2|}\sqrt{\frac{kT}{\epsilon_2}} \qquad (9)$$

Here K_{th} is the value of K_o at the threshold points indicated by dots on the curves in fig. 40. It is not a very strong function of concentration, and with an error not greater than 10%, may be taken as 9. Thus eq. (9) becomes a useful approximation for the threshold field strength for pearl-chain formation:

$$E_{th} = 1.7\ a^{-\frac{3}{2}}\ \frac{\epsilon_1 + 2\epsilon_2}{|\epsilon_1 - \epsilon_2|}\sqrt{\frac{kT}{\epsilon_2}} \qquad (10)$$

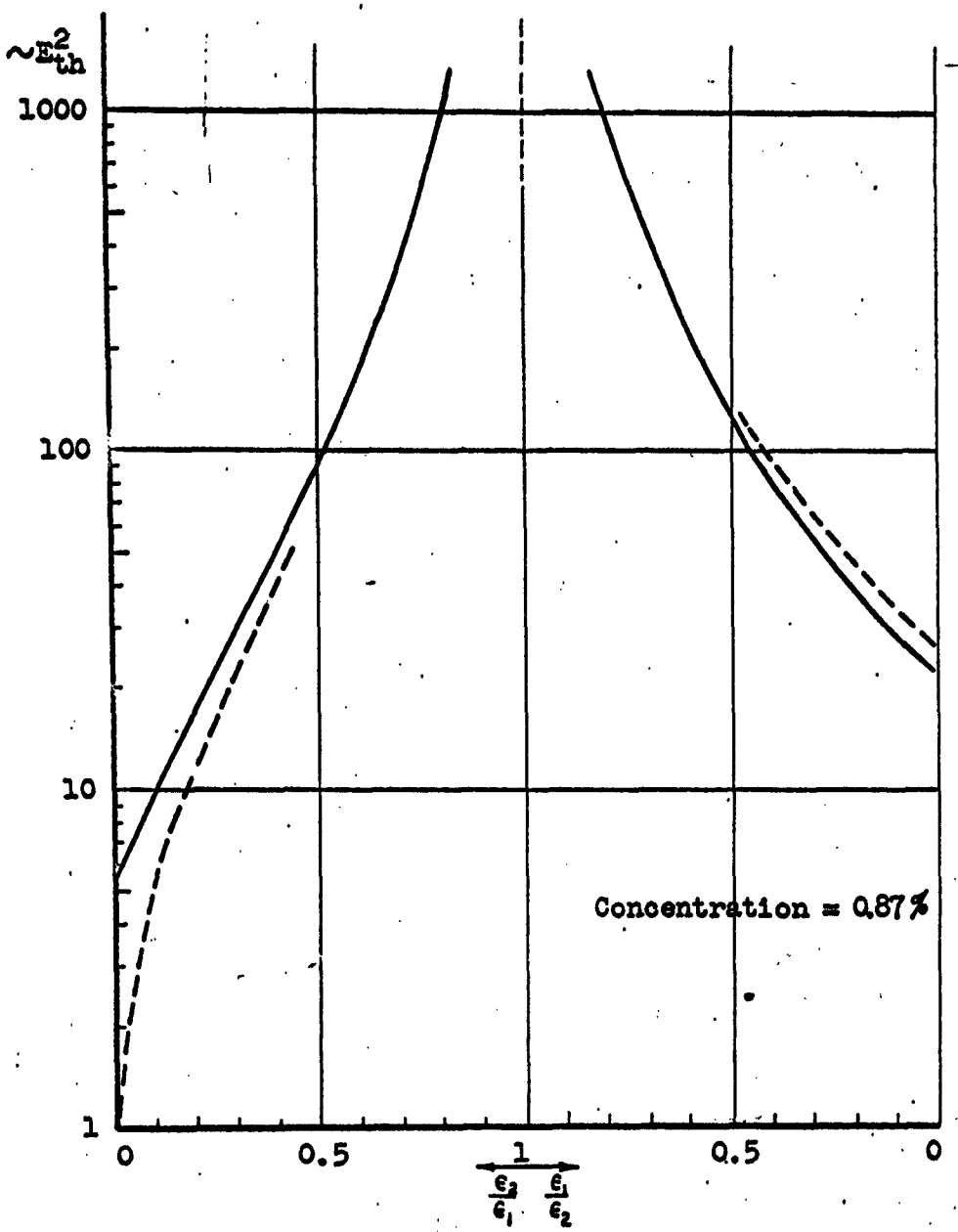

Figure 42. Comparison of threshold field strengths predicted by "exact" theory (dotted lines) and by "dipole approximation" theory (solid lines). Ordinate is proportional to square of threshold field strength.

4. Lossy dielectric spheres in a lossy dielectric medium; dipole approximation--revision of theory of M. Saito

An approximate formula, analogous to eq. (10), has been derived for the more complicated case of lossy dielectric media. Unfortunately, the exact assessment of its validity requires a large computer and has not yet been done. However, since fig. 42 shows that the dipole approximation is satisfactory except for cases of $\epsilon_1 \gg \epsilon_2$, it can be hoped that similar validity will prevail here except for cases of $|\epsilon_1^*| \gg |\epsilon_2^*|$.

It is assumed that spheres A and B (refer to fig. 43) are producing dipole fields independently[71]. Then the potential energy associated with the presence of sphere B in the dipole field of A is given by (cf. section IV, eq. 1)

$$\Delta U = \frac{1}{2} \operatorname{Re} \int_{V_B} \tilde{\epsilon}_2^* \left(1 - \frac{\epsilon_1^*}{\epsilon_2^*}\right) (\mathbf{E}_1 \cdot \tilde{\mathbf{E}}_A)\, dv \qquad (11a)$$

where V_B = volume of sphere B

$\epsilon_1^*, \epsilon_2^*$ = complex dielectric constants of sphere, medium

$\mathbf{E}_1$ = effective (r.m.s.) field inside sphere B

$\mathbf{E}_A$ = effective value of the dipole field from particle A which is impressed on particle B (sufficient separation is assumed to provide the necessary local homogeneity of $\mathbf{E}_A$)

$\sim$ = complex conjugate

But the potential energy associated with the presence of sphere A in the dipole field of B has the same value. Therefore, the total potential energy associated with the interaction of A and

---

[71] That is, the presence of the pre-existing homogeneous field, $\mathbf{E}_o$, has been disregarded, since it is manifest to the spheres only through the creation of dipoles.

B is just twice that given for one sphere:

$$\Delta U = \mathrm{Re} \int_{V_B} \tilde{\epsilon}_2^* \left(1 - \frac{\epsilon_1^*}{\epsilon_2^*}\right) (\mathbf{E}_1 \cdot \tilde{\mathbf{E}}_A)\, dv \qquad (11b)$$

Then E_1 is given by (cf. section IV, eq. 2)

$$E_1 = - \frac{3\epsilon_2^*}{\epsilon_1^* + 2\epsilon_2^*} E_0 \qquad (12)$$

If V_A is the potential of the dipole field of A,

$$V_A = - \frac{\epsilon_1^* - \epsilon_2^*}{\epsilon_1^* + 2\epsilon_2^*} a^3 E_0 \frac{\cos\theta}{(2r)^2} \qquad (13)$$

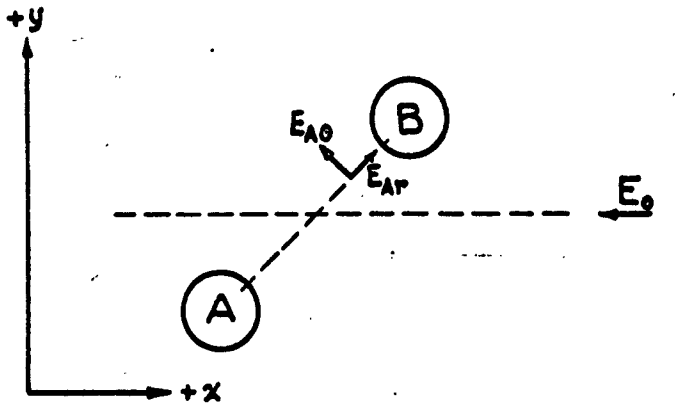

Figure 43. Two-particle model for dipole-approximation treatment of the pearl-chain formation with lossy dielectric media

then

$$E_{Ar} = - \frac{\partial V_A}{\partial(2r)} = -2 \frac{\epsilon_1^* - \epsilon_2^*}{\epsilon_1^* + 2\epsilon_2^*} \left(\frac{a}{2r}\right)^3 E_0 \cos\theta \qquad (14)$$

$$E_{A\theta} = - \frac{1}{2r} \frac{\partial V_A}{\partial \theta} = - \frac{\epsilon_1^* - \epsilon_2^*}{\epsilon_1^* + 2\epsilon_2^*} \left(\frac{a}{2r}\right)^3 E_0 \sin\theta \qquad (15)$$

Now having expressions for the two electric fields in eq. (11), each can be resolved into components along the x and y axes and the dot product taken:

$$E_1 \cdot \tilde{E}_A = - \frac{3\epsilon_2^*}{\epsilon_1^* + 2\epsilon_2^*} E_o^2 \frac{\tilde{\epsilon}_1^* - \tilde{\epsilon}_2^*}{\tilde{\epsilon}_1^* + 2\tilde{\epsilon}_2^*} \left(\frac{a}{2r}\right)^3 (1 - 3\cos^2\theta) \tag{16}$$

Substituting this expression into eq. (11), and making the necessary simplifications, there results

$$\Delta U = \left|\frac{\epsilon_1^* - \epsilon_2^*}{\epsilon_1^* + 2\epsilon_2^*}\right|^2 3E_o^2 \left(\frac{a}{2r}\right)^3 (1 - 3\cos^2\theta) \left(\int_{V_B} dv\right) (\mathrm{Re}\, \tilde{\epsilon}_2^*) \tag{17}$$

from which

$$\Delta U = 4\pi a^3 E_o^2 \left(\frac{a}{2r}\right)^3 \epsilon_2 \left|\frac{\epsilon_1^* - \epsilon_2^*}{\epsilon_1^* + 2\epsilon_2^*}\right|^2 (1 - 3\cos^2\theta) \tag{18}$$

By definition, K_o is the energy lost in the complete longitudinal alignment of two spheres ϵ_1^* in medium ϵ_2^*, in units of kT. That is,

$$K_o\, kT = -\Delta U\Big|_{\theta=0°,\ r=a} \tag{19}$$

the minus sign being used because of the use of the term "energy lost" rather than "energy change." From eq. (18) and (19),

$$K_o\, kT = \pi a^3 E_o^2 \epsilon_2 \left|\frac{\epsilon_1^* - \epsilon_2^*}{\epsilon_1^* + 2\epsilon_2^*}\right|^2 \tag{20}$$

At the threshold for pearl-chain formation, eq. (20) becomes

$$K_{th} kT = \pi a^3 E_{th}^2 \epsilon_2 \left|\frac{\epsilon_1^* - \epsilon_2^*}{\epsilon_1^* + 2\epsilon_2^*}\right|^2 \tag{21}$$

so that

$$E_{th}^2 = \frac{K_{th}}{\pi} a^{-3} \left|\frac{\epsilon_1^* + 2\epsilon_2^*}{\epsilon_1^* - \epsilon_2^*}\right|^2 \frac{kT}{\epsilon_2} \tag{22}$$

If a value of $K_{th} = 9$ is assumed, similar to the last case of perfect dielectrics (eq. 8), then

$$E_{th} = 1.7\, a^{-\frac{3}{2}} \left|\frac{\epsilon_1^* + 2\epsilon_2^*}{\epsilon_1^* - \epsilon_2^*}\right| \sqrt{\frac{kT}{\epsilon_2}} \tag{23}$$

which is the final result. Note that eq. (9) is a special

case of eq. (23). Equation (23) together with fig. 42 is the best available estimate of the theoretical threshold field strength for pearl-chain formation with lossy dielectric media.

5. Graphical presentation of dipole approximation for threshold field strength--extension to theory of M. Saito

Although eq. (23) relates E_{th} to frequency, the form of this relation is hidden in the algebra. It may be elucidated with the following graphical representations of E_{th} as a function of $\frac{\epsilon_1^*}{\epsilon_2^*}$, and $\frac{\epsilon_1'}{\epsilon_2'}$ as a function of ω.

If eq. (22) is rewritten, letting $K_{th} = 9$, then

$$E_{th}^2 = 2.9\, a^{-3}\, \gamma\, \frac{kT}{\epsilon_2} \tag{24}$$

where

$$\gamma = \left| \frac{\epsilon_1^* + 2\epsilon_2^*}{\epsilon_1^* - \epsilon_2^*} \right|^2 \tag{25}$$

Alternatively,

$$\gamma = \left| \frac{\frac{\epsilon_1^*}{\epsilon_2^*} + 2}{\frac{\epsilon_1^*}{\epsilon_2^*} - 1} \right|^2 \tag{26}$$

By letting $\frac{\epsilon_1^*}{\epsilon_2^*} = x + iy$, it follows that (27)

$$\gamma = \left| \frac{x + 2 + iy}{x - 1 + iy} \right|^2 \tag{28}$$

or

$$\left(x - \frac{\gamma + 2}{\gamma - 1}\right)^2 + y^2 = \frac{9\gamma}{(\gamma - 1)^2} \tag{29}$$

Any one of this family of circles, shown in fig. 44 , with

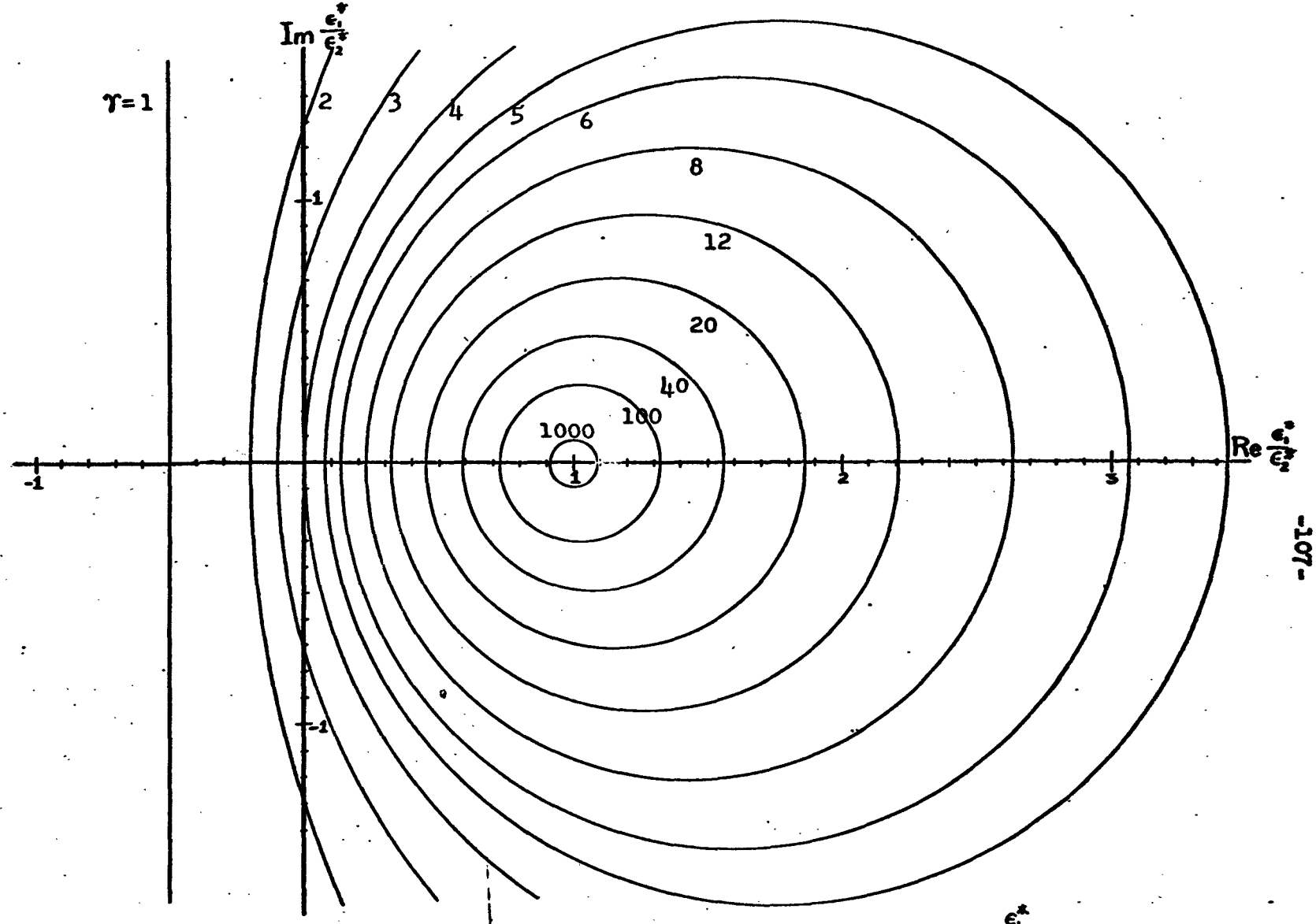

Figure 44. Family of loci, each of which is the locus of all values of $\frac{\epsilon_1^*}{\epsilon_2^*}$ for which γ (or $E_{th}^2 \epsilon_2$) is a constant. If $\epsilon_2 \neq \epsilon_2(\omega)$, then each represents a constant value of E_{th}.

center at $\left(\frac{\gamma+2}{\gamma-1}, 0\right)$ and radius equal to $\frac{3\sqrt{\gamma}}{\gamma-1}$, represents the locus of all values of $\frac{\epsilon_1^*}{\epsilon_2^*}$ for which γ (or E_{th}) is a constant.[72] (The relation between γ and E_{th} is given in eq. 24)

Although only the right half plane in fig.44 corresponds to physical reality, the family of circles is shown to extend slightly into the left half plane. But all such circles, corresponding to $1 < \gamma \leq 4$, are at least partly in the right half plane where their meaning is clear.

If media 1 and 2 are such that ϵ_1, ϵ_2, K_1, and K_2 are frequency-independent, then the variation of $\frac{\epsilon_1^*}{\epsilon_2^*}$ with frequency is easily established:

(a) The variation of $\frac{\epsilon_1^*}{\epsilon_2^*}$ in the complex plane is always a semicircle starting and ending on the real axis.

(b) The function $\frac{\epsilon_1^*}{\epsilon_2^*}$ assumes a value which always travels clockwise around the semicircle as ω increases; the ends of the semicircle correspond to the values of $\frac{\epsilon_1^*}{\epsilon_2^*}$ at zero and infinite frequency.

(c) At $\omega = 0$, $\frac{\epsilon_1^*}{\epsilon_2^*} = \frac{K_1}{K_2}$, and at $\omega = \infty$, $\frac{\epsilon_1^*}{\epsilon_2^*} = \frac{\epsilon_1}{\epsilon_2}$.

(d) The central angle, θ, generated by the clockwise movement of $\frac{\epsilon_1^*}{\epsilon_2^*}$ is related to ω by the relation

$$\tan \theta/2 = \omega T_2 \qquad (30)$$

where $T_2 = \frac{\epsilon_2 \epsilon_r}{K_2}$. The inscribed angle generated in the same way is given by

$$\tan \alpha = \omega T_2 \qquad (31)$$

Of course, $\theta = 2\alpha$ by simple geometry. An example of the use of these rules and relations is given in fig.45 .

---

[72] It is assumed here that ϵ_2 is a constant--certainly true for aqueous media for $f < 3000$ Mc.

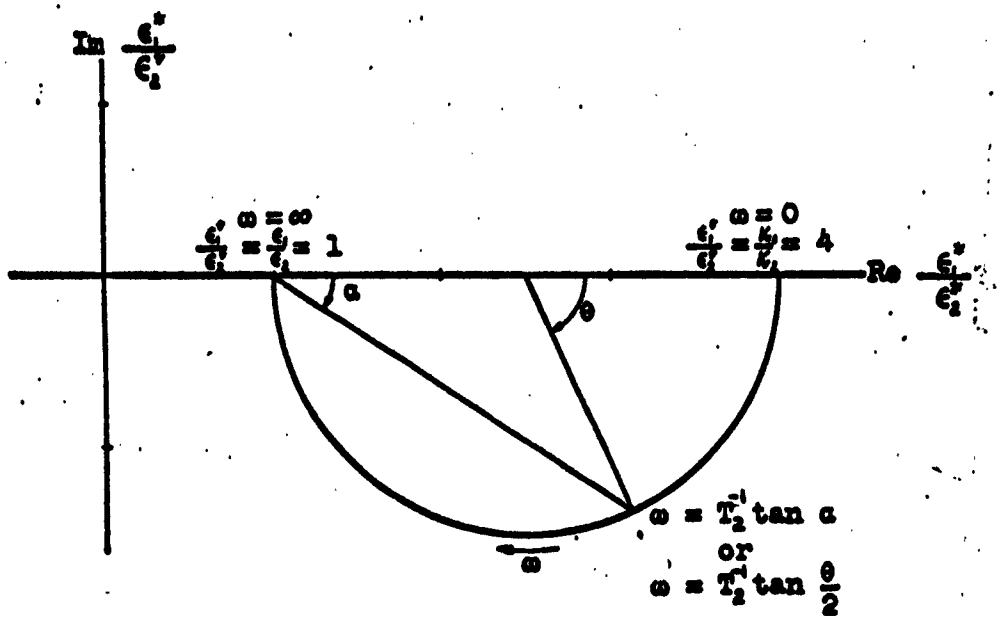

Figure 45. An example of the semicircular dependence of $\frac{\epsilon_1^*}{\epsilon_2^*}$ on frequency. It is assumed that $\kappa_1/\kappa_2 = 4$ and $\epsilon_1/\epsilon_2 = 1$, the four separate parameters being frequency-independent. Using only these data and the rules (a) through (d), the above semicircle may be drawn immediately. Note that one decade of change in ω, centered about the value $\omega = 1/T_2$, is sufficient to drive θ over almost the entire semicircle. If the κ's and ϵ's vary with frequency, a curve may still be drawn, although it will no longer be a simple semicircle. However it often may be sufficiently simple so that the graphical method will still be useful.

The results in fig. 44 and fig. 45 may now be combined as a graphical method for evaluating E_{th} vs. ω from eq. 23. Equation (24) shows how E_{th} varies with γ. Figure 44 shows how γ varies with $\frac{\epsilon_1''}{\epsilon_2''}$. And fig. 45 shows how $\frac{\epsilon_1''}{\epsilon_2''}$ varies with ω for a given pair of materials. The method works most easily for substances whose conductivities and dielectric constants are frequency-independent, so that $\frac{\epsilon_1''}{\epsilon_2''}$ vs. ω is a semi-circle. Superposition of the semi-circle onto fig. 44 then gives a series of intersections which relate γ to θ, or E_{th} to ω. An example of this method is shown in fig. 51 and its related text.

For substances whose conductivities and dielectric constants are functions of frequency (in the frequency range of interest), the method is a little more cumbersome. The curve showing $\frac{\epsilon_1''}{\epsilon_2''}$ vs. ω, no longer a semicircle, must be superimposed onto fig. 44. Intersections again give paired values of γ and θ, but now eq. (24) must be used in the conversion to paired values of E_{th} and ω.

6. Time constants--summary of results of M. Saito[73]

The foregoing theory tacitly has assumed that only the r.m.s. value of the applied field has an influence on the threshold. The position of a particle was described in terms or r and θ but not of t (time). By assuming this statistical steady state, the threshold field strengths found were functions only of the r.m.s. value of the applied field. However, a pulsed field and a CW field with the same r.m.s. value may have different effects on pearl-chain formation. To analyze this possibility, the position of the particle also must be considered to be a function of time. The statistical steady-state is replaced with the statistical transient state, giving the probability density for finding a particle at a given r and θ as a function of time. In particular, the total time necessary for two particles to go from randomness to pearl-chain formation (or vice versa) is calculated and is called the time constant for these particles.

The time constants are calculated for two cases: (a) For zero field strength, and (b) for weak field strengths, not greatly exceeding E_{th}. The meaning of the time constant for $E_o < E_{th}$ is the time necessary for pearl chains completely to break up, and for $E_o > E_{th}$, is the time necessary for pearl chains to form from a completely random distribution of particles.

---

[73] Saito, M. and Schwan, H.P.: The time constants of pearl-chain formation, in Vol. 1 of Biological Effects of Microwave Radiation. Plenum, New York, 1961. It is being prepared for publication in detail.

The results of these calculations for τ, the time constant, may be summarized as follows:

$$\begin{aligned} \tau &\sim a^3 \quad (a = \text{radius}) && \text{, for all } E_o \\ &\approx \text{constant} && \text{, for } E_o \ll E_{th} \\ &\sim E_o^{-2} && \text{, for } E_o > E_{th} \end{aligned} \tag{31a}$$

The transition of τ from the constant value to the dependence on E_o^{-2} occurs at about the threshold field strength for pearl-chain formation, E_{th}. The actual calculations for the dependences, especially for $E_o > E_{th}$, are subject to large errors--even approaching an order of magnitude--so no values will be stated. More exact values for large field strengths must await computer solutions. For zero field, however, the dependence on size has been calculated with fairly good accuracy (probably not more than 10% in error): At room temperature for a volume concentration of 1.6%, the time constant for a particle of 1μ radius is 2.2 seconds, and, as stated above, it varies as the cube of the radius.

It must be emphasized that these results are at least as approximate as the definition of the time constant itself.

C. Experimental considerations

1. Definition of experimental threshold

The choice of a criterion for establishing an experimental threshold for pearl-chain formation was limited by two constraints: The criterion had to be experimentally feasible; and it had so to relate to the theoretical definition of threshold that a good comparison of experimental and theoretical results would be possible. Examining the theoretical definition (see eq. 5 and fig. 40), it can be seen that K_o varies by a factor of about 4 between maximum mean separation and contact of the spheres. This variation implies (cf. eq. 8) that E_o varies by a factor of about 2. So it is likely that the observed values of E_{th} will show a maximum spread of a factor of 2. But a narrower spread of data obviously would be desirable. Experimental feasibility also demands a more refined operational definition.

Possible definitions of an experimental threshold vary from the most mathematically precise to a complete dependence on undefinable inner feelings, the former having the advantage of precision, the latter of simplicity. Examples of the former type were those whose criterion was satisfied (a) when a fixed percentage of the particles were in chains--say 50% or 99%; (b) when the chains exceeded a pre-established degree of straightness, straightness being measured by the mean square deviation from a straight line; (c) when the average length of chains exceeded a preset number; and (d) when a fixed increment of field strength caused the greatest proliferation of chains. All of these ideas would require meas-

urements to be made from numerous photographs. However, it never became possible to take such photographs, for the technical difficulties are formidable. Furthermore it was not clear that such measurements would have more significance than those which could be taken by easier methods. As examples of intermediate criteria, i.e., those combining measurement and opinion, were (a) the first appearance of 3-particle chains which were "correctly and firmly" oriented with the field and (b) the first appearance of 4-particle chains similarly disposed. This kind of criterion combines the worst features of the other kinds, so it was not seriously considered.

Finally, the threshold whose definition depends entirely on opinion was considered. It was decided that the sloppy qualities inherent in this kind of subjective definition could be reduced to a reasonable level if the opinion were based on the following simple, succinct, operational definition: Pearl-chain formation will be said to have occurred when it first can unequivocably be said that chain formation has appeared out of randomness. Such a definition is not trivial. The conscientious experimenter, after hours of trying to see the intangible threshold, will find that The Definition is the only solid footing he has in a morass of indecision and uncertainty. Thus simplicity is bought at the price of despair. To say when, with an overcast sky, night has turned into day is an equivalent challenge. To repeat this decision assiduously hundreds of times, one either finds

his principle or perishes.

It is important to realize that although this use of an operational definition will definitely narrow the spread of data, the average value of an infinite number of measurements still may not coincide with the theoretical value of E_{th}. The reason is that there is no guarantee that the operational and theoretical definitions coincide. One can only presume that an improvement in the average value of the obseved threshold has been obtained. However, if a frequency dependence is found in the data, it will be more clearly defined than in the absence of this operational definition. For this reason, data could be said to show or not to show a frequency dependence of consequence even though the absolute values were slightly uncertain.

2. Difficulties in measuring the threshold

While experimental difficulties are inherent in all experimentation, those encountered here have such a direct bearing on the experimental results that some discussion may be justified. Also a repetition or adaptation of this work by another investigator would proceed more smoothly if the various problems could be forseen. The difficulties presented by making subjective measurements of the threshold are indicated above, so that issue will be omitted here.

Difficulties may be described loosely by the following terms. A discussion of each term follows.

a. Particle size
b. Settling
c. Slowness
d. Conductivity
e. False chains
f. Dielectric pumping
g. Concentration
h. Electrophoresis

a. Particle size

The threshold field strength varies with the radius of the particle used according to eq. (23): $E_{th} \sim a^{-\frac{3}{2}}$. Thus larger particles line up in weaker fields. No such variation in E_{th} is encountered when the particles are as uniformly graded as polystyrene spheres--hence their popularity. But a significant problem arises in emulsions, which have a roughly Gaussian distribution of particle sizes. As the applied field strength is reased, the large particles will give one threshold (low), the median sizes a second (medium), and the small particles a third (high). In fact the largest sizes will usually be all lined up by the time the field strength reaches the threshold value for the median sizes. And they, in turn, will be lined up when the smallest begin to react to the field. However, if the field strength is raised so quickly that the median sizes are seeking partners before the large particles have found each other, then chains of mixed sizes will occur. An extreme case of these mixed chains is shown in fig. 46. Prevention of this phenomenon is simply done by raising the field strength slowly and by using freshly diluted emulsions. But the variation of threshold with size still must be consi-

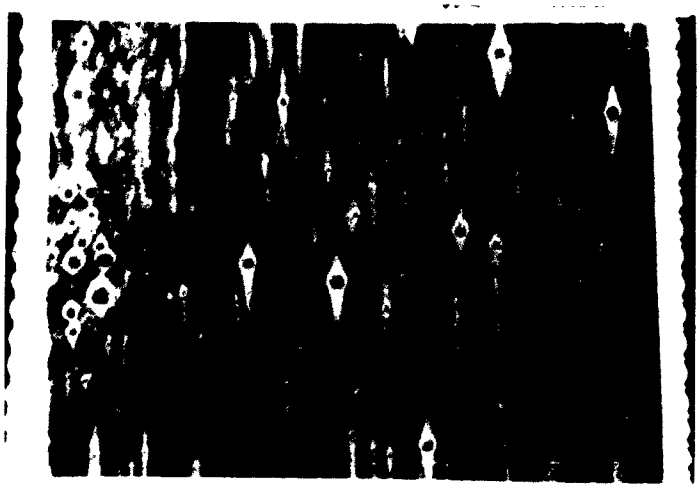

Figure 46. Pearl chains of particles with different sizes. One large particle is capable of attracting numerous smaller ones. The suspension is a highly diluted silicone emulsion in which coalescence has occurred to make very large particles. Freshly diluted emulsions do not have time to coalesce.

To get consistent threshold values from an emulsion with a mixture of particle sizes, the procedure found to be most satisfactory was to measure the length of a straight chain of the median (most common) size and to deduce from that, the median size. Subsequent observations would be confined to particles of that size, larger sizes being ignored. Smaller sizes never would form pearl chains, since E was limited to the threshold value for the median size.

It is interesting to note that the method of measuring the length of a straight chain in order to determine the particle size could also be applied to the polystyrene sphere

case, for which the answer was known. This measurement was done twice. At first the measurement of chain length was made by visual comparison with the calibrated eyepiece reticle. It was found that a chain of 11 particles was longer than the sum of 11 diameters. The difference divided by the number of interspaces gave a space between "touching" spheres that was about 0.21μ, which is 18% of one diameter. A second, more accurate measurement was made from a photograph[74] of a different 12-particle chain (fig. 47.). A space of 0.19μ was found between "touching" spheres.

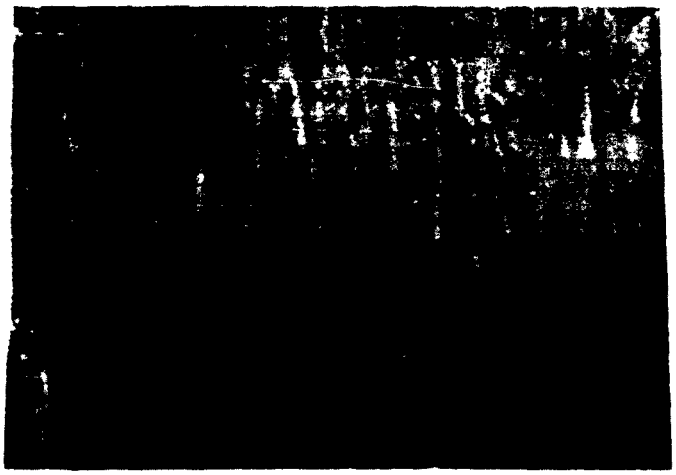

Figure 47. 1.17μ polystyrene spheres exposed to a 26 Mc electric field of 660 v/cm. A 12-particle section of one chain is indicated. Scale of photograph: 1 mm = 1.234μ .

---

[74]The scale on a photograph can be determined very accurately by comparison with another photograph, taken under the same conditions, of a calibrated slide (2mm divided into 200 parts).

If the chain were not exactly straight, the separations found would be smaller than the actual average separation. Therefore, if crookedness plays a part, it does so in the "wrong" direction. In the absence of further work, several explanations are possible: (a) The pearl-chain formation does not bring the particles into contact at this field strength (which is about three times the threshold value); (b) there is some form of "shield" or "shell" around the particles which prevents their closest approach; or (c) the particles are larger than 1.17μ.

The first possibility, (a), certainly has a measure of validity. Fig. 40 shows that the spheres do not snap together like magnets but rather are forced into closer and closer contact as the field strength increases. However, the two-particle model loses its validity once chains have formed, so no theory is available for estimating the mean separation in this case. Possibility (b) arises from the presence of a detergent whose very function is to keep the particles separate. But the detergent layer probably does not account for the whole 1000Å-thick "shell." Possibility (c) is unlikely at best.

b. Settling

For particles greater than 1μ in diameter, buoyancy forces generally are at least comparable with forces which tend to maintain the suspension or emulsion (electrostatic repulsion, Brownian movement). For example a silicone emulsion with 2μ particles settles, while one with 0.6μ particles does not. Since 100μ of settling is sufficient to cause most particles to rest on or near the bottom of the cell,

only a few minutes to about an hour are available if no anti-settling procedures are used. Within this period satisfactory measurements may be made in the bulk of the solution.

Two means exist to prevent or retard settling and one to live with it. Clearly settling may be prevented by inverting the cell for half of the time, with a frequency which depends upon the settling rate. The method is not without its problems, however, as several particles will stick to the glass during each period, until visibility is impaired. Also measurements cannot conveniently be made while the cell is inverted, which is usually 5 out of every 10 minutes. The second means of

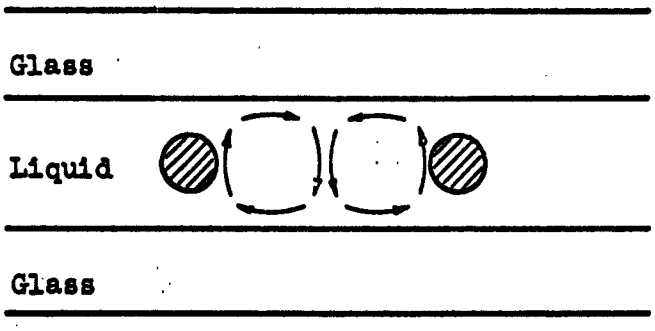

Figure 48. Thermal convection currents in the suspending liquid. More heat is produced near the wires (cross-hatched) than in the bulk of the liquid because of field inhomogeneities.

retarding or even reversing settling is to force enough current through the liquid so as to cause thermal convective stirring, as illustrated in fig. 48. Again the method has faults, the primary one being a tendency for particles to accumulate in the center of the bottom glass. There is a way of making measurements, however, on a settled sample. It

is necessary first to clear up the dense packing on the bottom glass with a thermal convective stir, then to focus on a plane just above the bottom glass where the Brownian motion will kick enough particles off the bottom to maintain a fairly concentrated suspension. One or another of these methods was regularly used for particles which settle.

It is noteworthy that if a particle is immobilized by being stuck to the glass, pearl chains form on this particle at significantly lower field strength than would occur if it were free to move. Theoretically this result is very reasonable, since the normal competition between electrical "ordering" forces and thermal "disordering" forces is biased in favor of the former.

Some particles which were both large and heavy, such as glass spheres or erythrocytes, could not be kept in suspension for periods exceeding a very few minutes. Measurements on glass spheres were not made at all and on erythrocytes to a minor extent (another severe problem, "slowness," exists in this case).

c. Slowness

The procedure for determining the threshold field strength for pearl-chain formation was to gradually increase the field until the phenomenon was observed. But the question was how gradual was "gradual?" As an example consider that chain formation would take about 1 second at the threshold of 100 v/cm. Then an increase of 10 v/cm/sec would cause the measurement to give 110 v/cm, instead of the correct

value of 100. In this case the solution is simple, requiring only a slightly slower rate of increase in field strength. But the time constant varies as the cube of the particle size (see eq.31a), and is very roughly 1 second for 1μ diameter. So a large particle easily can have a time constant of three minutes. Then the rate of increase of field strength cannot be more than 10% of the threshold per three minutes if an intolerable error is to be avoided. Repetitive observation of the threshold for pearl-chain formation under these circumstances is virtually impossible. Should the threshold be exceeded, about three minutes would be required for the return to some semblance of randomness. Only estimates can be made for the threshold in these cases.

The median particle size in the SM 70 silicone emulsion[75] is 2.3μ (diameter). The time constant for this particle is in the order of several seconds, roughly, between about 2 and 10 seconds by observation. This time constant was found to be near the maximum value tolerable for repetitive measurements.

d. Conductivity

The threshold field strength for pearl-chain formation is a function of particle size. According to the dipole appoximation formula (eq. 23), the threshold varies as $a^{-3/2}$, where "a" is the radius of the particle. But the heat developed in the suspending fluid varies as E^2. Thus it can be seen that the heat developed at the threshold field strength varies as a^{-3}. In other words the liquid in a suspension of

---

[75] General Electric Silicone Products Dept., Waterford, N.Y.

small particles may get very hot, with violent thermal convection currents (as in fig. 48), before the chains form. For example, a suspension of 0.557μ polystyrene spheres, with a conductivity of about 10^{-4} mho/cm, may require more than 600 v/cm for pearl-chain formation. But with this field strength, there is ohmic heating at the rate of about 9 cal/cm^3/sec. This amount of heating renders measurements virtually impossible.

The obvious solution, reducing the conductivity of the liquid suspending medium, does help somewhat. But the reduction in conductivity is necessarily linked to a change in the ionic character of the liquid, and, as a consequence, the particles assume a new behaviour, described next.

5. False pearl chains

In order to make a suspension or emulsion stable, a detergent is usually employed. The function of the detergent is to coat each particle with molecules, one end of which is attracted to the particle and the other to the suspending fluid. If the fluid is water, the latter end is called hydrophilic and the former hydrophobic. This coating of detergent molecules on a particle or globule acts as a protective layer by keeping other particles or globules at a distance. If one attempts to change the suspending medium in which such particles have been prepared, the detergent phase may be upset and the protective coating may become ineffective.

Attempts to reduce the conductivity of a 0.557μ polystyrene sphere suspension by repeated resuspension in dis-

tilled water (10^{-6} mho/cm) caused the resultant conductivity to change from 2×10^{-4} mho/cm to 5×10^{-6} mho/cm. But when a field was applied, the pearl chains that formed did not readily break up when the field was turned off. In fact the suspension then had numerous 3 and 4 particle chains with no field applied. Reapplication of the field would cause these "linear clumps" to align with the field direction, thereby obscuring a proper threshold measurement. (The threshold for alignment is less than for pearl-chain formation.) Since 0.6μ particles were available in the SM-61 silicone emulsion, further attempts to make threshold measurements on the 0.557μ polystyrene spheres were abandoned.

It is possible that this untoward reaction may be turned to advantage for some purposes. For example an acceleration of clumping might be useful for removing suspended material from a liquid. Other purposes, such as in polymerization processes, also may be found.

f. Dielectric pumping

A dielectric particle in a medium of different dielectric constant will experience a force either with or against the gradient of the electric field, as described in section IV. If the field is homogeneous, i.e., grad $\vec{E} = 0$, then the force vanishes. Although this phenomenon was already discussed at some length, it has a particular reference to measurements of the threshold for pearl-chain formation. For these measurements to be valid, the concentration of particles in the observed region must be great enough to make chain

formation possible in a reasonable time. Of course the initial sample concentration of particles is sufficient, but due to inhomogeneities in the field, certain regions become partially or completely evacuated after a short time. The problem usually is not severe, but in certain cases it is surprisingly troublesome. For example, it may be seen in the studies of field configurations inside the cell (fig. 12) that inhomogeneities are more severe in the viewing area when the wire spacing is small. In such a case, application of a high field strength may clear out the entire viewing area, since simple diffusion vainly tries to restore the concentration of particles in the evacuated area. The appearance resembles a pumping action, hence the name of dielectric pumping.

g. Concentration

It has just been pointed out that measurements are difficult or impossible in suspensions whose particle concentration is very small. In principle, pearl-chain formation should be possible with any finite concentration. But the threshold, and more significantly, the time necessary are increased with small concentrations, so that it is practical only to make measurements in the presence of enough particles to make collisions common. Too great a concentration is even worse, however, since it is then not possible to see properly, as was mentioned in the section on design of the cell. In practice, concentrations of about 0.1% to 1% are optimum.

Three factors affect the concentration in the viewing

area, once the cell has been completed: gravitational settling, dielectric pumping, and diffusion. Settling already has been adequately discussed. Dielectric pumping may be helpful if the concentration is too great for good viewing. One needs only to increase the field until the viewing area is partially cleared of particles. Diffusion very slowly (hours) will restore the initial uniform concentration.

h. Electrophoresis

Alternating electrophoresis is readily apparent for polystyrene and silicone particles when the frequency is below about 500 cps[76]. When the field is applied, individual spheres appear to be elongated by a fraction of a diameter to several diameters. Under these conditions, to determine whether one is seeing a single particle or a chain of several particles is very difficult. In general, the lowest frequency at which threshold measurements for pearl-chain formation could be made was between 0.1 and 1 kc.

---

[76]The dependence of the amplitude of alternating electrophoresis on field strength and frequency is given in section V, eq. (11).

D. Experimental results

The observation of pearl-chain formation had to be limited to particles larger than about 0.4μ in diameter in order not to fall below the limit of optical resolution. The upper limit was vaguely set by the problem of time constants, which has already been mentioned. Measurements consisted of slowly raising the applied field strength until the threshold for pearl-chain formation was reached. The pertinent values were noted and the measurement was then repeated.

Measurements of threshold were carried out on five systems:

(i) General Electric SM-61 silicone emulsion: silicone globules of fairly uniform 0.6μ diameter suspended in an aqueous medium.

(ii) General Electric SM-70 silicone emulsion: silicone globules of median size 2.3μ (range is about 0.8μ to 3.0μ) suspended in an aqueous medium.

(iii) Polystyrene spheres: 1.17μ diameter in an aqueous medium[77].

(iv) The bacteria E. coli: a prolate spheroid with major and minor axes of about 1.2μ and 0.6μ respectively, suspended in water (see section VI, B for details).

(v) Human erythrocytes: 7μ in diameter, suspended in physiological saline.

---

[77]Kindly supplied by J. W. Vanderhoff of the Dow Chemical Co., Midland Mich.

1. Threshold field strength vs. frequency

The dipole approximation theory for the threshold shows that a frequency dependence may occur if at least one of the two following conditions prevails:

(a) The values of ϵ_1, ϵ_2, κ_1, and κ_2 are frequency-independent; but the value of $\frac{\epsilon_1^*}{\epsilon_2^*}$ is sufficiently frequency-dependent so that γ (or E_{th}) is subject to significant departures from constancy (see eq. 26 or its graphical equivalent in fig. 44). The resultant dependence of threshold on frequency will be most marked within about one decade above and below ω_2, (see fig. 45), where

$$\omega_2 = \frac{1}{T_2} = \frac{\kappa_2}{\epsilon_2 \epsilon_r} \qquad (32)$$

(b) The values of ϵ_1, ϵ_2, κ_1, and/or κ_2 are frequency-dependent. Each case of this type must be investigated separately, although a graphical analysis may still be performed, as described in relation to fig. 45.

a. E_{th} vs. f for 1.17 polystyrene spheres

No significant frequency dependence could be noted between 1 kc and 100 Mc (refer to fig. 49). Each of the points is an average of 10 to 20 measurements, except for the point at 1 kc which is the average of five measurements. The indicated spread represents $\pm$ one standard deviation. The dotted line at 174 v/cm shows the average of all of the individual measurements, assuming no frequency dependence.

This apparent frequency-independence of E_{th} may be interpreted in terms of the involved electrical parameters. In the case of the suspending medium, ϵ_2 is known to be frequency-

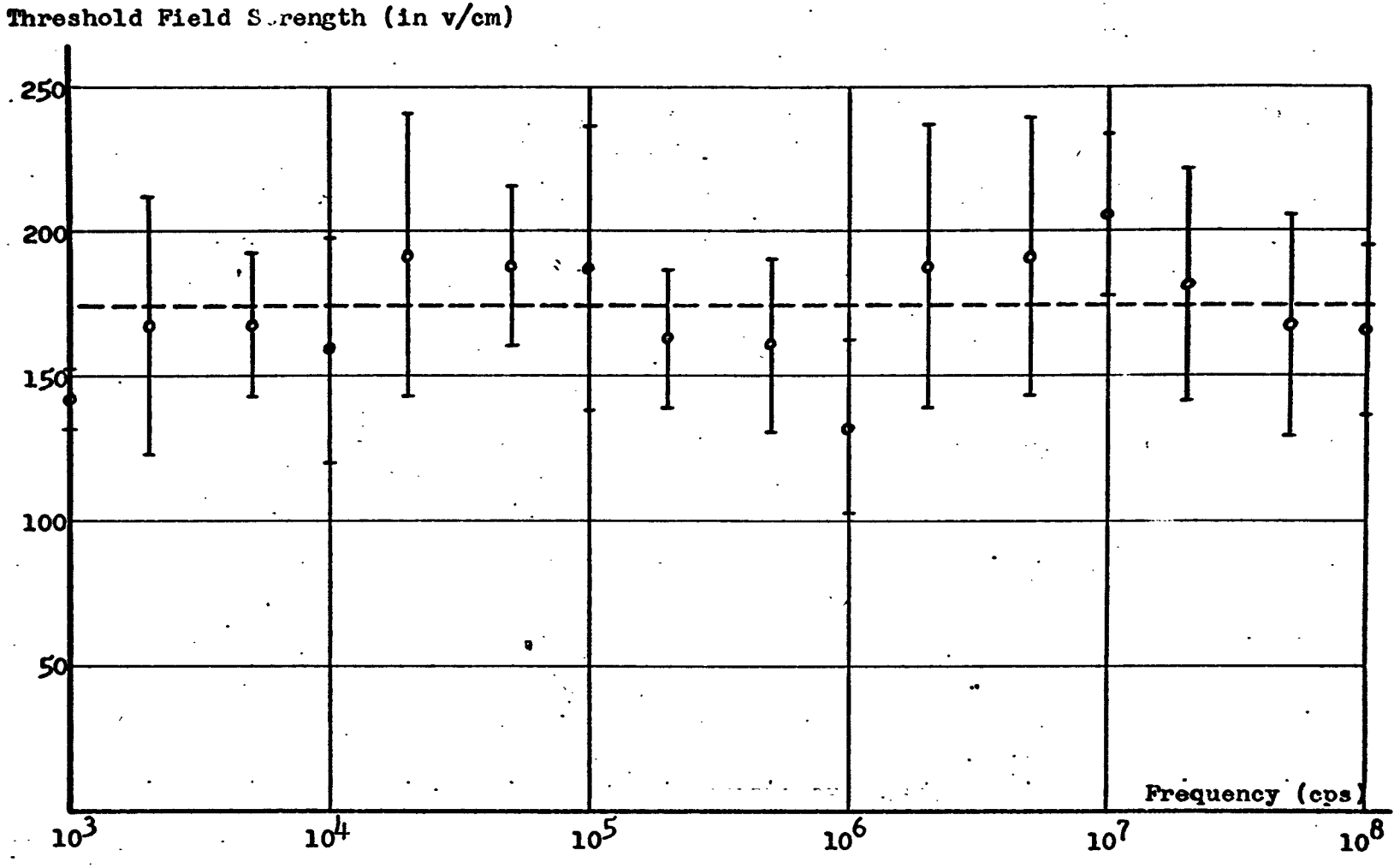

Figure 49. Threshold field strength for pearl-chain formation vs. frequency for 1.17 polystyrene sphere suspension. Bars indicate ± one standard deviation.

independent for $f < 100$ Mc. The frequency dependence of κ_2 depends somewhat on its value at low frequencies, κ_{20}. For $f \ll$ 20 kMc, it increases with frequency according to the relation[78]

$$\kappa_2 = \kappa_{20} + 0.8\,(f/f_0)^2 \qquad (33)$$

where $\kappa_{20} \cong 10^{-4}$ is the low frequency value of κ_2 (in mho/cm);

$f_0 = 20$ kMc is the characteristic frequency for the dielectric dispersion of water

At 100 Mc, $\kappa_2 = 1.2\,\kappa_{20}$. It too is therefore essentially independent of frequency over this range. The polystyrene sphere has a dielectric constant ϵ_1 which is constant above ~10 kc and which rises to very high values (~10^4 to ~10^5) at very low frequencies[79] (<600 cps). But even if $\epsilon_1 = 10^3$ at 1 kc, the particle still appears to be conductive, as will now be shown. The surface conductivity, G_s, and hence the equivalent homogeneous conductivity κ_1, of the polystyrene sphere also has a low-frequency dispersion, in the low kilocycle region. But as G_s changes from 10^{-10} to 10^{-9} mho, the value of κ_1, given by

$$\kappa_1 \simeq 2\,\frac{G_s}{a} \qquad (34)$$

changes over a range (~10^{-6} to ~10^{-5} mho/cm) small enough so that $\frac{\kappa_1}{\kappa_2}$ is essentially constant. Furthermore, $\kappa_1 > \omega\epsilon_1\epsilon_0$ by at least one order of magnitude. Thus, over this range of frequency, the particle continues to appear as a poorly conducting sphere in a conducting liquid. In conclusion, it can be seen that

---

[78] This formula is just the low-frequency ($f \ll f_0$) approximation to the usual dispersion relation

$$\kappa = \kappa_0 + (\kappa_\infty - \kappa_0)\,\frac{(f/f_0)^2}{1 + (f/f_0)^2}$$

where $\kappa_\infty - \kappa_0 = (\epsilon_0 - \epsilon_\infty)\,2\pi f_0 = 0.8$ mho/cm.

[79] Schwan, H.P. et al.: Ref. cit.

the four parameters, ϵ_1, ϵ_2, κ_1, and κ_2 may be considered to be frequency-independent above 1 kc for the purpose of calculating thresholds for pearl-chain formation.

The semicircular dependence of $\frac{\epsilon_1^*}{\epsilon_2^*}$, assuming frequency-independent parameters, starts from $\frac{\kappa_1}{\kappa_2}$ (at low frequency) and ends at $\frac{\epsilon_1}{\epsilon_2}$ (at high frequency). The values of these two end points are $\frac{\kappa_1}{\kappa_2} = \frac{2G_2}{a\kappa_2} \cong 0.02$ and $\frac{\epsilon_1}{\epsilon_2} = \frac{2.5}{78} \cong 0.03$. Therefore the semicircle is very small and yields virtually no frequency dependence of E_{th}.

For these particles, the theoretical prediction for E_{th} from the dipole approximation is 200 v/cm. Comparison with the experimental value of 174 v/cm is well within the experimental error, as is shown in fig. 54.

Interpretation of the frequency-independent experimental results for 1.17μ polystyrene spheres in water has been shown to be particularly simple. The same type of reasoning may now be used for the 2.3μ silicone emulsion (SM 70).

b. E_{th} vs. f for SM 70 silicone emulsion

The median particle size of 2.3μ is about the largest size for which many measurements may be made, since the time constant of these particles almost is too long for both rapid and precise measurements (see discussion on experimental problem of "slowness," p. 121). Nevertheless, the number of measurements made, about 7 per plotted average point, (fig. 50), shows a small tendency for the threshold to decrease with frequency. The bars illustrate the total spread of data for each average value plotted. The points at 0.5 and 1.0 kc are averages of less than five measurements and their values are

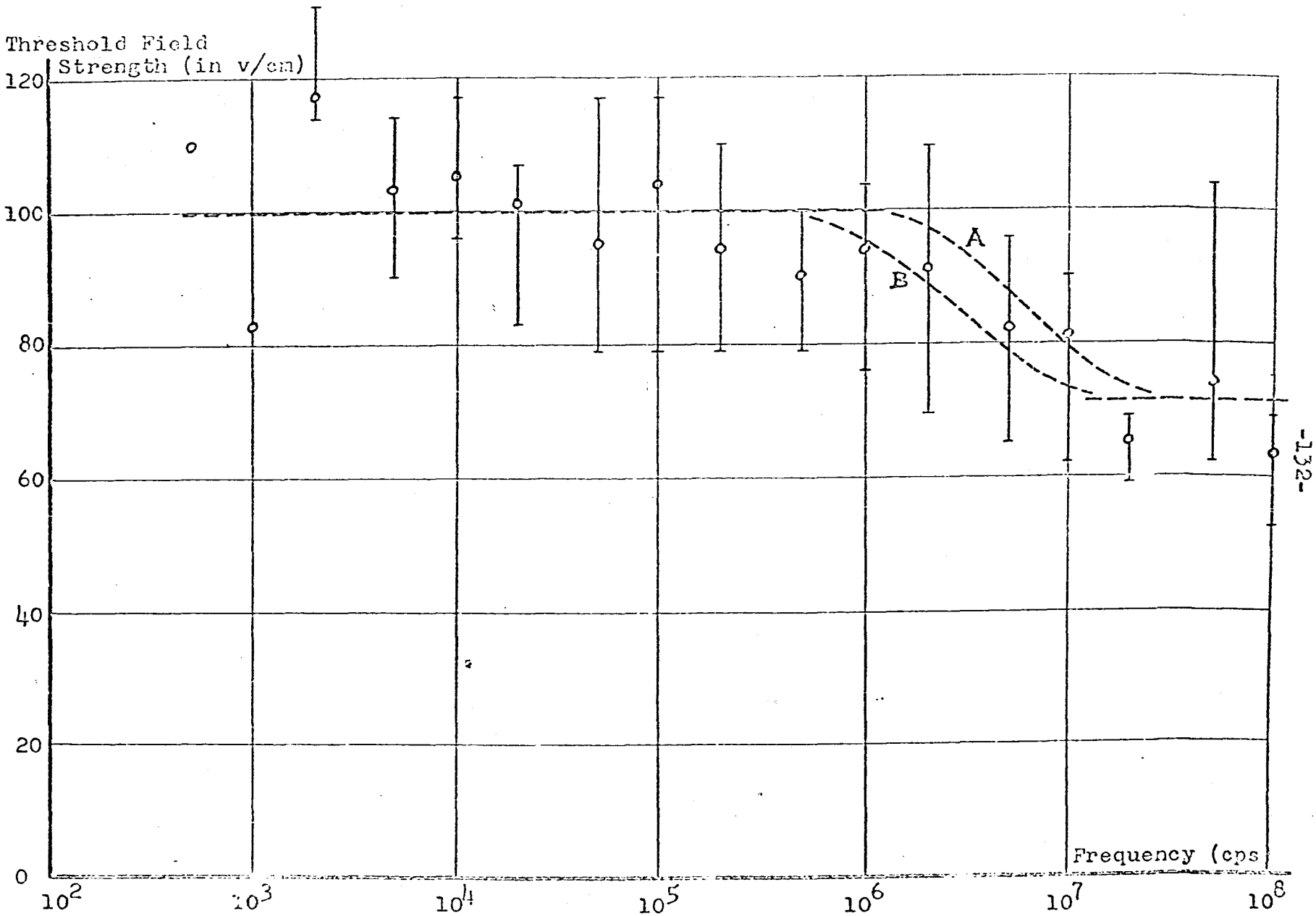

Figure 50. Threshold field strength for pearl-chain formation vs. frequency for SM 70 silicone emulsion (particle size = 2.3μ). Curves A and B are theoretical possibilities.

not well established, because of the interference of AC electrophoretic behaviour. No bars are given for these points.

To compare theory with experiment, it must first be pointed out that the considerations of the frequency independence of ϵ_2 and κ_2 given in the last discussion (for 1.17 polystyrene spheres) are equally applicable here. Also the dispersions of ϵ_1 and κ_1 are of even less concern here than in the previous case: The larger size of these particles causes the dielectric constant ϵ_1 to be fairly constant until the frequency is below 500 cps; and the larger size also suppresses the contribution of surface conductance (see eq. 34) to values lower than those found negligible for polystyrene. Therefore, the parameters ϵ_1, ϵ_2, κ_1, and κ_2 may be regarded as constants over the frequency range of 500 cps to 100 Mc.

If the data are interpreted as two constant levels joined by a transition zone between 1 and 10 Mc, then agreement with the dipole approximation theory is particularly good. The constant levels shown for $f < 1$ Mc and $f > 10$ Mc are the averages of all individual measurements in these respective ranges of frequency. The two connecting curves are theoretically derived from the dipole approximation, as will now be discussed.

Application of the dipole approximation theory for this case is most easily done graphically. Figure 51 repeats an earlier plot (fig. 44) which shows circular loci, each of which represents the locus of all values of $\frac{\epsilon_1^*}{\epsilon_2^*}$ for which E_{th} is a constant. On this family of circles are superimposed the two possible semicircles which (a) have the experimentally

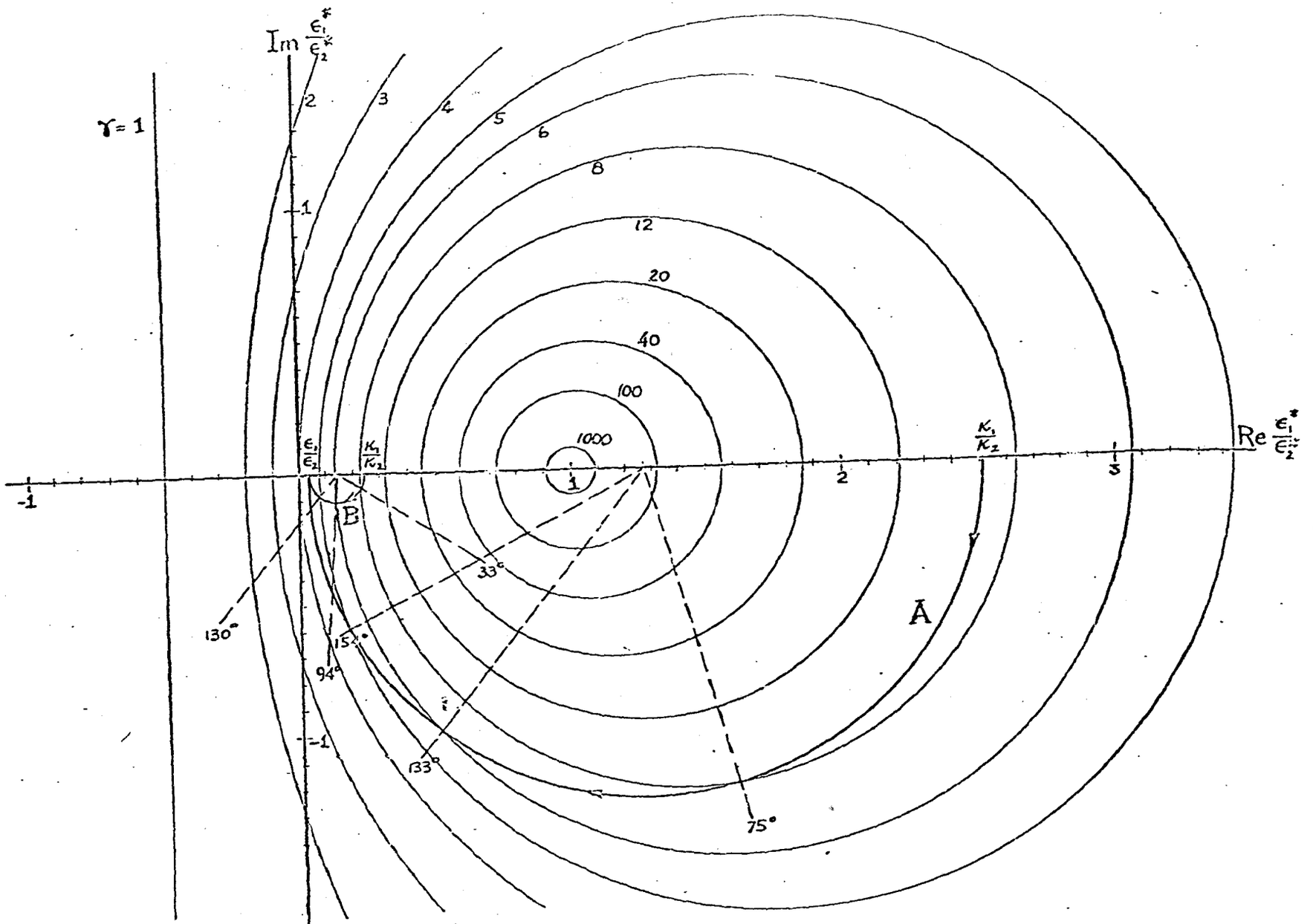

Figure 51. Graphical solution for E_{th} vs. ω (in eq. 23) using data from SM-70 silicone emulsion. From this plot, two possible "solutions," A and B, are seen to fit the data (fig.50).

observed E_{th}-values at their termini and (b) have the known $\frac{\epsilon_1}{\epsilon_2} = 0.035$ value at their high-frequency end. Each of these semicircles, A and B, predicts a distinct E_{th} vs. f behaviour which is shown in fig. 50. Each also shows a value of $\frac{\kappa_1}{\kappa_2}$, from which κ_1 and hence the unknown surface conductance, G_s, may be calculated. These operations are summarized below.

The high-frequency end of the semicircles is fixed by the known value of $\frac{\epsilon_1}{\epsilon_2}$. But the low-frequency end may appear in either one of the two places where the appropriate circle of constant E_{th} crosses the real axis. This circle, a member of the family illustrated (fig. 51), may be found from the experimentally-found, low-frequency value of E_{th}, 100 v/cm. Evaluating eq. (24), it follows that for this case

$$E_{th} = 33.7\sqrt{\gamma} \qquad \text{(in v/cm)}$$

$$100 = 33.7\sqrt{\gamma}$$

$$\gamma = 8.8$$

Corresponding to this value of γ is a circle with center at (1.384, 0) and radius of 1.142 (see top of p. 108). Then the intersections of this circle with the real axis are at 2.526 and 0.242. These intercepts are the two values of $\frac{\kappa_1}{\kappa_2}$ which correspond to the low-frequency threshold field strength, 100 v/cm; and for each value of $\frac{\kappa_1}{\kappa_2}$, there is a corresponding value of G_s (refer to eq. 34):

$$G_s = \frac{a\,\kappa_1}{2} = \frac{a\,\kappa_2}{2}\,\frac{\kappa_1}{\kappa_2}$$

where $\kappa_2 = 1.44 \cdot 10^{-4}$ mho/cm is calculated from the cell's resistance and geometry. Thus,

$$G_s = 2.01 \cdot 10^{-8} \text{mho} \quad \text{(gives semicircle A)}$$

or

$$G_s = 2.00 \cdot 10^{-8} \text{mho} \quad \text{(gives semicircle B)}$$

One hopes that a comparison of the A and B predictions of (E_{th} vs. f) with the experimental data will be sufficient to say that A or B is the correct semicircle. These predictions, shown in fig. 50, are calculated from the construction in fig. 51 using the methods described on pp. 106-110. It can be seen that the distinction cannot be made with certainty.

In summary, the high frequency value of E_{th} can be predicted by a knowledge of $\frac{\epsilon_1}{\epsilon_2}$; it also can be measured, as is done in fig. 50. The two values are virtually indistinguishable at 71.5 v/cm. Similarly, the low-frequency value of E_{th} can be predicted from a knowledge of the value of $\frac{K_1}{K_2}$; but this value is unknown. However it can be measured (again in fig. 50). So the measured value of E_{th} at low frequencies is used to calculate $\frac{K_1}{K_2}$, and subsequently G_s. Two distinct and very reasonable[80] values of G_s result.

Two surprising observations may be made here. One is that two and only two distinct values of G_s come out of the data, and these values are fairly sensitive functions of the thresholds found. One is naturally led to speculate on the possible usefulness of pearl-chain formation threshold measurements for a study of surface conductivities. The second is the very close prediction of the high-frequency E_{th} made by the dipole approximation formula. Figure 54 shows this coincidence graphically.

---

[80] Schwan, H.P., Schwarz, G., Maczuk, J., and Pauly, H.: Ref. cit.

Figure 52. Pearl chain formation in the SM 70 silicone emulsion The spread of particle sizes around the mean of 2.3μ can be seen. A higher field strength would cause the chain to be straighter. Notice that small particles have not formed into chains, since their threshold field strength has not been reached.

c. E_{th} vs. f for SM 61 silicone emulsion

This emulsion contains 0.6μ silicone globules which are difficult to see and which have a pronounced Brownian activity. They react very quickly (in time) to a sufficiently strong applied field, so that the measurements, even though sometimes difficult to make, tend to have a fairly small spread. This small spread is evident in the curve (fig.53) of E_{th} vs. f, where each value plotted is the average of five measurements whose total spread is indicated. Other threshold measurements on this system, not plotted here, have the same general form but have a slightly different rate of change of E_{th} at low frequencies. The slight difference must be due to some aspects of the dilution or other preparatory procedures. To get a curve with the maximum definition, just this one run of E_{th} vs. f is plotted.

The frequency-independent nature of E_{th} for $2 \cdot 10^7 > f > 10^5$ cps follows from previously stated reasoning: ϵ_2 and κ_2 are frequency-independent over this range of frequency and the ϵ_1 and κ_1 are clearly at the high-frequency-limit values of their α-dispersions. The ratios $\frac{\epsilon_1}{\epsilon_2} = \frac{2.75}{78} = 0.035$ and $\frac{\kappa_1}{\kappa_2} \lesssim 0.2$, if G_s is assumed to be $\lesssim 0.5 \cdot 10^{-9}$ mho, so that the semi-circular dependence of $\frac{\epsilon_1^*}{\epsilon_2^*}$ is a minor one. If there is any appreciable frequency-dependence from this semi-circular behaviour, it must be between 1 and 10 Mc (see eq. 32). There may be such a minor frequency dependence in the data but it is difficult to say with certainty. In any event, the value of G_s is certainly less than 10^{-9} mho, and probably is less

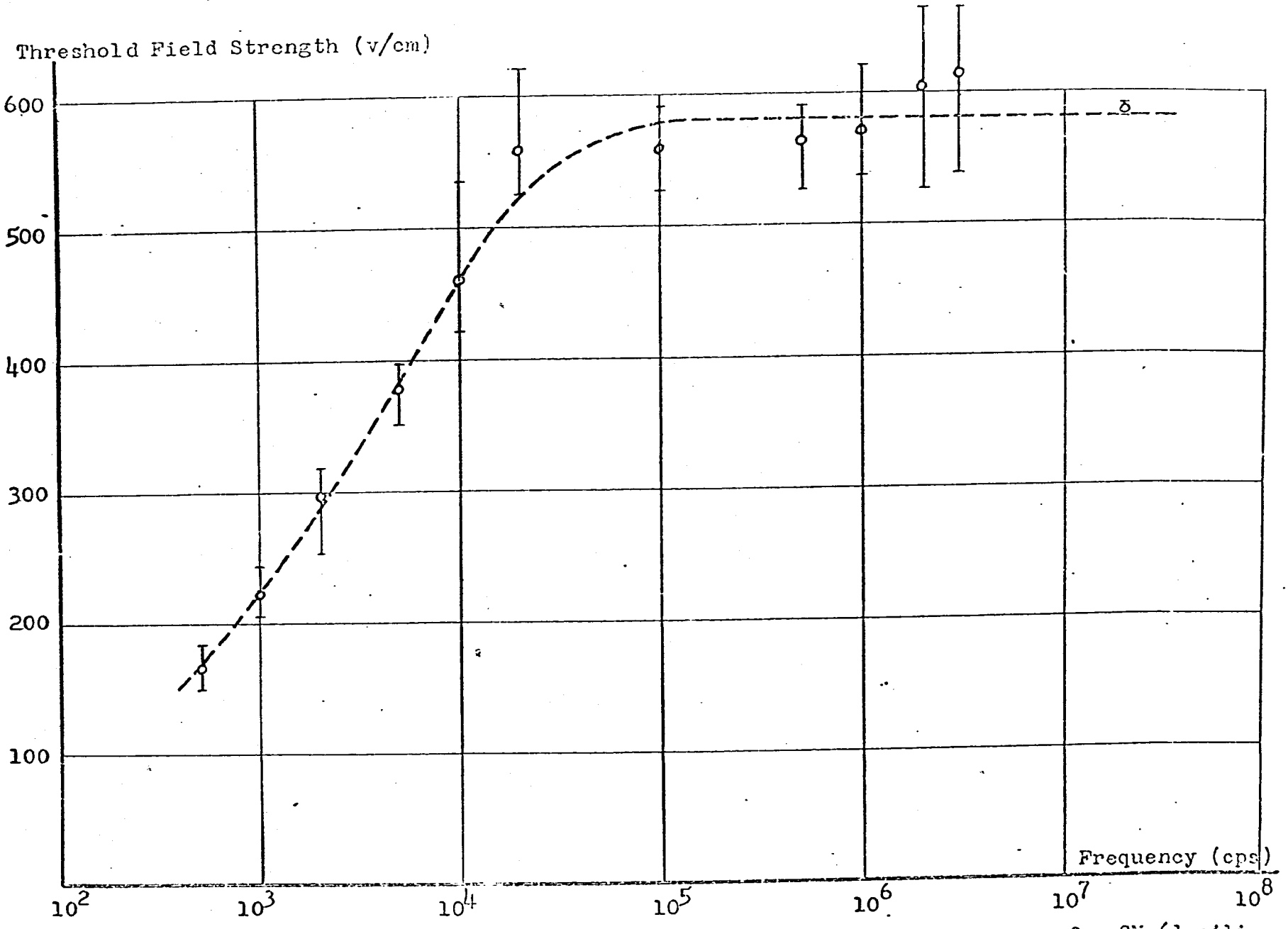

Figure 53. Threshold field strength for pearl-chain formation vs. frequency for SH 61 silicone emulsion (particle size = 0.6μ). Bars show spread of five measurements.

than $0.5 \cdot 10^{-9}$ mho. The dipole approximation formula predicts a value of 508 v/cm, 11% lower than the observed "high-frequency" average value of 574 v/cm.

The strong frequency dependence at low frequencies is probably related only in part to the α-dispersion for these small particles. It may be seen from the dipole approximation formula (eq. 23) that for these particles

$$E_{th} = 254\sqrt{\gamma} \qquad (35)$$

It was shown in fig. 44 that γ is never less than unity and may only approach unity for $\left|\frac{\epsilon_1^*}{\epsilon_2^*}\right| \gg 1$. In this case, $\left|\frac{\epsilon_1^*}{\epsilon_2^*}\right| < 1$ if $G_s \leq 10^{-9}$ mho. So it appears as if no recourse to the dipole approximation formula <u>per se</u> can help to form a complete understanding of the low thresholds found at low frequency. The most likely recourse is to fig. 42 which shows that, at least in the case of perfect dielectric materials, the dipole approximation is greatly in error (high) when $\frac{\epsilon_1}{\epsilon_2} \gg 1$. If the same fault exists for $\left|\frac{\epsilon_1^*}{\epsilon_2^*}\right| \gg 1$, then the low values of observed E_{th} may be explainable. But this idea is only intuitive.

The low-frequency electrical properties of the undiluted SM 61 silicone emulsion were measured[81] in an effort to explain the threshold data. Although ϵ_1 was shown to exhibit a strong increase at low frequencies, it occurred below 1 kc. The value of κ_1 increases slowly with increasing frequency over a large range of frequency, but no clear dispersion could be distinguished either in magnitude or center frequency. There is therefore no completely adequate theory and no completely accurate data on SM 61 to allow a thorough analysis of the

---

[81] Many thanks to Dr. J. Maczuk who made these measurements.

strong E_{th} dependence at low frequencies. Plausible mechanisms may be hypothesized, but as yet this analysis is incomplete.

2. Threshold field strength vs. size

The dipole approximation formula (eq. 23) shows that, other things being equal,

$$E_{th} \sim a^{-\frac{3}{2}} \qquad (36)$$

where "a" is the radius of a spherical particle. If the discussion is restricted to high frequencies, where $\frac{\epsilon_1'}{\epsilon_2'} = \frac{\epsilon_1}{\epsilon_2} = 0.035$, at least for polystyrene and silicone particles, then the formula may be explicitly stated as

$$E_{th} = 88.2\, a^{-\frac{3}{2}} \left(\text{v/cm}\right) \qquad (37)$$

Figure 54 shows this theoretical curve, a straight line with slope = -1.5, together with points representing the average of the pooled high-frequency data for each of the particles. For example, for a given point, five average values (say), each containing 10 measurements (say), are averaged together to give the value shown. The vertical bar shows the spread of these five average values.

For E. coli, the abscissa was chosen to be the long dimension, 1.2μ. For erythrocytes, a diameter of 7μ was assumed. For the SM 70 emulsion, a small spread in the diameter (see fig. 52) is shown to indicate that the particle size is not exactly uniform. The large spread of the two measurments on erythrocytes reflects the extreme difficulty in making these measurements. The time constant must surely be at least one

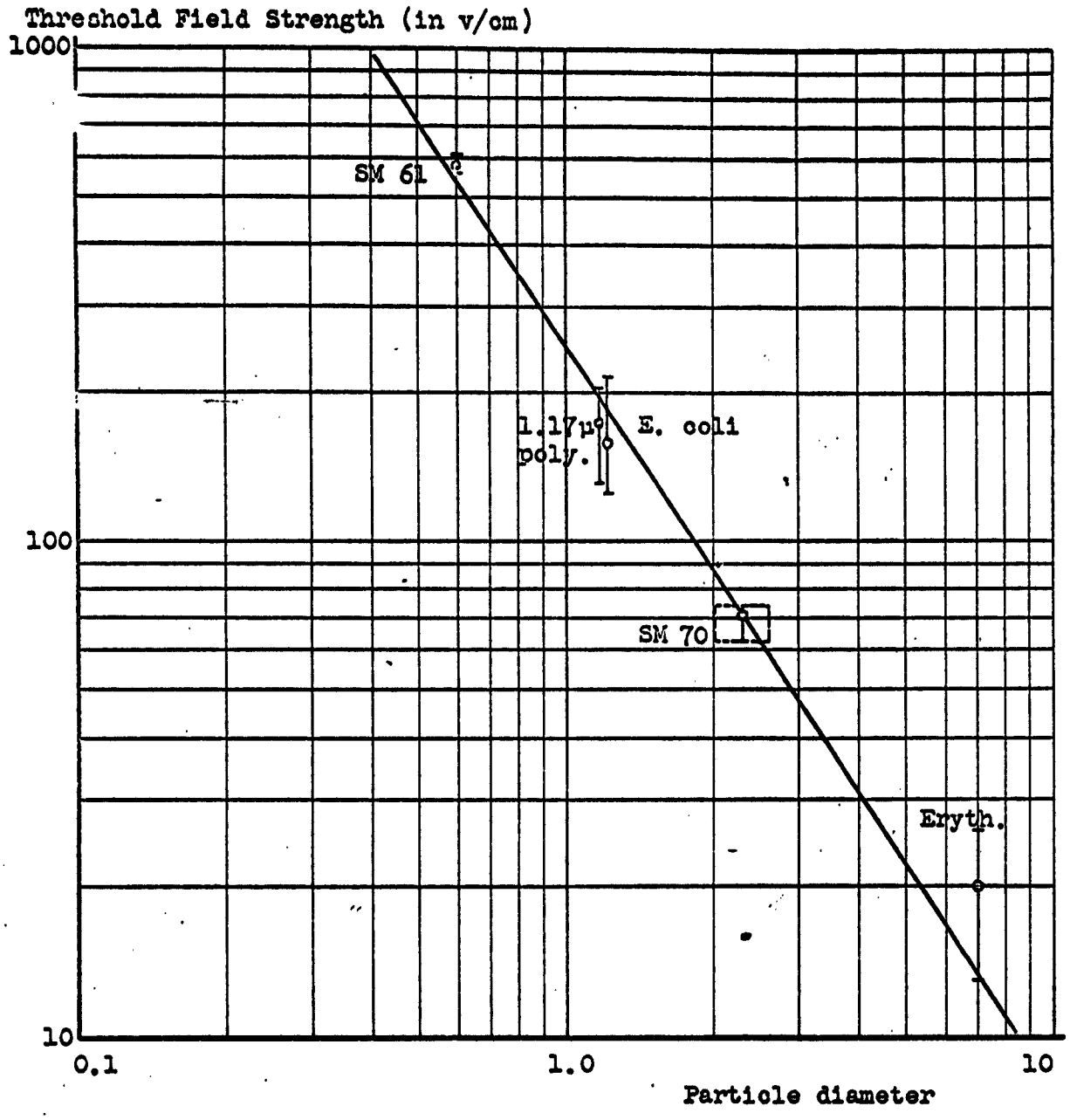

Figure 54. Threshold field strength vs. particle size for pearl-chain formation. For the silicone and polystyrene, the points shown are the "high-frequency" average values. For E. coli, the point is the average value of all measurements. For erythrocytes, the point is the average of two measurements taken at 1 kc and 17 Mc. Line is theoretical prediction.

minute, and may be ten. The large spread of the E. coli data reflects the frequency dependence, shown in fig. 36, which was averaged out for this plot.

The very attractive match between experiment and theory shows that the relationship $E_{th} \sim a^{-\frac{3}{2}}$ must surely be correct.

3. Time constants vs. size

The theory for the transient behaviour of pearl-chain formation shows that the time constant, τ, characterizing the rate of formation or dissolution of pearl chains (whichever is applicable) has the following functional dependences:

$$\tau \sim a^3 \quad , \text{for all } E$$
$$\approx \text{constant} \quad , E \quad E_{th}$$
$$\sim E^{-2} \quad , E \quad E_{th}$$

No formal attempt was made to measure the time constants for pearl-chain formation. The time constant ranges shown in fig. 55 for the three sphere-suspensions are only the subjective estimates of this experimenter. The estimates are for $E = E_{th}$ and were made verbally before being plotted. The circles indicate the geometric means between the upper and lower estimates. For the 0.6μ particles, no lower estimate could be made (obviously), so the geometric mean was chosen on the basis of the average factor involved in the other two means. A straight line of slope = +3 was then fitted (by eye) to the points. The second (dotted) straight line (of slope = +3) shows the theoretical prediction for the zero-field-

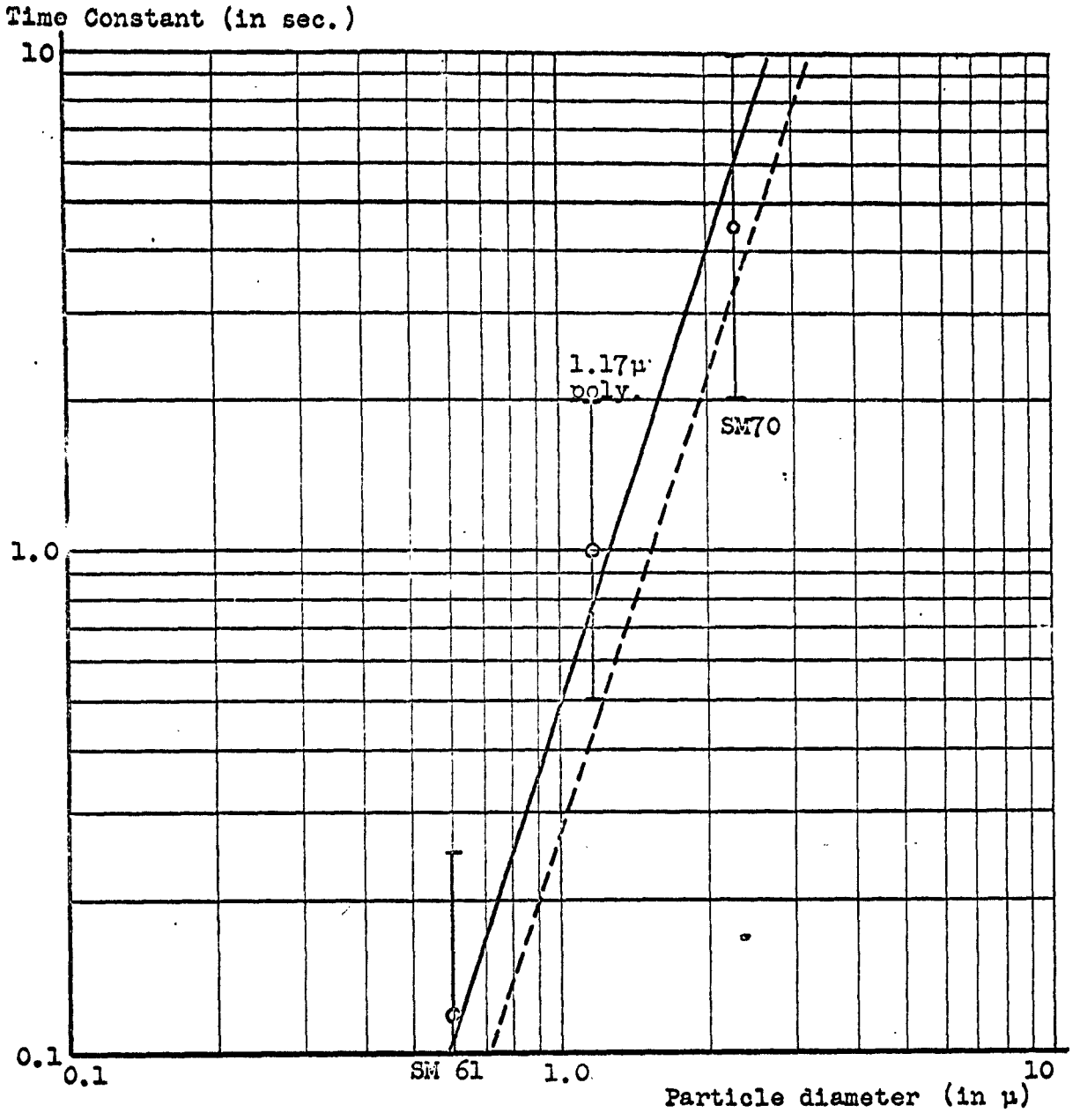

Figure 55. Time constant vs. particle diameter for pearl-chain formation. Points are geometric mean values of the estimates shown by bars. Solid line has slope of +3 and is fitted to the points by eye. Dotted line has same slope but is theoretical prediction under the condition that E = 0.

strength time constants. No similar estimate is available for τ at the threshold field strength; however it should be less than that at zero field strength, but not less by an order of magnitude. That is, the dotted line representing $\tau\big|_{E=E_{th}}$ (not plotted) would compare less favorably with the experimentally observed values. However, in view of the many approximations made in the theory, it is likely that the theoretical time constant magnitudes are significantly in error (too low). It is also likely that the prediction that $\tau \sim a^3$ is correct.

Objective measurements of the time constants may be possible with the use of micro-cimenatography. This work is currently in progress.

E. Conclusion

Pearl-chain formation has been experimentally demonstrated in five organic and inorganic particulate suspensions. Measurements of the threshold field strength have been made and have been compared with the theory, some of which was derived or adapted for this purpose. The results of these comparisons lead to the following conclusions:

(a) The dipole approximation theory generally has proved adequate ($\pm 25\%$) to predict the frequency dependence of the threshold field strength. The exception is for one particular case of small particles at low frequencies; it is likely that this (relative) failure of the dipole approximation theory is just a reflection of its expected range of validity (see fig. 42).

(b) The threshold field strength has been shown to depend on the particle size according to the theoretical prediction $E_{th} \sim a^{-3/2}$. In the case of non-spherical particles, it seems to be the largest dimension which is of importance.

(c) The time necessary for pearl chains to form has been shown roughly to be proportional to the cube of the size, as predicted. It is possible that the theory has underestimated these times for the condition $E = E_{th}$ by at least a factor of two.

VIII. BIOLOGICAL IMPLICATIONS

Four distinct mechanical effects of AC fields on particles dispersed in a liquid have been discussed. It is now desired to translate these results to the case of a biological organism irradiated by or exposed to an AC field.

A. Incident microwave fields

An extreme case will be chosen for this purpose--a human being (or large animal) exposed to an incident microwave power density of 100 milliwatts/cm^2 in air. This example is used because of its current interest and because the presently accepted maximum tolerance dosage for continuous, whole-body, microwave irradiation of human beings is 10 mw/cm^2[82], absorbed dose. From recent studies of the microwave absorption and scattering properties of human beings[83], it can be generalized that about 50% of the incident power is absorbed. Therefore, for whole body irradiation, the example chosen is an extreme; but for microwave diathermy, which irradiates only small parts of the body, it is more of a mean. According to the stated assumptions, there will be about 50 mw/cm^2 of absorbed power, P, just inside the top layer of skin. For watery tissues, such as skin and muscle, E is related to P through the relation

$$P = \frac{E^2}{|Z_o|} \cos\theta \qquad (1)$$

where $\frac{|Z_o|}{\cos\theta} \approx 30$ ohm[82]. Then for the above data,

---

[82] Schwan, H.P. and Li, K.: Hazards due to total body irradiation by radar. Proc. I.R.E., 44, 1572, (1956).

[83] Anne, A., Saito, M., Salati, O.M., and Schwan, H.P.: Penetration and thermal dissipation of microwaves in tissues. Report no. 62-13, Dept. of Biomed. Electronic Eng., Univ. of Pa.

$$E = 1.2 \text{ v/cm} \qquad (2)$$

Under pulsed conditions, assuming a 1 μsec pulse every msec,

$$P_{peak} = 10^3 P_{ave} \qquad (3)$$

and in muscle,

$$E^2_{peak} = 10^3 E^2_{ave} \qquad (4)$$

$$= 10^3 (1.5)$$

$$E_{peak} = 40 \text{ v/cm} \qquad (5)$$

This figure says that the field strength inside the body will not exceed ~40 v/cm with usual pulsed systems, and will have that high value only near the surface. The implications for pearl-chain formation (refer to fig. 54) are that on no account can "biological" pearl-chain formation appear for particles smaller than ~3μ (diameter) without risking overheating of the tissues. But such large particles have time constants in the order of seconds, so that they would respond only to the r.m.s. value of the field, not to the peak value. On this basis, particles smaller than about 30μ (diameter) would not form pearl chains. But freely moveable particles of this size are not available in the body. In conclusion, then, it can be said with certainty that pearl-chain formation will not occur due to microwave irradiation (by usual pulsed or CW systems) of human beings who are even loosely observing the thermal tolerance threshold.

It was shown in fig. 36 that orientation will occur at about three times lower field strength than will pearl-chain formation. Using the above assumptions, one can see that the peak value of E, ~40 v/cm, corresponds to the thresh-

old for orientation of a non-spherical particle whose major dimension is at least 2μ. But the same consideration of time constants leads to the conclusion that such particles cannot respond to the peak value of the field. Therefore, it can be said that structures shorter than about 15μ will not be oriented by pulsed or unpulsed fields which do not overheat the tissues. It is unlikely that any histological structure exists which is superficial, sufficiently large, and free to be oriented. Therefore, on the basis of the somewhat sparse data for orientation, it can be said that significant biological orientation within human beings or large animals is very unlikely.

Biological implications of AC electrophoresis are particularly simple to discuss. In view of the inverse relation between amplitude and frequency (section V, eq. 11), it is clear that for any reasonable value of mobility and for the electric fields described above, the amplitude is vanishingly small above audio frequencies. As a tool for biological or other research, it does have promise. It will receive future consideration in this regard.

The gradient of an incident microwave field is largest at the surface of the body. If a peak field of 40 v/cm is considered, and a depth of penetration of only 0.12 cm is chosen (corresponding to 10,000 Mc), the gradient will be of the order of only 40/0.12 = 300 v/cm/cm. It was shown in section IV that gradients of the order of 10^4 v/cm/cm were required to provoke effects with 1μ particles. Therefore,

it can again be concluded that incident microwave fields offer virtually no chance that any effect due to forces in inhomogeneous fields will be significant.

B. Ionic fields

Although the fields in this study have always been alternating, there is no reason to exclude from present considerations the very strong DC fields which exist in the close proximity of an ion. Consider the field surrounding an elementary charge in a physiological medium (assume $\epsilon = 50$):

$$E = \frac{1}{4\pi\epsilon\epsilon_r}\frac{q}{r^2} \qquad \text{(in MKS units)} \qquad (6)$$

Then

$$E \text{ (in v/cm)} = \frac{3 \cdot 10^9}{r^2} \qquad (7)$$

where r is in Ångstrom units. Thus, within a distance of at least 50 Å, the field exceeds 10^6 v/cm. Also

$$|\text{grad } E| = \frac{6 \cdot 10^9}{r^3} \qquad (8)$$

so that within a distance of at least 15 Å, the gradient exceeds 10^6 v/cm/cm.

Of course the extrapolation of macroscopic laws to these small dimensions is fraught with error. But if one can still judge the orders of magnitude, it can be seen that within the stated distances, pearl-chain formation and orientation are easily conceivable for "particles" of 1 Å ! Forces due to the inhomogeneity per se are probably overpowered by electrostatic forces, especially at that close range.

While it is not possible to say with any assurance what will actually happen on this scale of sizes, the possibilities

for pearl-chain formation and orientation a
tive.